

CORROLES

Thesis by

Jeremy John Weaver

In Partial Fulfillment of the Requirements for the

Degree of

Doctor of Philosophy

CALIFORNIA INSTITUTE OF TECHNOLOGY

Pasadena, California

2005

(Defended May 5, 2005)

© 2005

Jeremy John Weaver

All Rights Reserved

ACKNOWLEDGEMENTS

At once the easiest and the hardest part of a thesis to write, the acknowledgements give me a chance to thank all the people who helped me get to the point where I even had a thesis to write. To anyone who falls in that category who I leave out (and I can virtually guarantee there will be at least one), I'm sorry. It's a reflection of my faulty memory, not your contribution.

First and foremost, I must thank my wife, Susanna Widicus Weaver. From when we first met (and both actually remember it) that first day of orientation and decided to be good friends, to our first date (at Fuddrucker's *not* Shanghai Garden) when we decided maybe we could be more, to our wedding and the start of our life together, you have been a wonderful part of my life. The bright spot on otherwise dark days, and an even brighter spot to make the good days that much better. I love you, and thank you for everything.

My career at Caltech has, of course, been greatly influenced by the man who first called me to tell me I had gotten into Caltech, Harry Gray! Unfortunately I was on break and didn't get the call personally, but even over voice-mail Harry's enthusiasm for everything comes across loud and clear. Once in the presence of the man, it's difficult not to be excited about chemistry. His knack for explaining things so that they sound so simple, without making you feel stupid for not seeing it in the first place, is amazing and is what led to all the results presented here. I have learned a tremendous amount from you, and if I manage to retain only a fraction of it, I'll be set for life.

The other half of my grad student parentage came from Zeev Gross, without whom I would have spent my entire time here trying to synthesize my second corrole. His generous gifts of his time and insights into the work were extremely valuable in getting to this point.

Along these same lines, I must thank Dr. Atif Mahammed for his help along the way. When I was still struggling to make that second corrole he came to the States to show me how it was done.

Of course, getting to the first corrole was especially important, and for that I have to thank Dr. Alexandre Meier. From the first time I met with him to hear about the project he was extremely helpful and kind. His work in starting the corrole project in the group was amazing, and I am indebted to him for getting me started as well.

Now furthering the project are Dr. Karn Sorasaenee, Don Walker, and Mayra Sheikh who all bring great things to the lab. Karn was there through the endless experiments with HSA. Take out a mL of sample, put in a mL of buffer. Repeat times 30. Both in lab and out, Karn has been a great co-worker and friend. Without Don, there would be no 6th chapter to this thesis, pure and simple. I helped him with the compounds, but it was his expertise with solar cells that got the interesting stuff. I had the opportunity to work with Mayra over a couple summers and a year's worth of school terms, and was consistently amazed by her knowledge and enthusiasm. Without her there would be no Appendix B, which is not an official chapter only by virtue of being so much more her toil in the lab than mine.

As for the members of the group who didn't work directly on the project, the list of those who helped it along is still numerous. Dr. Jay Winkler provided much help in data interpretation and in teaching me to really think about all the factors in setting up an experiment so I only had to do it once. Dr. Steve Contakes provided the insight that finally led to a clean synthesis of indium corrole. Drs. Alex Dunn, Kristine Jensen, Judy Kim, Jenn Lee, and Randy Villahermosa, as well as Wendy Belliston Bittner, Brian Leigh, Melanie Pribisko, and Don all helped with the laser experiments and with trying to teach me how to run them myself, a skill I never quite picked up. Drs. Oliver Wenger and John Magyar provided the most non-laser related help. Over the years I had the opportunity to share space in Noyes with Gitrada Arjara, Wendy, Steve, Dr. Pierre Kennepohl, Bert Lai, Brian, Dr. Jeremiah Miller, Yen Ngyuen, Melanie, Crystal Shih, Karn, Don, Dr. Will Wehbi, and Keiko Yokoyama. All of them managed to make it one of the best places to work, full of laughter and fun, and just a great place to spend the days.

Of course, the influence of others is not limited strictly to those in the Gray group. As this is where I'm most likely to forget individual names, let me give blanket thanks to the Peters, Bercaw, Lewis, and Barton groups for help, resources, and equipment usage over the years. And specific thanks must go out to my committee members, Profs. Jackie Barton, Pat Collier, and Jack Richards for all their help along the way.

As well, I must thank Catherine May and Rick Jackson, without whom nothing would get done in the BI, and Pat Anderson and Kathleen Hand, without whom nothing would get done in Noyes. Any problem I had, one them always seemed to have an answer.

Without Dian Buchness, I'm sure I wouldn't be at this point either. She was always there to make sure we were on the right track, or just to give us a place to sit and talk for a few minutes when we needed it.

I also want to thank Mona Shahgholi, Mike and Steve from the machine shop, Tom Dunn, Tony Solyom, and Rick Gerhart for providing help with mass specs, lab equipment, and glassware whenever I asked.

Dr. Mike Day is a wonderful teacher, and I am happy to have had the opportunity to TA for him.

On the road to getting me to Caltech, I must first thank Dr. Jim Hembre, my high-school chemistry teacher, who taught me to love chemistry in the first place and gave me something to fall back on when I decided medicine wasn't for me. At Gustavus, Drs. Tom Gover, Gretchen Hofmeister, Brian O'Brien, Larry Potts, Jon Smith, and Al Splittgerber all made sure I continued to love the field.

As for those who helped keep me sane outside of research, foremost must be Andrew Waltman, my first roommate at Caltech, and later my Best Man. One of the greatest friends a guy could ask for. Rebecca Connor, Rachel Niemer, Brian and Amanda Sisk, Andrew Udit, and Lauren Webb all also fall into this category. Always there whenever needed for a laugh and a good time. Dr. Jeff Johnson, from fifty-page-long p-chem reports and studies on the physics of high-velocity water-balloon collisions with windows to emergency groomsman duty, you've always been a great friend and cohort. Shantanu

Sharma has been a wonderful friend and ally since he arrived at Caltech. Anytime I see a guy with three-inch-thick glasses, I'll think of you.

Ben Edelson, I didn't know you half as well as I would've liked, but still well enough to know Chemistry is worse off without you.

Dorothy Holm was one of the best neighbors I ever had, and I am happy for the chance to know her.

And of course, I could have never made it this far without my family. Mom, Dad, and Toni, thank you for the support, encouragement, and everything else you gave me along the way.

And lastly, partly because as an inorganic chemist I love symmetry, and partly just because I want to, I'll bring this back around to where it started. Susanna, thank you for putting up with me during the writing of the following 100+ pages. You deserve another degree just for that. Storm clouds may gather and stars may collide, but I'll love you until the end of time. Come what may, I will love you until my dying day.

ABSTRACT

Corroles, porphyrin analogues, are the center of a rapidly growing field of research. By virtue of a missing meso-carbon, corroles retain the aromaticity of porphyrins, but become tribasic ligands in place of the dibasic porphyrin. This thesis is a study of synthetic methods for corroles, as well as their photophysical properties and potential applications.

New synthetic methodologies for the free-base molecules have been used to obtain corroles with pentafluorophenyl meso substituents in both water-soluble and non-water-soluble forms. Closed-shell metallocorrole complexes have been synthesized by introducing Ga(III) and Sn(IV) ions into the macrocycle. Likewise, an open shell transition metal corrole utilizing Mn(III) has been made. Problems arising from making a third type of closed shell metallocorrole by introduction of In(III) are also discussed. Among other characterizations of these complexes, Gouterman's four-orbital model for porphyrins is reinterpreted under the reduced symmetry of the corrole macrocycle to explain the absorption and singlet emission spectra of the molecules. Evidence of a triplet excited state is also presented.

The application of corrole complexes to other aspects of chemistry is then examined in two different areas. The interactions of the water-soluble corroles with human serum albumin were investigated to assess their usefulness as diagnostic agents and drugs for cancer research. These highly colored compounds have also been introduced as the dye component of dye-sensitized solar cells, and various aspects of the cells, including overall efficiency, have been tested.

This thesis concludes with a summary of results obtained from collaborations on the interactions of corroles in cellular systems and synthetic attempts toward new types of water-soluble corroles, including an imidazole substituted chromium corrole and a sulfonated manganese nitrido corrole.

TABLE OF CONTENTS

Acknowledgements	iii
Abstract	viii
Table of Contents	x
List of Tables, Schemes, and Figures	xii
Molecule Abbreviations	xv
Chapter I: Introduction	1
Chapter II: Syntheses	5
General Synthetic Procedures	5
pK _a of 2	12
Materials	18
Detailed Syntheses	20
¹ H NMR Data	27
Mass Spectral Data	28
Chapter III: Electronic Structures and Absorption Spectra	35
Gouterman Four-Orbital Model	35
Corrole Four-Orbital Model	35
Conclusions	44
Chapter IV: Photophysics	46
Singlet Emission and the Four-Orbital Model	46
Singlet Lifetimes	54
Singlet Quantum Yields	54
Triplet States	58
Conclusions	61
Chapter V: Interactions with HSA	62
Introduction	62
Experimental Procedures	66
Results and Discussion	67

Concluding Remarks	83
2-Sn /HSA Interactions	84
2-Sn /HSA Conclusions	87
Chapter VI: Solar Cells.....	89
Introduction.....	89
2-Ga versus Ruthenium Dyes	90
2 , 2-Ga , and 2-Sn Dyes versus N3	93
Conclusions.....	100
Appendix A: Anti-Cancer Drugs.....	101
Appendix B: Work with Mayra Sheikh	104
Bibliography	112

LIST OF TABLES, SCHEMES, AND FIGURES

Chapter 1

Figure 1.1. Skeletal structures of porphyrin, corrin, and corrole	2
---	---

Chapter 2

Scheme 2.1. Synthesis of 1	8
Scheme 2.2. Synthesis of 2	9
Scheme 2.3. Metallation reactions of 1	10
Scheme 2.4. Metallation reactions of 2	11
Figure 2.1. Skeletal structures of free-bases 1 and 2	6
Figure 2.2. Protonation and deprotonation processes for 2	13
Figure 2.3. UV-vis pH titrations of 2	15
Figure 2.4. Fluorescence pH titrations of 2	16
Figure 2.5. X-ray structure of 1	17
Figure 2.6. Measured and predicted mass spectra of 1	29
Figure 2.7. Measured and predicted mass spectra of 2	30
Figure 2.8. Measured and predicted mass spectra of 1-Ga and 2-Ga	31
Figure 2.9. Measured and predicted mass spectra of 1-Sn	32
Figure 2.10. Measured and predicted mass spectra of 2-Sn	33
Figure 2.11. Measured and predicted mass spectra of 2-Mn	34

Chapter 3

Table 3.1. Absorption peaks and epsilons	39
Figure 3.1. Porphyrin HOMOs and LUMOs.....	36
Figure 3.2. Orbital and state diagrams for porphyrins and corroles	38
Figure 3.3. Absorption spectra of 1 and 2	40
Figure 3.4. Absorption spectra of 1-Ga and 2-Ga	41
Figure 3.5. Absorption spectra of 1-Sn and 2-Sn	42

Chapter 4

Table 4.1. Emission peaks.....	47
Table 4.2. Quantum yields	59
Table 4.3. Triplet lifetimes	60
Figure 4.1. Emission spectra of 1-Ga and 2-Ga	48
Figure 4.2. Emission spectra of 1-Sn and 2-Sn	49
Figure 4.3. Emission spectra of 1 and 2	51
Figure 4.4. Emission spectra of 1 , 2⁻ , and 2	52
Figure 4.5. Emission spectra of 2⁻ , 2 , and 2⁺	53
Figure 4.6. Idealized structure of 2⁺	55
Figure 4.7. Fluorescence emission decay and fit for 1	56

Chapter 5

Table 5.1. Association constants of HSA:porphyrinoid conjugates	64
Figure 5.1. HSA/corrole titrations by UV-vis	68
Figure 5.2. UV-vis spectral changes at selected wavelengths	70
Figure 5.3. HSA/corrole titrations by corrole fluorescence	72
Figure 5.4. Fluorescence peak intensity as a function of added HSA	73
Figure 5.5. HSA/corrole titrations by visible CD	75
Figure 5.6. HSA/corrole titrations by UV-CD	76
Figure 5.7. HSA/corrole titrations by HSA fluorescence.....	78
Figure 5.8. Normalized HSA emission as a function of added corrole	79
Figure 5.9. Structural models depicting four potential binding sites	82
Figure 5.10. HSA/ 2-Sn titrations by UV-vis and CD	85
Figure 5.11. HSA/ 2-Sn titrations by corrole fluorescence.....	86
Figure 5.12. HSA/ 2-Sn titrations by HSA fluorescence	88

Chapter 6

Table 6.1. Efficiency parameters for 2-Ga vs. ruthenium dyes.....	95
--	----

Table 6.2. Efficiency parameters for corrole dyes vs. N3	97
Figure 6.1. TiO ₂ slides coated with 2-Ga and N3	91
Figure 6.2. Model diagram of CV curve showing efficiency parameters.	92
Figure 6.3. CV curves for 2-Ga vs. ruthenium dyes	94
Figure 6.4. CV curves for corrole dyes vs. N3	96
Figure 6.5. Absorption spectra of corrole dyes and N3 on TiO ₂ slide	98
Figure 6.6. IPCE curves for corrole dyes vs. N3	99

Appendix A

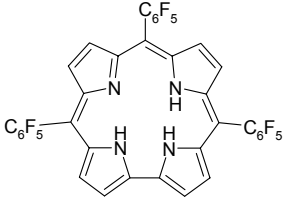
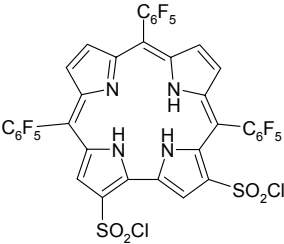
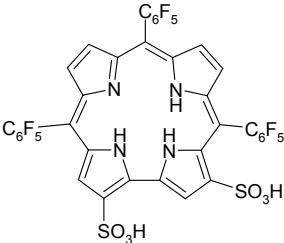
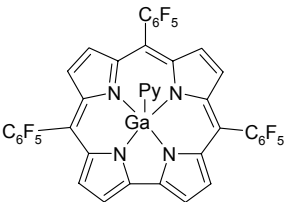
Figure A.1. Micrographs of corrole delivery to cells	102
--	-----

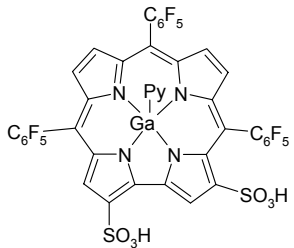
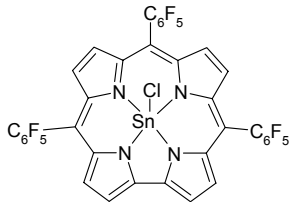
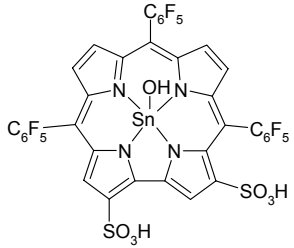
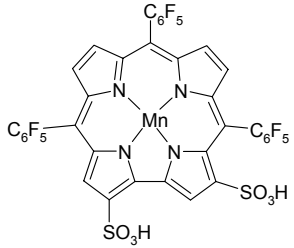
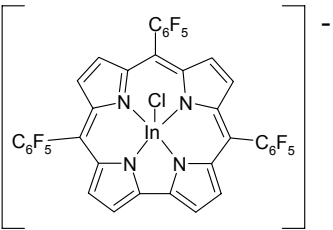
Appendix B

Figure B.1. Skeletal structure of 4	106
Figure B.2. Mass spectra of imidazole substituted corrole	107
Figure B.3. Possible structures of bismethylimidazole corrole.....	109
Figure B.4. Mass spectrum of water-soluble chromium corrole.....	110

MOLECULE ABBREVIATIONS

Below is a list of the compounds synthesized in this work, along with their structures and the abbreviations used in the text.

Abbreviation	Structure	Name
1		5,10,15-tris(pentafluorophenyl)corrole
Cl-2		2,17-bis(chlorosulfonato)-5,10,15-tris(pentafluorophenyl)corrole
2		2,17-bis(sulfonato)-5,10,15-tris(pentafluorophenyl)corrole
1-Ga		5,10,15-tris(pentafluorophenyl)corrolato-gallium(III) monopyridine

Abbreviation	Structure	Name
2-Ga		2,17-bis(sulfonato)-5,10,15-tris(pentafluorophenyl)corrolato-gallium(III) monopyridine
1-Sn		5,10,15-tris(pentafluorophenyl)corrolato-tin(IV) chloride
2-Sn		2,17-bis(sulfonato)-5,10,15-tris(pentafluorophenyl)corrolato-tin(IV) hydroxide
2-Mn		2,17-bis(sulfonato)-5,10,15-tris(pentafluorophenyl)corrolato-manganese(III)
1-In		5,10,15-tris(pentafluorophenyl)corrolato-indium(III) chloride anion

Chapter 1

INTRODUCTION

Corroles are tetrapyrrolic molecules, maintaining the skeletal structure of corrin, with its three meso carbon positions and one direct pyrrole-pyrrole linkage, and possessing the aromaticity of porphyrins (see figure 1.1). First reported by Johnson and Kay in 1965^[1], corroles were the end product of a many step synthetic scheme, finally being formed by the photocyclization of a,c-biladienes. While this last step was simple, with 20-60% yields, the route to a,c-biladienes was far from easy. Indeed, the overall reaction from readily available starting materials to corrole was a multi-step synthesis, with poor yields in many of the reactions. Thus, while corroles have been known for more than 40 years, research in the field was slow to progress. It wasn't until the discovery of new synthetic methods for corroles developed in 1999 by different groups working independently that research in this area really started to expand^[2].

This is not to say, however, that the field of corrole research was non-existent prior to the development of the new methodologies. While it was slow growing after the initial publication, it was far from stagnant, and many of the interesting properties of corroles were investigated by different groups. Among these properties is their ability to stabilize unusually high formal oxidation states of metal ions, such as iron(IV), cobalt(IV), and cobalt(V)^[3,4]. In fact, one particular corrole available through a method developed by Zeev

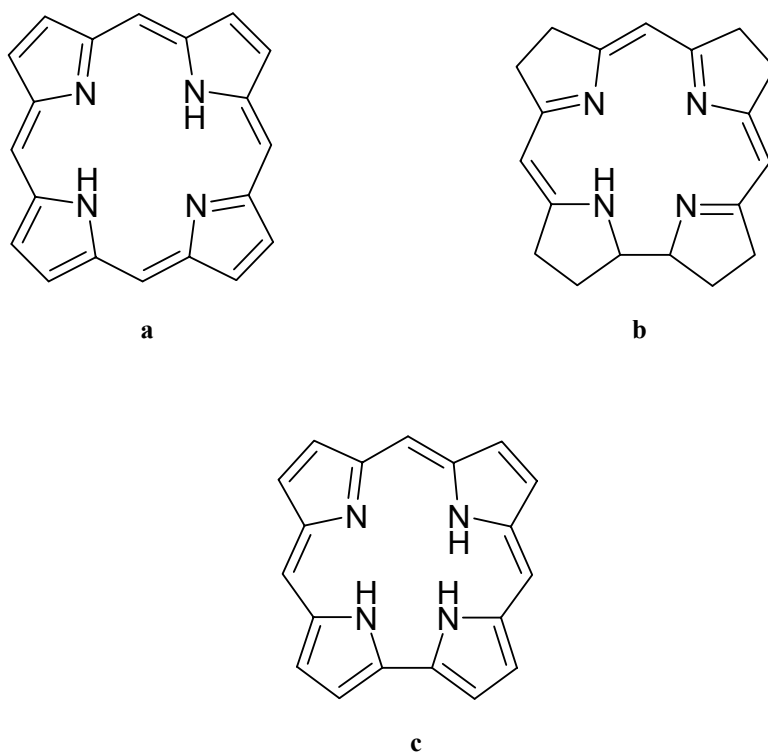


Figure 1.1. Skeletal structures of a) porphyrin, b) corrin, and c) corrole.

Gross, 5,10,15-tris(pentafluorophenyl)corrole, has been shown to stabilize four formal oxidation states of chromium, Cr(III, IV, V, IV)^[5].

Now that the synthesis of corroles has been made easier, the field of corroles has greatly expanded. A quick search of the literature reveals that of all the papers published on corroles in the 40 years since Johnson and Kay's initial publication, almost three-quarters have come out in the last 5 years.

So what makes corroles so interesting? Aside from their ability to stabilize metal ions in higher oxidation states, corroles also possess many other very remarkable properties. Once synthesized, the ligands have shown themselves to be very versatile toward substitution and metallation reactions, allowing for numerous corroles with varying solubility properties, making them useful in many different applications. Some of these corroles form very tight conjugates with proteins, opening up possibilities for use in biological systems^[6, 7].

Also among the interesting attributes of corroles are their photophysical properties. Corroles generally show porphyrin type spectra, with strong absorptions in the visible range associated with very highly colored compounds. As well, the direct pyrrole-pyrrole linkage seems to give corroles stronger fluorescence properties than their porphyrin counterparts^[8]. These properties open up potential for using corroles in many other applications, including such diverse areas as cancer diagnosis and treatment, and solar cell research.

With all these different areas of research opening up to corroles, it is becoming clear that they are a very important class of molecules. And while their uses in other areas are interesting, it has also become clear that a fundamental understanding of the properties of these new molecules is needed. In many respects, corroles are very similar to porphyrins, possessing the same types of properties, but to varying degrees. This raises the questions of just why does the removal of one meso carbon cause these differences, and do these differences in fact make corroles better or worse than porphyrins in regard to applications to other systems? This work investigates the fundamental properties of corroles, in an attempt to determine just how this small change in the structure of the molecule can lead to the various properties seen in corroles, as well as to quantify these properties in selected cases.

Chapter 2

SYNTHESES

While the initial synthesis of corroles was a very long procedure, the advent of a one pot synthesis by Gross and co-workers in 1999 revolutionized the process of making corroles. It is now possible to make hundreds of milligrams of free-base corrole in a single day, compared to weeks or even months of work with the previous methods. Detailed in this chapter are the synthetic methods used for the corroles studied in this work, including two different free-bases; gallium, manganese, and tin complexes of these free-bases; and work done toward the synthesis of an indium corrole.

The particular corrole free-bases used in this study were 5,10,15-tris(pentafluorophenyl)corrole, and 2,17-bis(sulfonato)-5,10-15-tris(pentafluorophenyl)corrole. The structures for these two molecules are shown in figure 2.1.

General Synthetic Procedures

All corroles used in this work are derived from the first of these, 5,10,15-tris(pentafluorophenyl)corrole (**1**), which in turn is synthesized from pyrrole and pentafluorobenzaldehyde. This can be accomplished by different methods, either involving a solid support, an acid to aid the reaction, or neat. All three methods will be described at the end of this chapter. However, in all cases, the synthesis of **1** is a condensation reaction

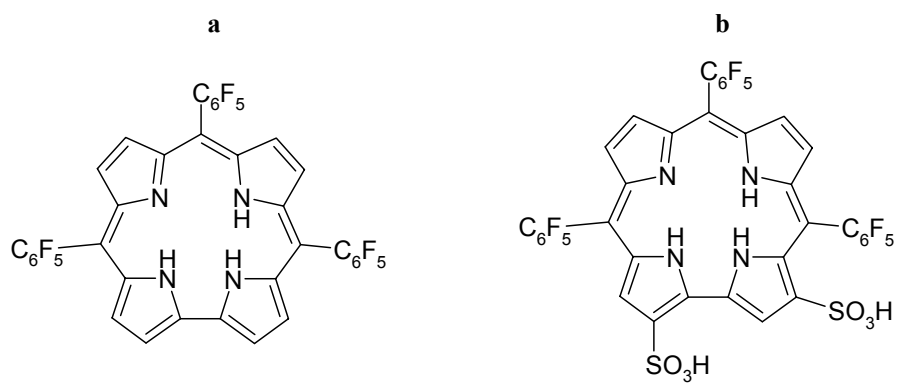


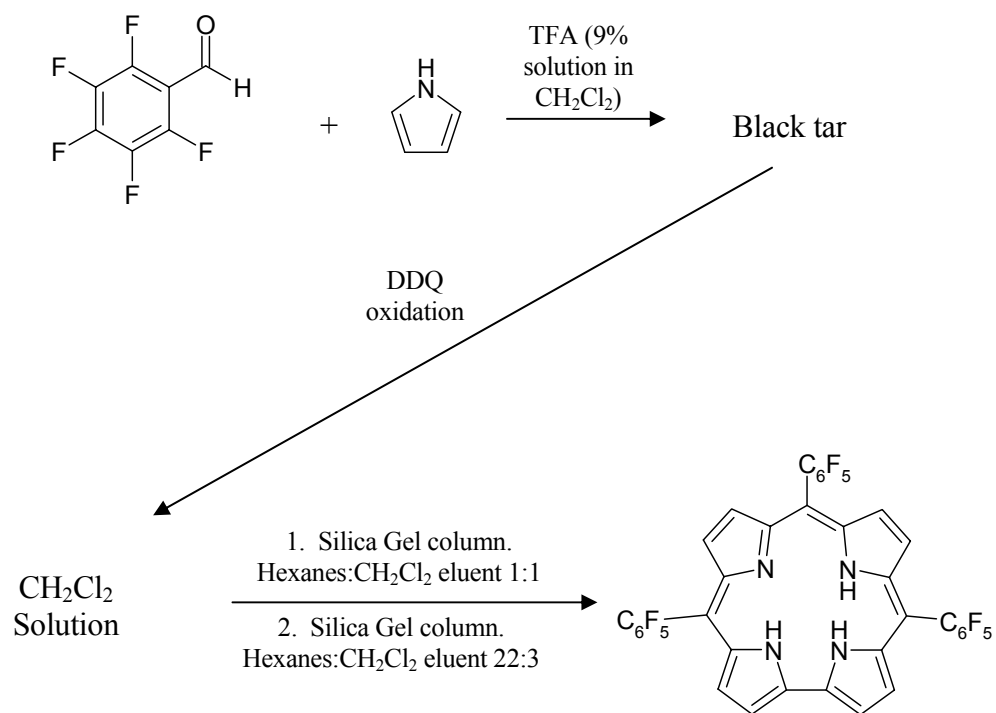
Figure 2.1. Structures of the two free-base corroles used in this study. a) 5,10,15-tris(pentafluorophenyl)corrole (**1**), and b) 2,17-bis(sulfonato)-5,10,15-tris(pentafluorophenyl)corrole (**2**).

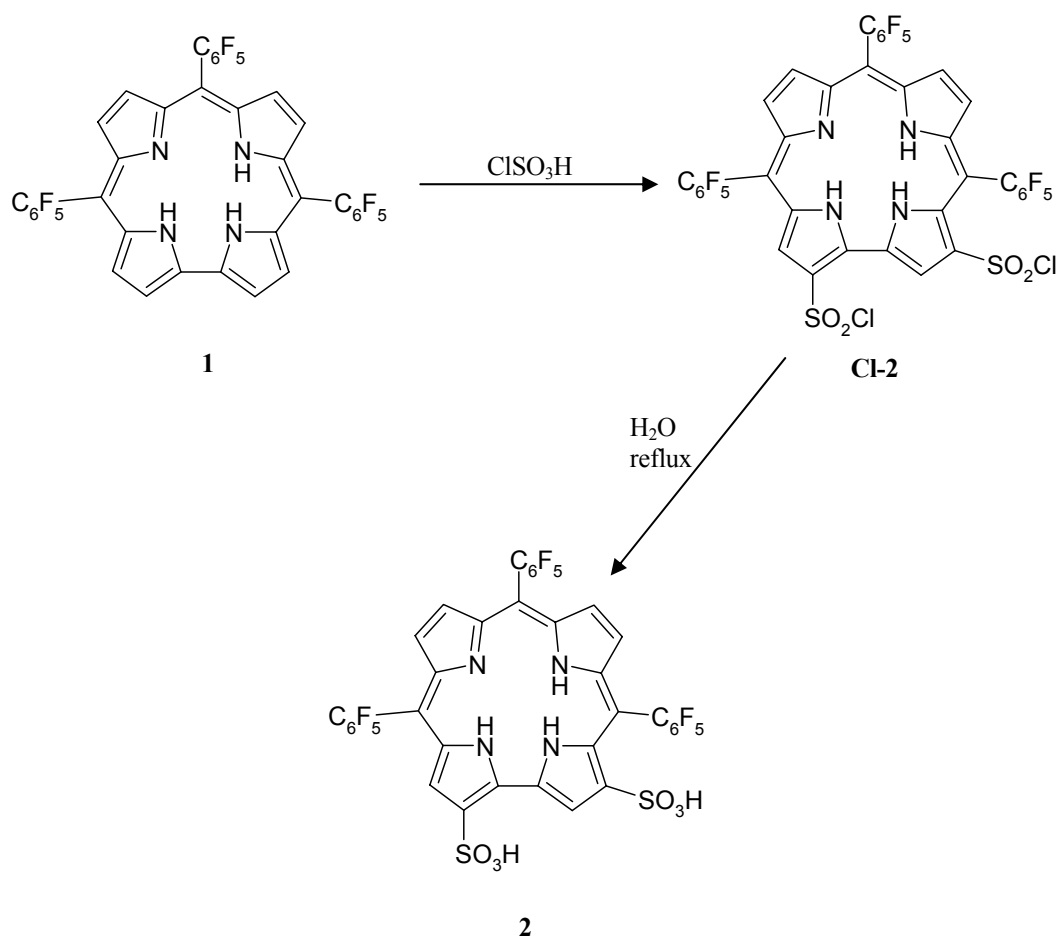
of pyrrole with pentafluorobenzaldehyde, followed by oxidation with 2,3-dichloro-5,6-dicyano-1,4-benzoquinone (DDQ) and column purification, as shown in scheme 2.1.

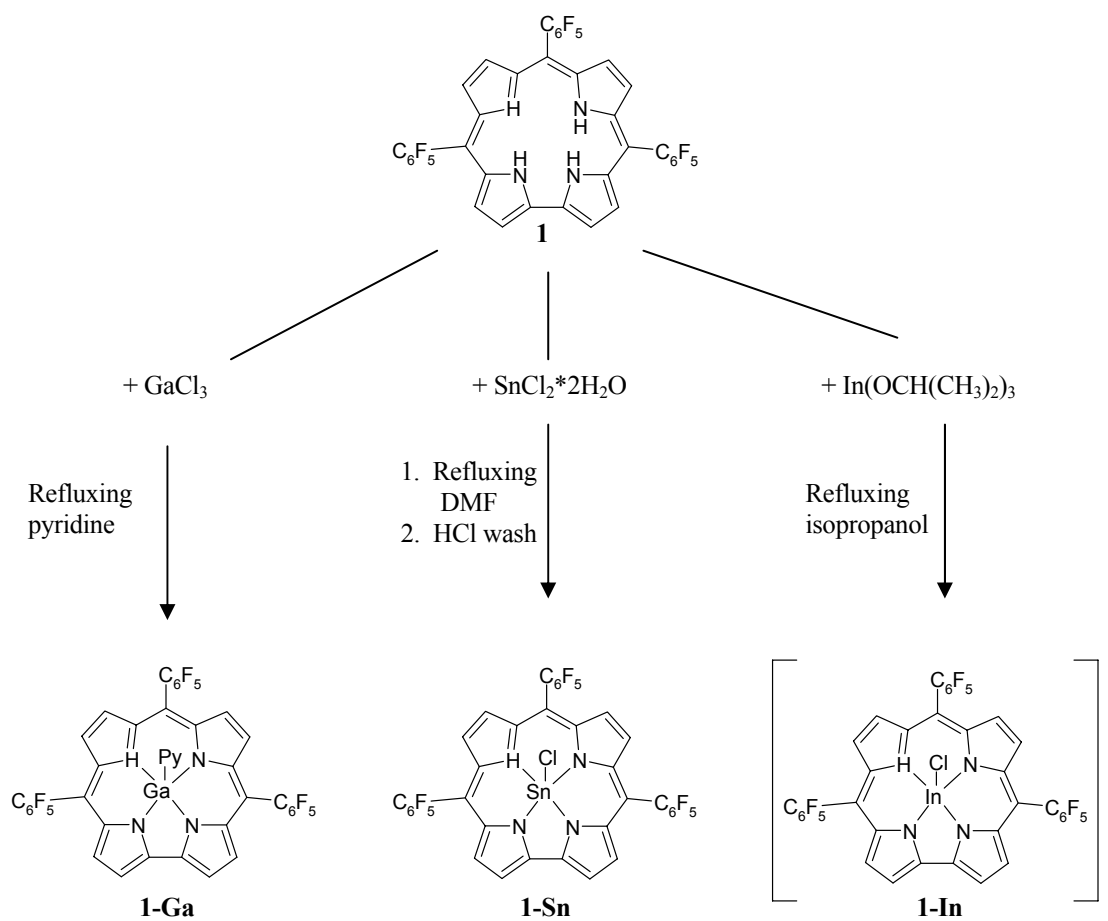
Once **1** has been made, chlorosulfonic acid can be used to substitute two of the β -hydrogens, and a subsequent hydrolysis step produces 2,17-bis(sulfonato)-5,10,15-tris(pentafluorophenyl)corrole (**2**) (see scheme 2.2).

The free-base corrole molecules **1** and **2** have shown themselves to be very versatile to metallation reactions. They are robust enough to survive reflux in high boiling solvents such as DMF, and the free-bases used here have shown no air-sensitivity. Indeed, the only factor requiring a metallation reaction to be performed under inert atmosphere is the stability of the starting metal salt. While it will be seen that the reactions with different metals vary somewhat in solvent and purification conditions, there are a great many similarities. For the most part the reactions described below involve refluxing the corrole free-base along with a metal salt (usually the chloride salt, as in the cases of gallium and tin corroles), followed by column purification, to provide the metallocorrole complex in high yield. Schemes 2.3 and 2.4 outline all the metallation reactions discussed below.

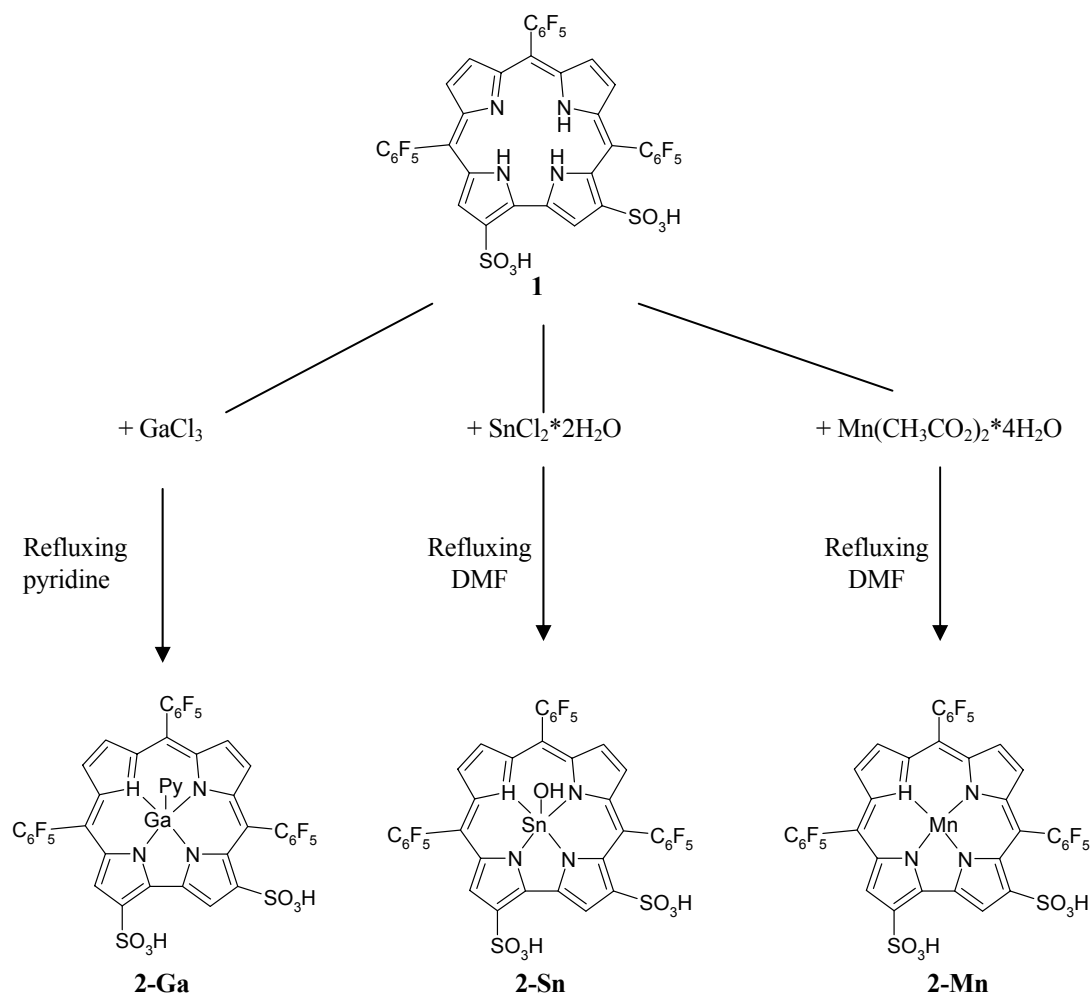
It has been seen that in considering a potential metallocorrole, size is an important factor. While the Ga(III) ion has been shown to form planar corroles^[9], In(III) has shown itself to be too large to form a stable corrole complex, both in **1-In**, which decomposed on attempts at purification, and in the only previously known indium corrole, an octamethylcorrole-indium complex, also seen to decompose upon any attempts to purify the product^[10].

Scheme 2.1. Current synthetic method used for **1**.

Scheme 2.2. Synthesis of **2**.



Scheme 2.3. Metallation reactions of **1**. Insertion of gallium requires column purification, **1-Sn** is purified through recrystallization, and no further purification was possible with the unstable **1-In** complex.



Scheme 2.4. Metallation reactions of **2**. All 3 metalloporphyrins are purified on a silica gel column.

pK_a of **2**

With the synthesis of **2**, a water-soluble corrole, it becomes easier to talk about pK_as of the inner core protons. A core neutral corrole has three protons and one nonprotonated nitrogen atom. By contrast, a core neutral porphyrin has two protons and two nonprotonated nitrogen atoms. The absolute pK_as for protonation and deprotonation of **2** were measured two different ways.

In the first method, buffer solutions were made to cover a wide pH range. Solutions were made from these buffers at a constant concentration of **2**, and the absorption spectra were measured. It had previously been observed that the protonated and deprotonated forms of **1** showed characteristic changes in their absorption spectra^[11]. The same effect is seen for **2**, and the spectra from this experiment show gradual transitions from protonated **2** (**2**⁺), to core neutral **2**, to deprotonated **2** (**2**⁻) as pH is increased. On the basis of these spectra, two rough pK_as can be assigned, at 2.5 and 5.2 for deprotonation of **2**⁺ and **2**, respectively (see figure 2.2).

These values were confirmed by a similar experiment monitoring pH effects on emission spectra of **2**. Again, previous work with **1** had shown a strong dependence of emission intensity on protonation state^[8]. As with the previous experiment, buffers were prepared at varying pHs and were used to make solutions of constant concentration in **2**. Spectra were obtained by exciting the samples at 420 nm, a point where all species have similar absorption coefficients. The spectra again show two transition points, corresponding to deprotonation of **2**⁺ and **2**, at pHs of 2.9 and 5.4, respectively. While this second value is

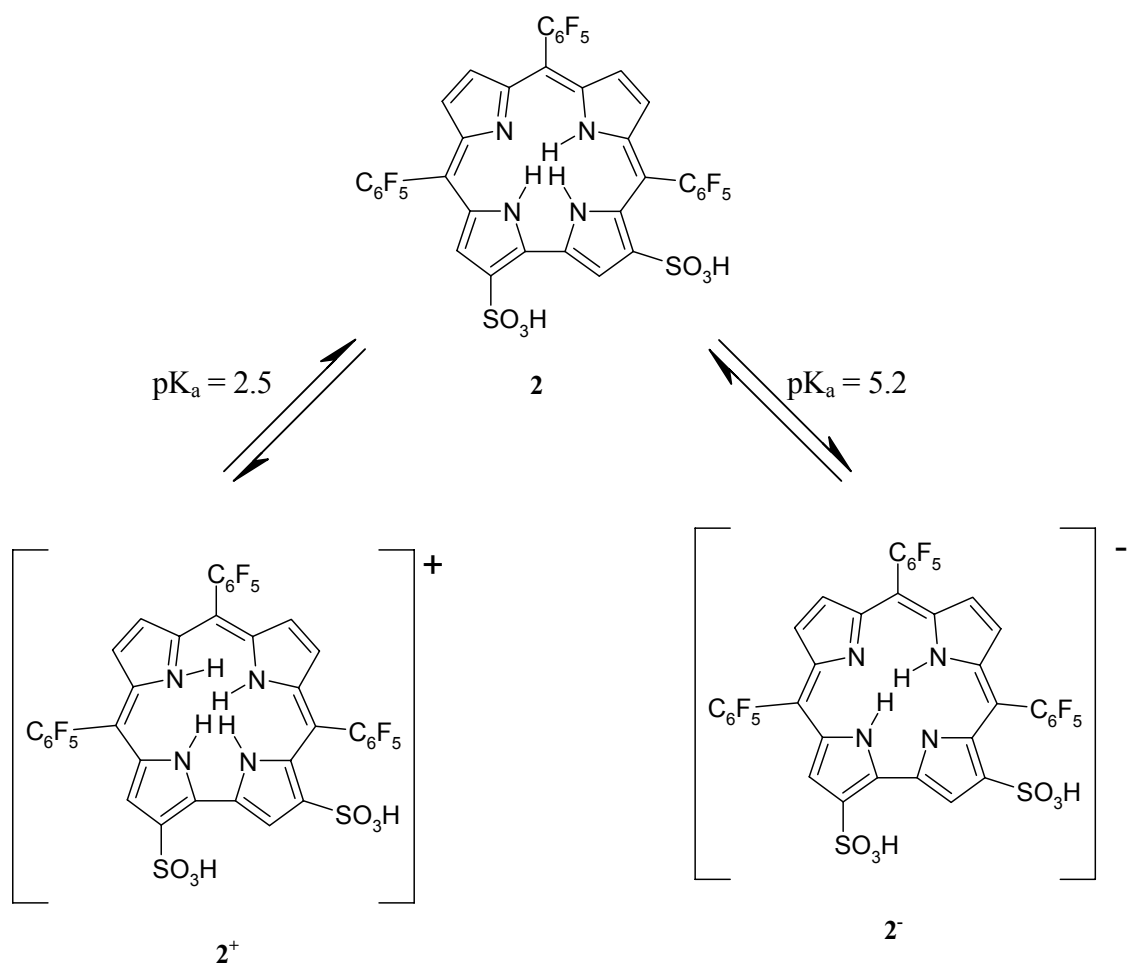


Figure 2.2. Protonation and deprotonation processes for **2**.

nearly identical to that from the first set of experiments, the first is farther off. However, given the lack of a perfect isobestic point for all the species, and given that the absorption change at 420 is greater at lower pH, greater error is expected in this number for the emission experiment. For this transition, the pK_a of 2.5 given by the first experiment is more reliable (see figures 2.3 and 2.4).

These pK_a values are especially interesting when compared to a representative water-soluble porphyrin, namely 5,10,15,20-tetra(*p*-sulfonatophenyl)porphyrin (**3**). The pK_a of this molecule is high enough that it can not be deprotonated in water. However, the value was measured in DMSO/water (4:1) and found to be 32.8^[12]. The acidity constant for protonation of **3**, however, was found to be 4.8 (it should be noted that this is a double protonation event; the singly protonated form of **3** has not been observed)^[13]. Upon inspection of these numbers, it becomes clear that the deprotonation equilibrium of corrole **2** is relatively closer to the protonation equilibrium of porphyrin **3** (the deprotonation equilibrium of **3**²⁺) than the deprotonation of **3**. This can be explained by considering the number of NH protons in each case rather than the formal charge. In both **2**⁻ and **3**, there are two NH protons in the core of the macrocycle. What can be gathered from the pK_a data, then, is that favorability of proton addition to either of these species is comparable, and core charge is not a large driving force for this reaction. Rather, sterics come into play. As seen in the crystal structure of **1** (figure 2.5)^[14], the three protons of a core neutral corrole are in close proximity, and the macrocycle experiences some distortion to be able to fit all three. Indeed, one of the protons of **1** is 0.89 Å out of the mean plane of the four nitrogen atoms. Presumably there is a similar steric penalty for the protonation of **3**, and

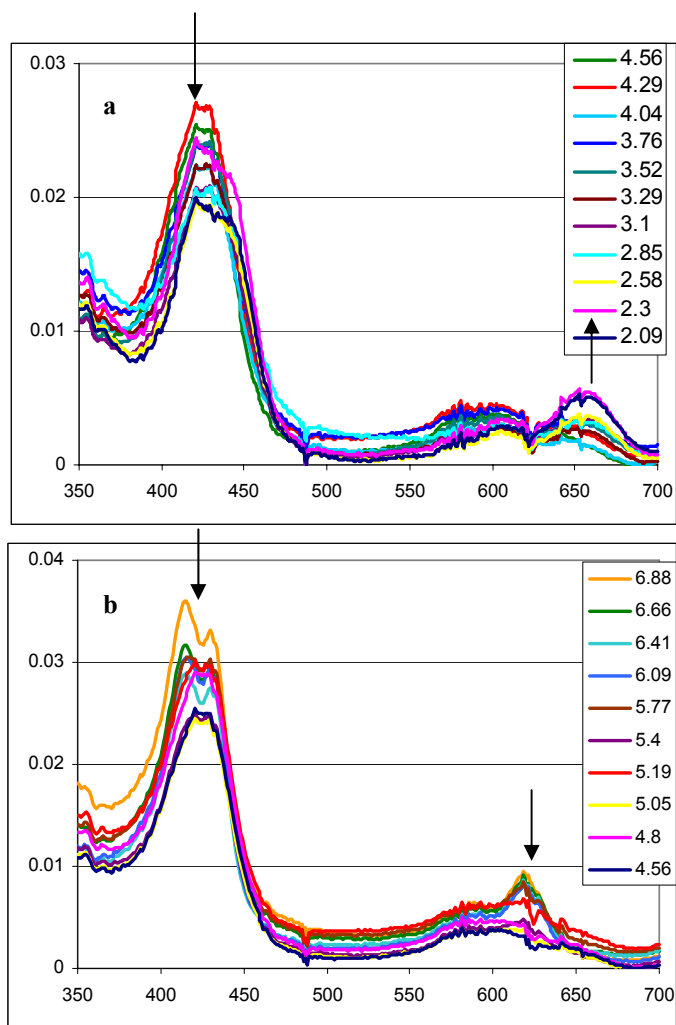


Figure 2.3. UV-vis spectra showing a) pH 4.56-2.09 ($2^{-}2^{+}$) and b) pH 6.88-4.56 ($2^{-}2^{-}$). General trends observed as pH is lowered have been noted.

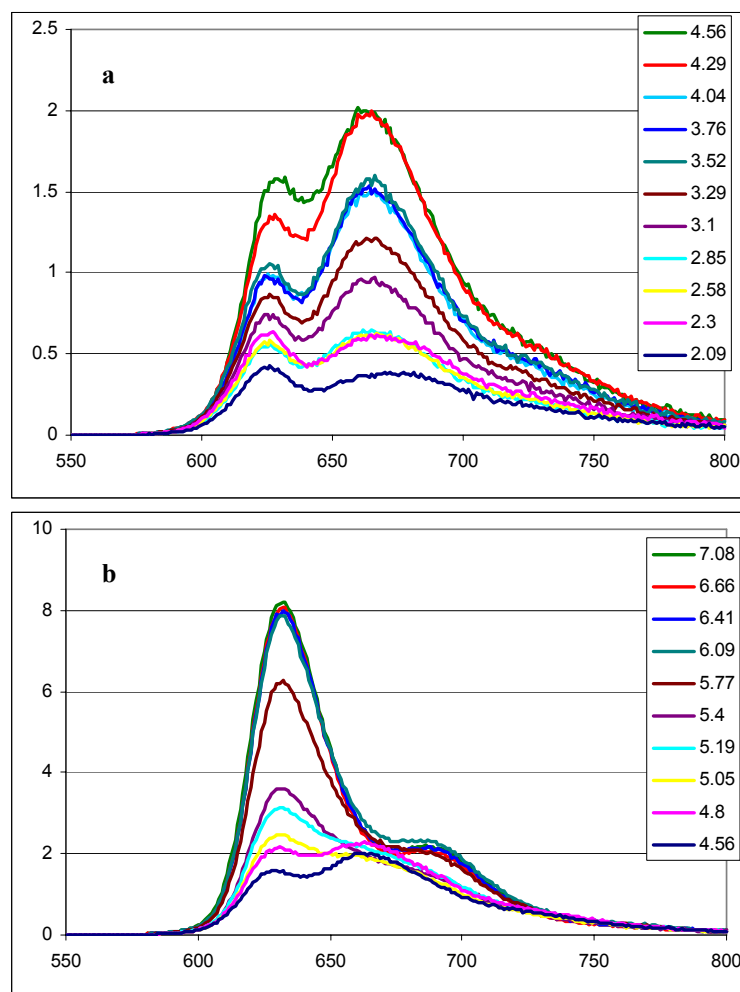


Figure 2.4. The pH-dependent fluorescence spectra: a) pH= 2.09 - 4.56. b) pH= 4.56-7.08. Note the different scales in (a) and (b).

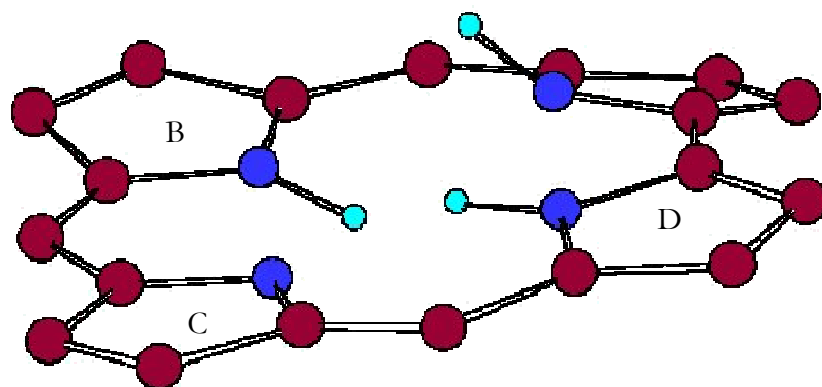


Figure 2.5. X-ray structure of **1**, with meso groups omitted for clarity. The protons on rings D, A, and B are -0.46 , 0.89 , and 0.1 Å out of the mean plane of the four nitrogens, respectively.

once either the corrole or porphyrin has three NH protons, there is no great steric inhibition to adding a fourth. This is evidenced by the small pH range in which **2** exists between 2^- and 2^+ , and the utter lack of a monoprotonated **3**, the molecule instead progressing directly to the diprotonated form.

Thus it can be seen that corroles are very versatile molecules, with interesting and useful spectroscopic properties. These properties will be discussed in greater detail in the following chapters.

Materials

All materials were purchased from Aldrich and used as received except where noted otherwise.

Pentafluorobenzaldehyde (98%, FW 196.07 g/mol, mp 20° , bp $164-166^\circ$, d 1.588 g/mL). Usually found as a solid except on particularly warm days. When solid, it was warmed to liquid with a heat gun prior to use. The liquid was then pipetted into a tared flask when measured by weight, or a particular volume was measured by syringe.

Pyrrole (98%, FW 67.09 g/mol, mp -23° , bp 131° , d 0.967 g/mL). While the bottle was stored in a refrigerator, the liquid did show evidence of photodecomposition products (the liquid was a dark yellow-brown). Prior to use the liquid was filtered through basic alumina to remove these excess products, affording a light yellow to colorless solution. The pyrrole was then pipetted into a tared flask to measure by weight, or a particular volume was measured by syringe.

Trifluoroacetic acid (TFA, 99%, FW 114.02 g/mol, mp -15.4°, bp 72.4°, d 1.480 g/mL).

Chlorosulfonic acid (99%, FW 116.52 g/mol, bp 151-152°, d 1.753 g/mL).

2,3-Dichloro-5,6-dicyano-1,4-benzoquinone (DDQ, 98%, FW 227.01 g/mol, mp 213-216°) was stored in a refrigerator.

Gallium(III) chloride (anhydrous beads, 99.99%, FW 176.08 g/mol, d 2.470 g/cm³) was stored in a dry box.

Tin(II) chloride dihydrate (98+%, FW 225.63 g/mol, mp 37-38°, d 2.710 g/cm³) was purchased from Fischer Scientific.

Manganese(II) acetate tetrahydrate (99+%, FW 245.09 g/mol, d 1.589 g/cm³).

Indium(III) chloride (anhydrous powder, 99.999%, FW 221.18 g/mol, d 3.460g/cm³) was stored in a drybox.

Indium(III) isopropoxide (5 w/v% solution in isopropanol, 99.9+%, FW 292.09 g/mol, d 0.808 g/mL).

Aluminum oxide, activated basic (standard grade, ~150 mesh, 58Å).

Silica gel 60 (particle size 0.040-0.063 mm) was purchased from EMD Chemicals through the VWR stockroom.

Sand was purchased from EMD Chemicals through the VWR stockroom.

All solvents were purchased from EMD Chemicals through the VWR stockroom.

Solvents used were generally Omnisolv[®] quality, though no particular purity was required, except where otherwise noted.

Detailed Syntheses

In the first of the three methods for synthesis of **1**, to 2.82 g (14.3 mmol) pentafluorobenzaldehyde were added first 10 mL dichloromethane (CH_2Cl_2) followed by 1 g (14.9 mmol) pyrrole. This mixture was then added to a 50 mL round bottom flask containing 3 g alumina. The mixture was stirred while heating to 60° C in an oil bath, causing CH_2Cl_2 to boil off. Once the solvent had been evaporated, the solid was maintained at 60° for four hours. After heating, CH_2Cl_2 was added to the flask to dissolve the black residue, and the liquid was filtered through a Büchner funnel to remove the alumina. To the liquid were added 1.5 g (6.6 mmol) DDQ, and the solution was stirred for one hour. After 1 hour, the mixture was checked by TLC (1:1 dichloromethane:hexanes eluent), and a purple band with strong fluorescence under long-wave UV light could be seen.

7 grams of silica gel were added to the flask, and the liquid was evaporated to afford the product mixture adsorbed onto the silica gel. A 2-inch inner diameter column (henceforth referred to as the large column) was packed to a height of ~7 inches with dry silica gel, followed by a ~0.5 inch layer of sand. The solid product adsorbed on silica gel was then scraped out of the flask and layered on top of the sand, followed by a second layer of sand. The column was then eluted with a 1:1 mixture of dichloromethane and hexanes. Progress

of the fluorescent corrole band could be monitored with UV light. Starting with the first colored fraction, all products were collected until the fluorescent band had completely eluted from the column. To the eluted products 2.5 g silica gel were added, and the solvents were evaporated. A 1-inch inner diameter column (henceforth referred to as the small column) was prepared in the same manner as the large column, with the adsorbed product layered between two sand fractions. The column was run with a 22:3 mixture of hexanes to CH_2Cl_2 and was monitored by UV light. The fluorescent corrole band was collected by itself.

Usually a third purification was performed by evaporating the solvent from the column eluent and by dissolving the residue in a minimum of dichloromethane and hexane (~3:1). The solution was then put in the freezer to induce crystallization. The crystals were collected in a Büchner funnel to provide extremely pure corrole. Normally 2-3 crops of crystals could be obtained from a single batch, providing ~150 mg (0.2 mmol, 5% yield) of 5,10,15-tris(pentafluorophenyl)corrole (**1**).

In the second, neat method, reaction between pentafluorobenzaldehyde and pyrrole was performed in six small vials with specially fitted stirrers. 0.45 g (2.3 mmol) pentafluorobenzaldehyde was added to each vial. While stirring, 150 μL (2.2 mmol) pyrrole were added. The reaction is exothermic, and some boiling could be seen initially. The mixture quickly turned black, and the viscosity increased to produce a tar. The vials were allowed to sit with no external heating for ~60 minutes. The tar in each vial was then dissolved in CH_2Cl_2 , and all six solutions were combined in a single flask. 1.5 g (6.6

mmol) DDQ were again added, and the reaction and purification proceeded as above.

This method afforded approximately the same yield as the original method. Both of these methods showed very little ability toward scaling up, with overall yield plummeting upon any attempt.

The third method for synthesis of free-base, and the one that is currently in use in the group, is a variation of the neat method. To a 250 mL round bottom flask were added, in order while stirring, 1.73 mL (14 mmol) pentafluorobenzaldehyde, 140 μ L of a prepared TFA solution (0.5 mL TFA in 5 mL CH_2Cl_2 , overall amount of TFA added was 0.17 mmol), and 1.46 mL (21 mmol) pyrrole. The mixture was allowed to react for 10 minutes, during which time the methylene chloride was evaporated by the exothermic reaction, leaving a black tar. The tar was then dissolved in \sim 100 mL CH_2Cl_2 , and 3.8 g (16.7 mmol) DDQ were added. This solution was allowed to stir for 5 minutes, after which 7 grams of silica gel were added and purification proceeded as above. Attempts to scale up this reaction reduced overall yield and ran into great problems with the first column, in that the amount of tar produced was too great to readily adsorb on the silica gel. Adding more silica gel resulted in larger product bands on the column, and overall separation was greatly reduced. However, given the short amount of time needed to run the reaction by this method, two batches could be prepared at once and run through the large column separately. The two runs could then be combined and separated together on the second column (which, conveniently, was the longer of the two). This method afforded \sim 250-300 mg of product (3.3-4% yield). While this was a slight decrease in overall yield of the reaction from the first method, the cost is outweighed by the more than two-fold decrease

in time necessary to obtain the same amount of corrole by the two methods. It should also be noted that these yields are those obtained by this researcher in this work. Reported yields for the first reaction are twice that obtained herein^[11]. The reaction for the current method is shown in scheme 2.1.

2,17-bis(sulfonato)-5,10,15-tris(pentafluorophenyl)corrole (**2**) was prepared from **1** in the following manner^[15]. 80 mg (0.1 mmol) of **1** were dissolved in ~2 mL chlorosulfonic acid, in a 50 mL round bottom flask, and the solution was stirred for 5-10 minutes at room temperature. The flask was then cooled in an ice bath, and ice chips were added directly to the solution to quench the acid. Care must be exercised at this point in the size of the chips added. A large chip would cause the solution to pop out of the flask. Once the reaction was quenched, as evidenced by no further gas evolution upon addition of more ice, the flask was filled with deionized water, and the liquid was poured into a 500 mL separatory funnel. The flask was then rinsed with CH₂Cl₂ to dissolve any residue left, and this was added to the funnel, along with ~20 mL more CH₂Cl₂. The funnel was shaken, and the two phases allowed to separate, followed by collection of the organic phase. The aqueous phase was washed with two more portions of methylene chloride, and these organic phases were combined with the previous one. The aqueous phase was then discarded, and the combined organic phases were washed three times with deionized water, with only the organic phase being kept between washings. Once washed, the solvent from the organic phase was evaporated, leaving a green residue, identified as a bis(chlorosulfonated) corrole (**Cl-2**). This solid could be scraped off the flask to afford a powder. The powder was added to a 250 mL round bottom flask along with ~150 mL deionized water, and the liquid

was refluxed 12-16 hours, during which time the solution changed from colorless to a dark green, indicating presence of the water-soluble **2**. After evaporation of the water, ~65 mg of **2** could be recovered (0.068 mmol, 68% yield from **1**). This is a remarkable reaction in its specificity. With no control over the number of substituents introduced to the β positions of the ring, there are 140 possible substitution patterns that are possible, ranging from unsubstituted to octasubstituted. This reaction provided one main isomer, with less than 5% contamination of a symmetrically substituted bis(sulfonated) isomer (3,17-bis(sulfonato)-5,10,15-tris(pentafluorophenyl)corrole).

Metallocorroles

5,10,15-tris(pentafluorophenyl)corrolato-gallium(III) monopyridine (**1-Ga**) was prepared from **1** by refluxing the free-base with a large excess of gallium(III) chloride in pyridine for one hour under inert atmosphere. Care must be exercised as gallium(III) chloride is very air sensitive. While the reaction can be done open to air, overall yield is reduced, and a larger excess of metal salt is needed. After the reaction was complete, the solvent was evaporated, and the compound was purified by use of the small column procedure outlined above, using a mixture of hexanes, methylene chloride, and pyridine (100:30:0.5) as eluent, and collecting the fluorescent fraction. The reaction provided **1-Ga** in overall ~80% yield.

2,17-bis(sulfonato)-5,10,15-tris(pentafluorophenyl)corrolato-gallium(III) monopyridine, **2-Ga**, was prepared in the same manner as **1-Ga**, starting from **2** and with the use of methanol:pyridine (19:1) as eluent for the column purification.

The synthesis of 5,10,15-tris(pentafluorophenyl)corrolato-tin(IV) chloride, **1-Sn**, started with dissolving **1** in DMF, followed by addition of 10-fold excess tin(II) chloride dihydrate. The solution was refluxed for 30 minutes, followed by evaporation of the solvent. The residue was dissolved in CH₂Cl₂ and filtered, and the filtrate was washed with concentrated HCl. The desired compound could be recrystallized from a mixture of hexanes and dichloromethane, with an overall yield of ~85%.

As with the gallium reactions, the initial metallation step in the synthesis of 2,17-bis(sulfonato)-5,10,15-tris(pentafluorophenyl)corrolato-tin(IV) hydroxide, **2-Sn**, was the same as its nonsulfonated counterpart, refluxing **2** in DMF with an excess of metal salt for 30 minutes. However, **2-Sn** is a water-soluble complex; therefore washing with concentrated HCl was not feasible, as the compound partitioned itself between the two layers. While the crude reaction mixture showed evidence of the tin corrole chloride, the Cl⁻ ligand exchanged for a hydroxide ligand over time. The transformation could be hastened by running the compound through a silica gel column, providing **2-Sn** in 90% yield.

2,17-bis(sulfonato)-5,10,15-tris(pentafluorophenyl)corrolato-manganese(III), **2-Mn**, was prepared from **2** and manganese(II) acetate tetrahydrate. Equal masses of the two compounds (a four-fold excess of manganese salt) were dissolved in DMF and refluxed for 15-30 minutes. After reflux, the solvent was evaporated and the compound was purified by running it through a small column using ethanol as eluent, giving **2-Mn** in ~90% yield.

The final metallocorrole synthesis considered in this project was that of 5,10,15-tris(pentafluorophenyl)corrolato-indium(III) chloride anion, **1-In**. Initial work with this compound focused on the addition of **1** to indium(III) chloride in refluxing DMF under argon. The crude reaction mixture showed evidence of **1-In** after 5 minutes and no further reaction after 30 minutes. However, attempts to separate this product from the numerous byproducts proved unsuccessful. When the same reaction was repeated in pyridine, in an experiment analogous to the synthesis of **1-Ga**, similar results were observed, and again numerous byproducts were seen. However, when the reaction conditions were changed, a very clean synthesis of **1-In** was discovered. In this synthetic pathway, **1** was added to a five-fold excess of indium(III) isopropoxide (5 w/v% in 2-propanol; used as solvent). Initially the reaction was stirred at room temperature and monitored by UV-vis. Under these conditions, there was evidence of a corrole product growing in at 30 minutes. Complete reaction took 36 hours. In later experiments, the solution was heated to reflux, and overall reaction time was reduced to 1 hour. Mass spectra of the crude reaction mixture revealed it to be very clean, with **1-In** the only corrole species evidenced. Note that this is without the deliberate addition of any chloride containing species, and the product was only observed as a monoanion. However, any attempts to perform further experiments with the compound, or even to store it for a period of time, showed it to decompose back to **1** and an unidentified indium salt (likely $\text{In}(\text{OH})_3$).

¹H NMR Data^[8, 11, 15, 16]

1 (CDCl₃) - δ = 9.10 (doublet, J = 4.4 Hz, 2H), 8.75 (doublet, J = 4.4 Hz, 2H), 8.57 (doublet, J = 4.4 Hz, 4H), -2.25 (broad singlet, 3H).

2 (CD₃OD) - δ = 9.68 (broad singlet, 1H), 9.14 (doublet, J = 4.8 Hz, 1H), 8.98 (doublet, J = 4.8 Hz, 1H), 8.90 (broad singlet, 1H), 8.86 (doublet, J = 4.8 Hz, 1H), 8.84 (doublet, J = 4.8 Hz, 1H).

Cl-2 (CDCl₃) - δ = 9.44 (singlet, 1H), 8.95 (singlet, 1H), 8.60 (doublet, J = 5.0 Hz, 1H), 8.50 (doublet, J = 5.0 Hz, 1H), 8.41 (doublet, J = 5.0 Hz, 1H), 8.18 (doublet, J = 5.0 Hz, 1H).

1-Ga (C₆D₆) - δ = 9.20 (doublet, J = 4.1 Hz, 2H), 8.88 (doublet, J = 4.4 Hz, 2H), 8.74 (doublet, J = 4.0 Hz, 2H), 8.66 (doublet, J = 4.6 Hz, 2H), 4.89 (triplet, J = 7.9 Hz, 1H), 4.32 (unresolved triplet, 2H), 2.84 (unresolved doublet, 2H).

2-Ga (CD₃OD) - δ = 9.77 (singlet, 1H), 8.77 (singlet, 1H), 8.70 (doublet, J = 4.8 Hz, 1H), 8.57 (doublet, J = 4.8 Hz, 1H), 8.48 (triplet, J = 4.3 Hz, 2H), 8.27 (broad singlet, 2H), 7.71 (unresolved triplet, 1H), 7.30 (broad singlet, 2H).

1-Sn (CDCl₃) - δ = 9.4 (doublet, J = 4.3 Hz, 2H), 9.0 (doublet, J = 4.9 Hz, 2H), 8.9 (multiplet, 4H).

2-Sn (CD₃OD) - δ = 10.04 (s, 1H), 9.04 (doublet, J = 4.8 Hz, 1H), 8.96 (singlet, 1H), 8.94 (doublet, J = 5.2 Hz, 1H), 8.84 (doublet, J = 4.3 Hz, 2H).

Mass Spectral Data

The mass spectrum for **2-Ga** was obtained from MALDI-TOF experiments. Other mass spectra were obtained by electrospray ionization. Species represented by each peak are given, where M is the parent molecule as shown in schemes 2.3 and 2.4. Percentages given are relative peak intensities. See figures 2.6-2.11 for actual versus predicted spectra.

1 – $m/z = 797.1 [M+H]^+$, $795.1 [M-H]^-$

2 – $m/z = 954.8 [M-H]^-$

1-Ga – $m/z = 941.7 [M+H]^+$

2-Ga – $m/z = 1021.9 [M-C_5H_5N]^+$

1-Sn – $m/z = 913.1 [M-Cl]^-$ (23.6%), $1001.0 [M+3(H_2O)-H]^-$ (100.0%)

2-Sn – $m/z = 1026.9 [M-OH+Cl-SO_3H]^-$ (100.0%), $1106.8 [M-OH+Cl-H]^-$ (60.8%)

2-Mn – $m/z = 1006.8 [M-H]^-$ (35.4%), $1029.0 [M-2H+Na]^-$ (100.0%)

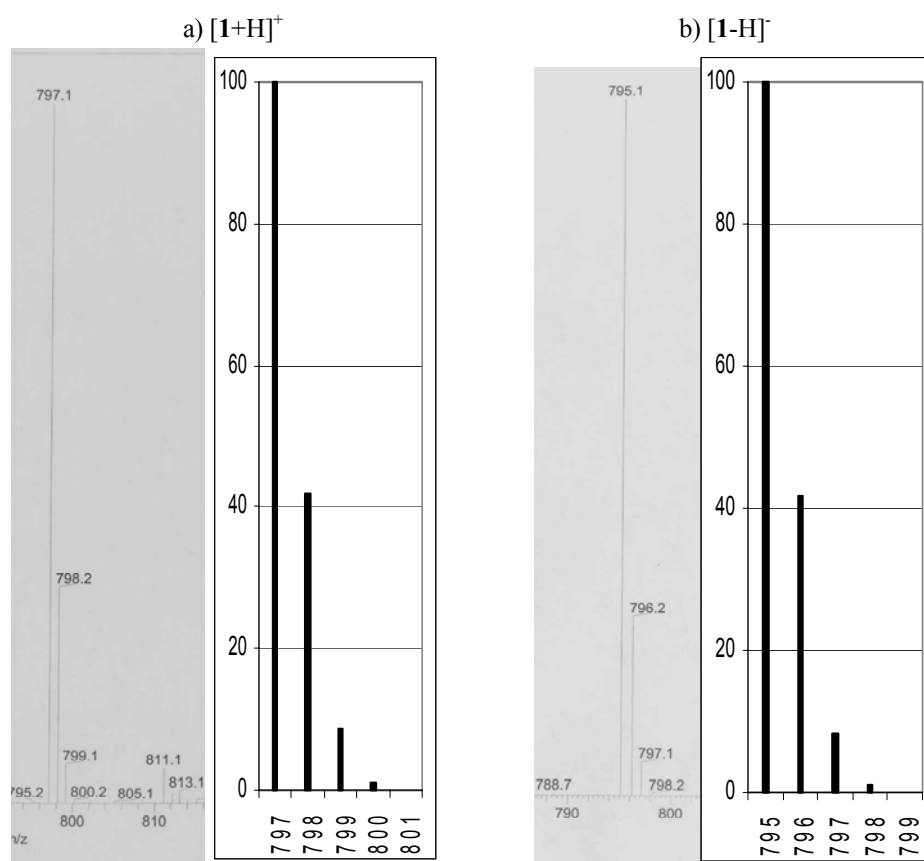


Figure 2.6. Actual (left) versus predicted (right) mass spectra for a) $[1+H]^+$ and b) $[1-H]^-$.

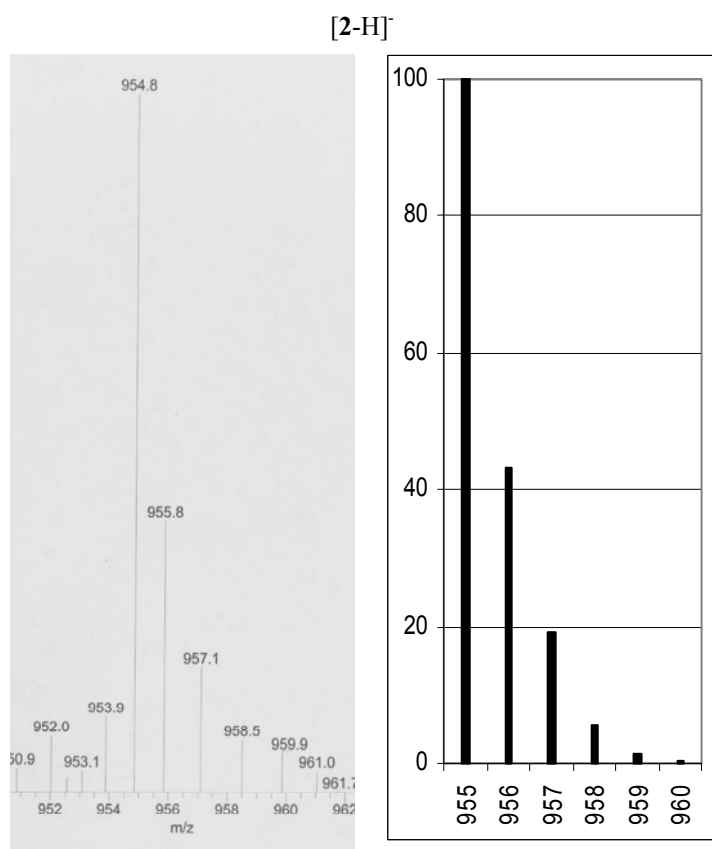


Figure 2.7. Actual (left) versus predicted (right) mass spectra for [2-H]⁻.

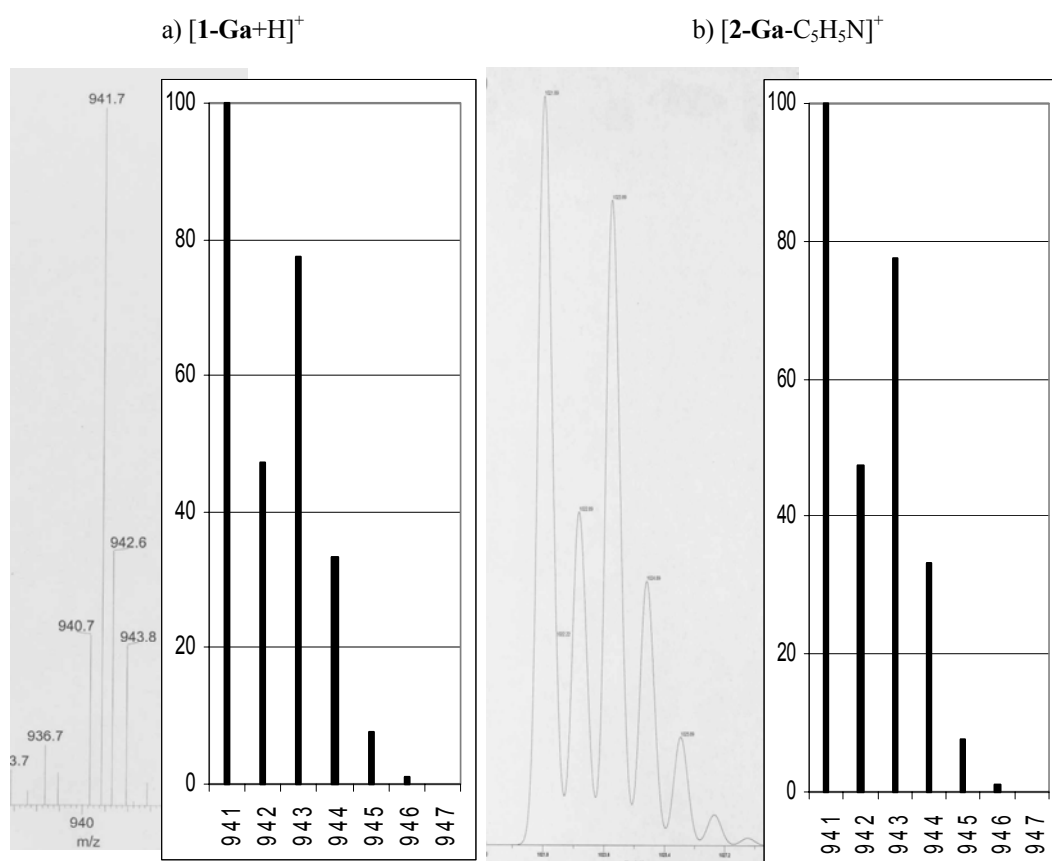


Figure 2.8. Actual (left) versus predicted (right) mass spectra for a) $[1\text{-Ga+H}]^+$ and b) $[2\text{-Ga-C}_5\text{H}_5\text{N}]^+$.

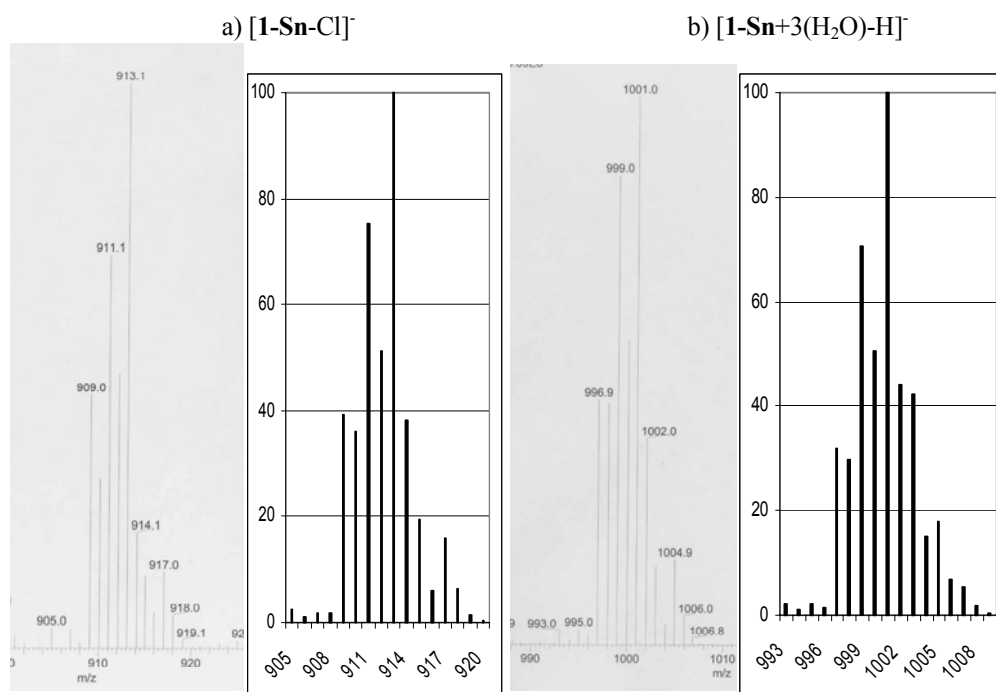


Figure 2.9. Actual (left) versus predicted (right) mass spectra for a) $[1\text{-Sn-Cl}]^-$ and b) $[1\text{-Sn}+3(\text{H}_2\text{O})\text{-H}]^-$.

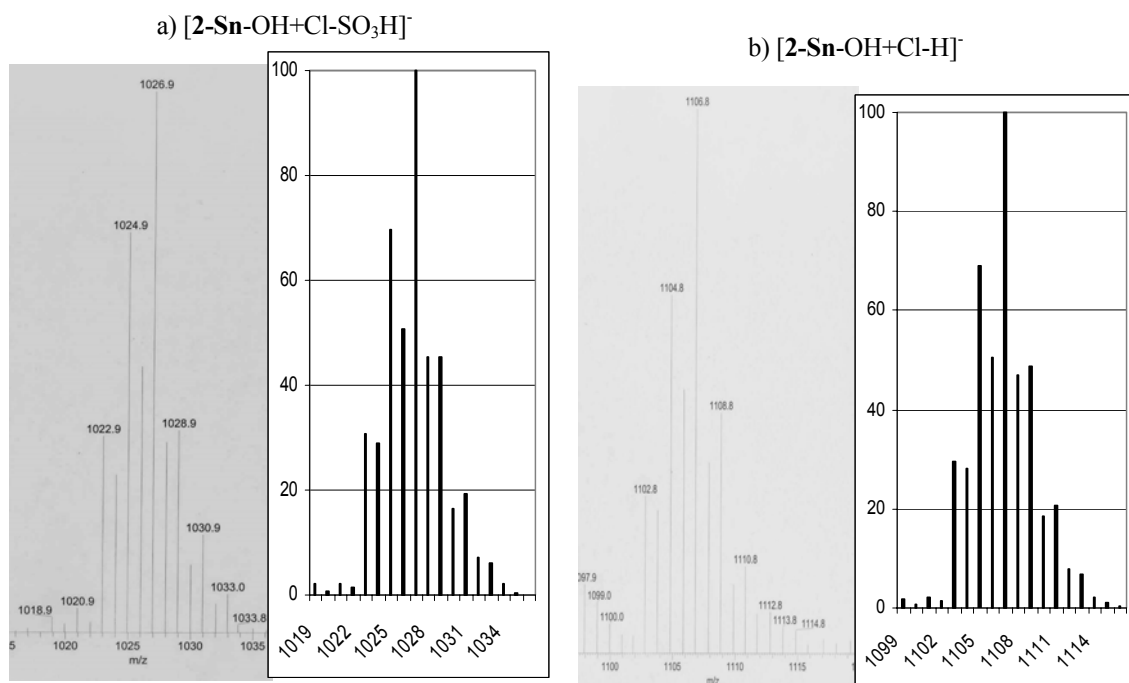


Figure 2.10. Actual (left) versus predicted (right) mass spectra for a) $[2\text{-Sn-OH+Cl-SO}_3\text{H}]^-$ and b) $[2\text{-Sn-OH+Cl-H}]^-$.

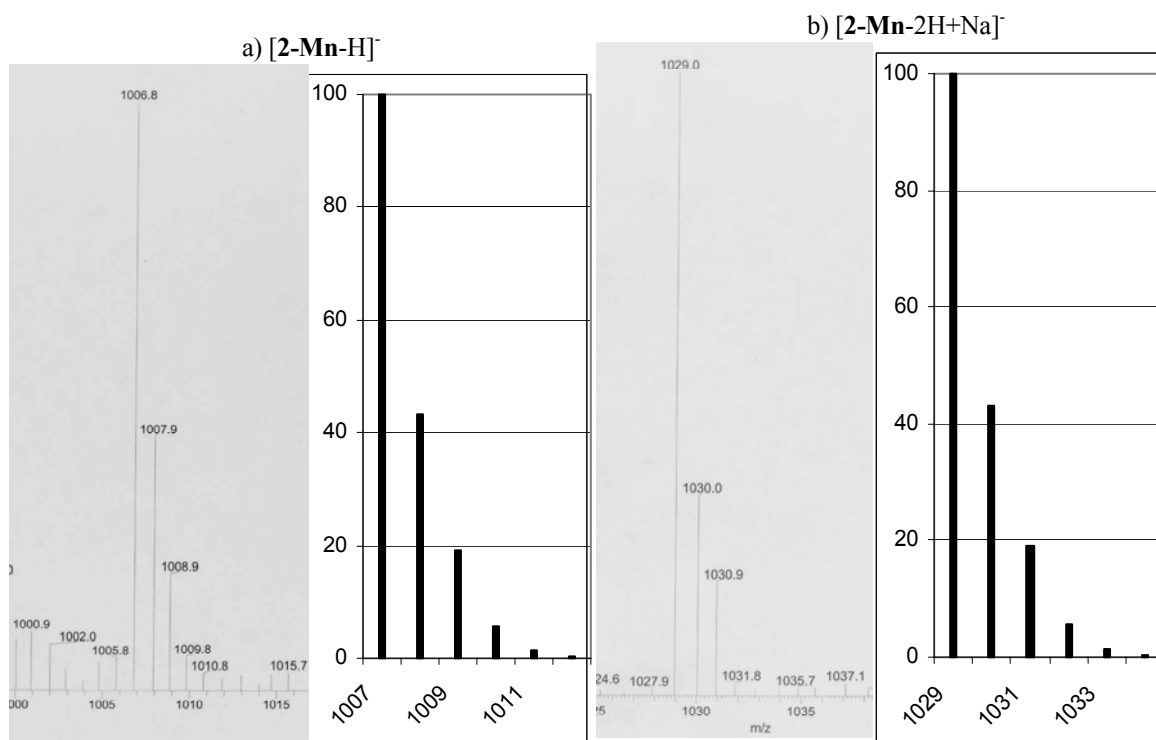


Figure 2.11. Actual (left) versus predicted (right) mass spectra for a) $[2\text{-Mn-H}]^-$ and b) $[2\text{-Mn-2H+Na}]^-$.

ELECTRONIC STRUCTURES AND ABSORPTION SPECTRA

Gouterman Four-Orbital Model

Martin Gouterman first proposed the four-orbital model in the 1960s to explain the absorption spectra of porphyrins^[17, 18]. According to this theory, the absorption bands in porphyrin systems arise from transitions between two HOMOs and two LUMOs, and it is the identities of the metal center and the substituents on the ring that affect the relative energies of these transitions. The HOMOs were calculated to be an a_{1u} and an a_{2u} orbital, while the LUMOs were calculated to be a degenerate set of e_g orbitals (see figure 3.1). Transitions between these orbitals gave rise to two excited states, both of 1E_u character. Orbital mixing splits these two states in energy, creating a higher energy 1E_u state with greater oscillator strength, giving rise to the Soret band, and a lower energy 1E_u state with less oscillator strength, giving rise to the Q-bands.

Corrole Four-Orbital Model

Work first by Hush and co-workers^[19], and later more quantitatively by Ghosh and co-workers^[20], has shown that this four-orbital model also holds for corrole systems. However, the quantitative treatment is not necessary for a basic understanding of the corrole four-orbital model. Instead, a qualitative understanding can be achieved by considering what happens to the porphyrin orbitals when the corrole C_{2v} symmetry is

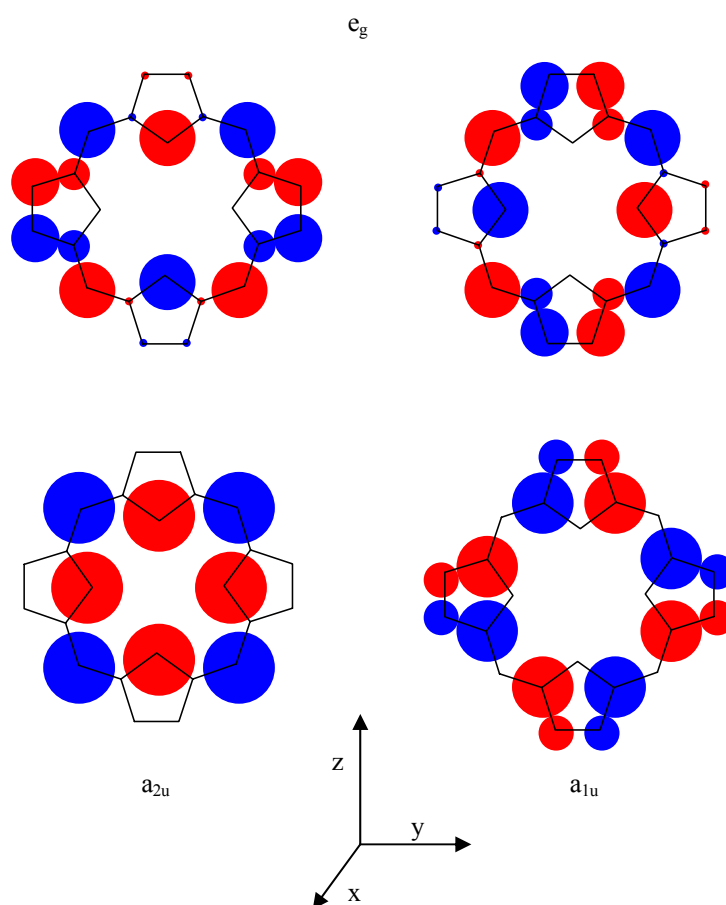


Figure 3.1. Porphyrin HOMOs (bottom row) and LUMOs (top row) (as shown in reference 17). In the corrole C_{2v} symmetry, the e_g orbitals transform as an a_2 and a b_1 ; the a_{2u} transforms as a b_1 ; the a_{1u} transforms as an a_2 orbital.

imposed. The a_{1u} and a_{2u} porphyrin HOMOs become a_2 and b_1 , respectively, and the e_g LUMOs split into another set of a_2 and b_1 orbitals. Transitions between these give rise to four excited states, two 1A_1 and two 1B_2 (see figure 3.2). Again, orbital mixing will split the relative energies of these states as shown in figure 3.2. This mixing will affect the relative oscillator strength of the states as with porphyrins, and the relative intensities of the bands remains unchanged, the Q-bands are still much weaker than the Soret (see table 3.1). As well, the Soret band of corroles would now be expected to split, unless the transitions to these states are accidentally degenerate. However, in the cases of the corroles studied here, the metal complexes show no splitting of the Soret band (not to be confused with the vibronic shoulder seen on this band for the metallocorroles). **1** does show a wider Soret band than in the metallocorrole cases, indicating some unresolved splitting, and in **2** the splitting is observed, though the peaks are not resolved to baseline (see figures 3.3-3.5).

In Ghosh's calculations, he showed that an unsubstituted gallium corrole (that is, with only hydrogens at the eight β and three meso positions) had two nearly degenerate HOMOs and two nearly degenerate LUMOs, and that these frontier orbitals were "well-separated energetically from the rest of the orbital energy spectrum."^[20] As well, his calculations showed that the HOMOs and LUMOs both did indeed consist of one a_2 and one b_1 orbital. In considering the relative energies for the two HOMOs, a crude approximation can be made by comparison to the a_{1u} and a_{2u} HOMOs of a metalloporphyrin. As stated above, theoretical desymmetrization of these orbitals transforms them to a_2 and b_1 , respectively. Thus, like the a_{1u} porphyrin orbital, the a_2 corrole orbital has very little to no amplitude at the meso positions, while the b_1 has large amplitude at these positions, as does the a_{2u} in the

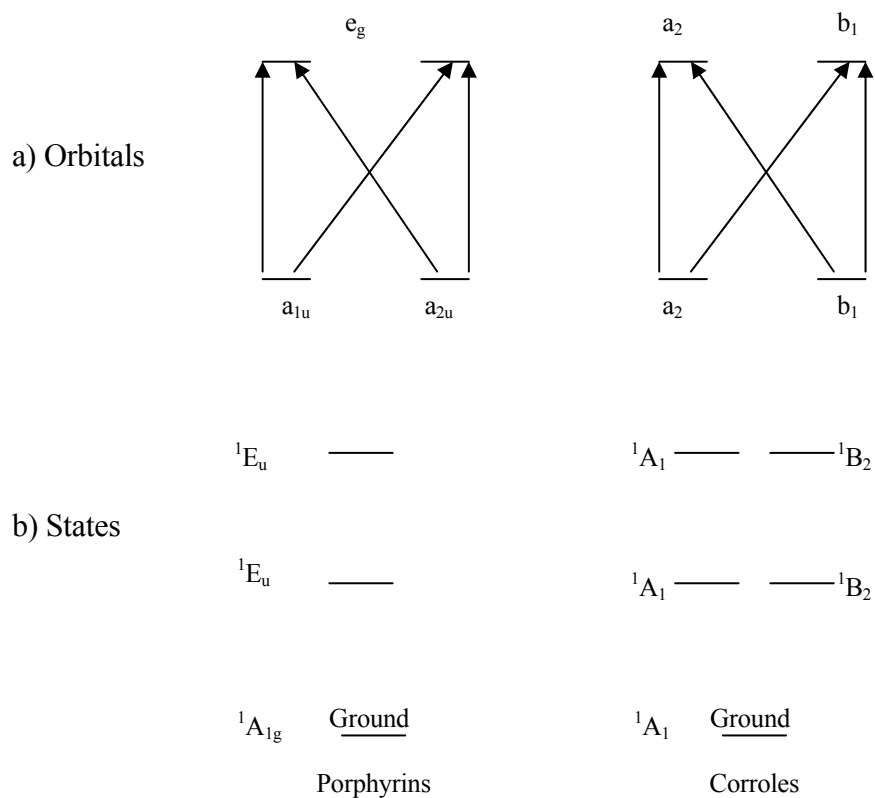


Figure 3.2. a) Orbital diagrams showing possible transitions for porphyrins and corroles. Note that while the HOMOs are shown to be degenerate in both cases, the actual relative energies will depend on the substitution of the rings. b) State diagrams showing possible excited states for porphyrins and corroles. Relative energies for the porphyrin case are taken from reference 17. In the absence of quantitative data for the corrole case, the states are shown as two sets of accidentally degenerate states.

Compound	Soret bands λ [nm] ($\epsilon \times 10^{-3}$ [$M^{-1} \cdot cm^{-1}$])	Q-bands λ [nm] ($\epsilon \times 10^{-3}$ [$M^{-1} \cdot cm^{-1}$])
1 (CH ₂ Cl ₂)	408 (114.0)	560 (17.6), 602 (9.3)
2 (pH 7.0 buffer)	414 (71.0), 430 (62.0)	588 (15.0), 620 (27.0)
1-Ga (CH ₂ Cl ₂)	398 (57.3), 420 (284)	568 (17.1), 594 (23.6)
2-Ga (pH 7.3 buffer)	424 (75.0)	588 (13.6), 610 (17.3)
1-Sn (CH ₂ Cl ₂)	396 (47.0), 416 (215)	566 (15.0), 588 (14.0)
2-Sn (MeOH)	424 (140)	582 (16.0), 602 (18.0)

Table 3.1. Absorption peaks and epsilons for the 6 closed shell corroles.

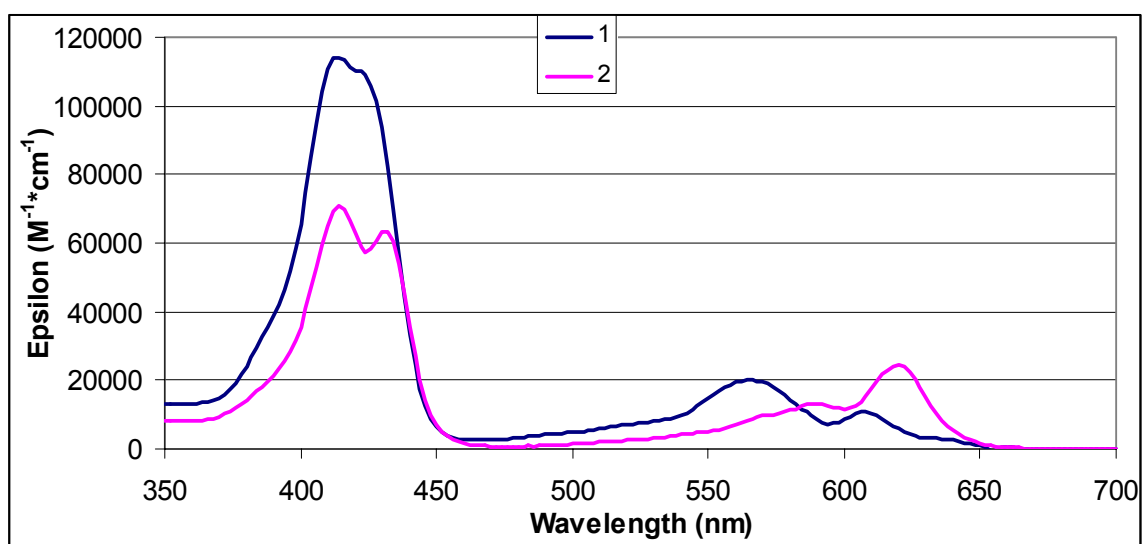


Figure 3.3. Absorption spectra of 1 (blue) and 2 (pink).

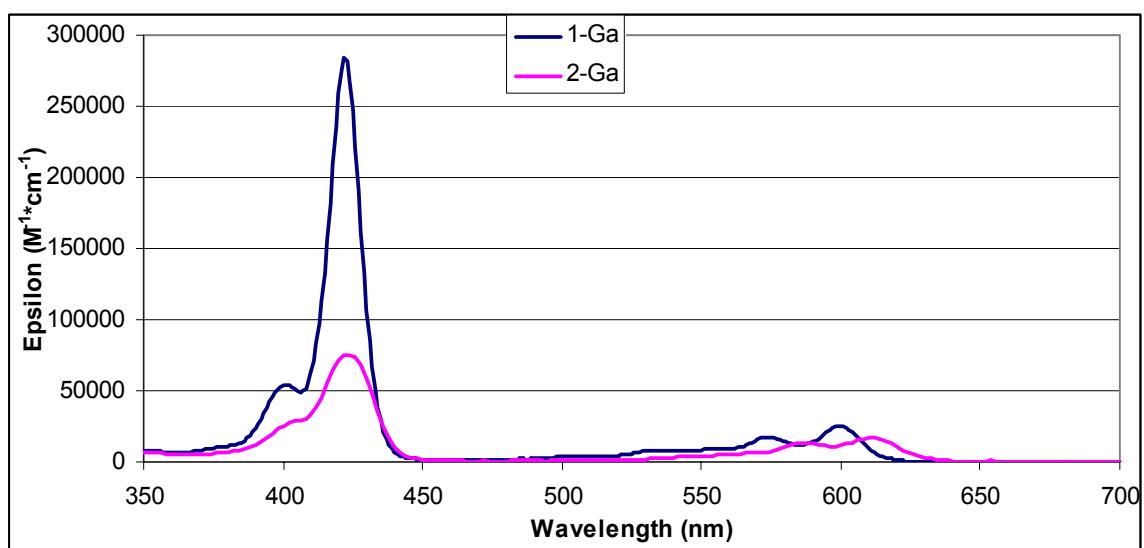


Figure 3.4. Absorption spectra of **1-Ga** (blue) and **2-Ga** (pink).

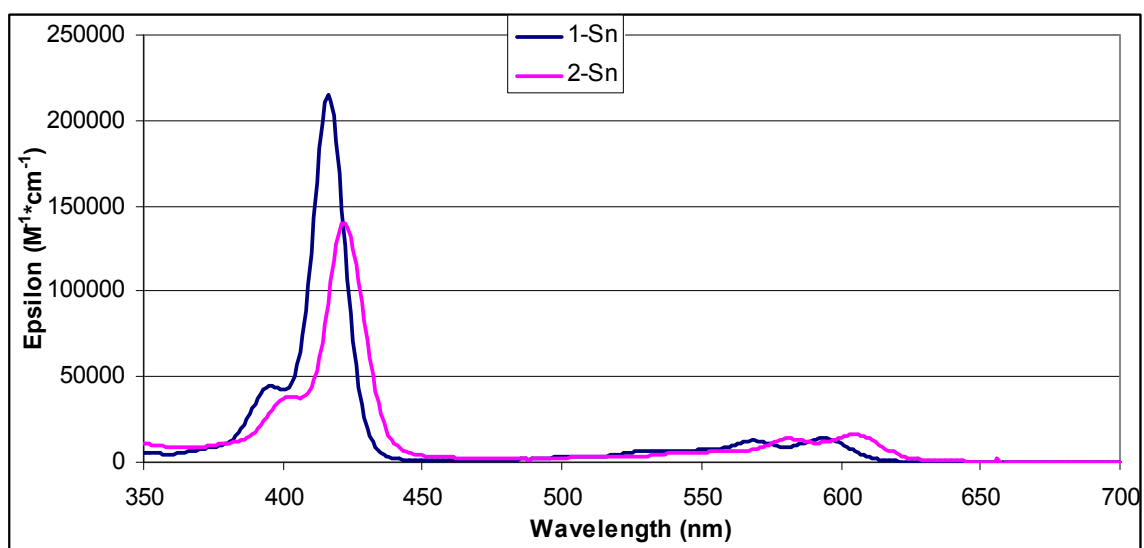


Figure 3.5. Absorption spectra of **1-Sn** (blue) and **2-Sn** (pink).

porphyrin case. Therefore, in the cases of the corroles used in this study, with very electron withdrawing pentafluorophenyl groups in the meso positions, the b_1 orbital should be stabilized (lowered in energy), making the a_2 orbital the higher of the two HOMOs when the degeneracy is broken. However, it has been shown with porphyrins that the main effect of a metal in the system is conjugation of its p_π orbital with the π electrons of the ring, and because of the nodal properties of the HOMOs, the metal can only interact with the a_{2u} orbital^[17], or the b_1 corrole orbital. A more electropositive metal will raise the energy of this orbital and can be evidenced by a red-shifting of the visible bands of the spectrum. Therefore the relative energies of the two HOMOs in a porphyrin or corrole will depend on the combination of these two factors.

These assumptions can be shown to hold by consideration of the absorption spectra of the free-bases, gallium, and tin complexes used in this study. Consider first the gallium versus tin species. In both the sulfonated and non-sulfonated cases, the bands of the gallium corrole are red-shifted with respect to those of the tin corroles. The ionization potential of the gallium(III) ion is 64 eV, and the ionization potential of tin(IV) is 72.28 eV^[21]. Thus, gallium(III) has a lower electron affinity and is expected to be more electropositive, and the red-shift of the absorption bands is as expected.

The effect of β substituents on the corrole ring is harder to predict qualitatively. However, if the HOMOs and LUMOs of the corrole do resemble their porphyrin counterparts, the b_1 HOMO should have little to no electron density on the β carbons, the a_2 HOMO should have electron density clouds with large lobes on the α carbons and smaller lobes on the β

carbons, and the LUMOs should have clouds with small lobes on the α carbons and large lobes on the β carbons. Thus a β substituent should not interact with the b_1 orbital, but should have some interaction with the a_2 orbital, and a larger interaction with the LUMOs. Therefore, to a first approximation, an electron withdrawing group, such as the sulfonyl groups used here, would be expected to stabilize the LUMOs more than the HOMOs, lowering the gap and producing an overall red-shift in the spectrum. The fact that this is indeed what is observed when comparing each non-sulfonated corrole to its sulfonated counterpart would give some credence to this theory. However, care must be taken in ascribing the absorption shifts to this effect. The relative energetics with regard to the β substituents on a corrole are delicately balanced, and the specific mechanisms producing the shifts are not fully understood.

Conclusions

Comparisons between corrole spectra and porphyrin spectra would seem to indicate that the Gouterman four-orbital model widely used to explain porphyrin absorption should be valid for corrole absorption as well. By imposing the symmetry restrictions of a corrole on the frontier orbitals of porphyrins, the model can be adapted for corroles, and it is seen that it does indeed describe the electronic spectra very well. Even under the reduced symmetry of corroles, the transitions between excited states show the same mixing effects as porphyrins, providing relatively high intensity Soret bands at lower wavelengths, and relatively low intensity Q-bands at higher wavelengths. Interestingly, while the Soret bands are no longer

required to be degenerate, only the free-base complexes show any evidence of splitting of these bands.

As well, by applying the corrole symmetry to the porphyrin orbitals, correlations can be made regarding the electronic nature of the corrole HOMOs and LUMOs, allowing first order predictions as to the effects of meso and β substituents, and the effect of the metal ion in metallocorroles. These predicted effects can be seen in the absorption spectra of the corroles, further validating the use of the four-orbital model for these systems.

Chapter 4

PHOTOPHYSICS

One only has to attempt the synthesis of **1** to truly appreciate the fluorescence properties of the molecule. On a column that is completely black with products, a single band shines brightly under long-wavelength UV light, identifying the corrole. A question that immediately comes to mind when observing this concerns the quantification of these properties.

Work on photophysics focused mainly on the excited singlet state of the corroles, though some work on characterization of the excited triplet state will be presented at the end of this chapter.

Singlet Emission and the Four-Orbital Model

Looking first at the metallocorrole complexes, the effects predicted by the four-orbital model can again be seen (see table 4.1). The fluorescence of the complexes with the more electropositive gallium(III) show a red-shift in comparison to their counterparts with the less electropositive tin(IV) centers. And, as with the absorption spectra, a red-shift is also seen when keeping the metal identity the same and changing the identity of the β substituents from hydrogen to sulfonate groups (see figures 4.1, 4.2). It can also be seen that each of the corrole emission spectra has a vibronic band $1300\text{-}1400\text{ cm}^{-1}$ to the red of each peak.

Compound	Emission Peak (nm)
1	648
2 (pH 7)	632
2 (pH 2)	628, 664
1-Ga	607
2-Ga	629
1-Sn	605
2-Sn	615

Table 4.1. Peak positions for singlet emission of the corroles used in this study.

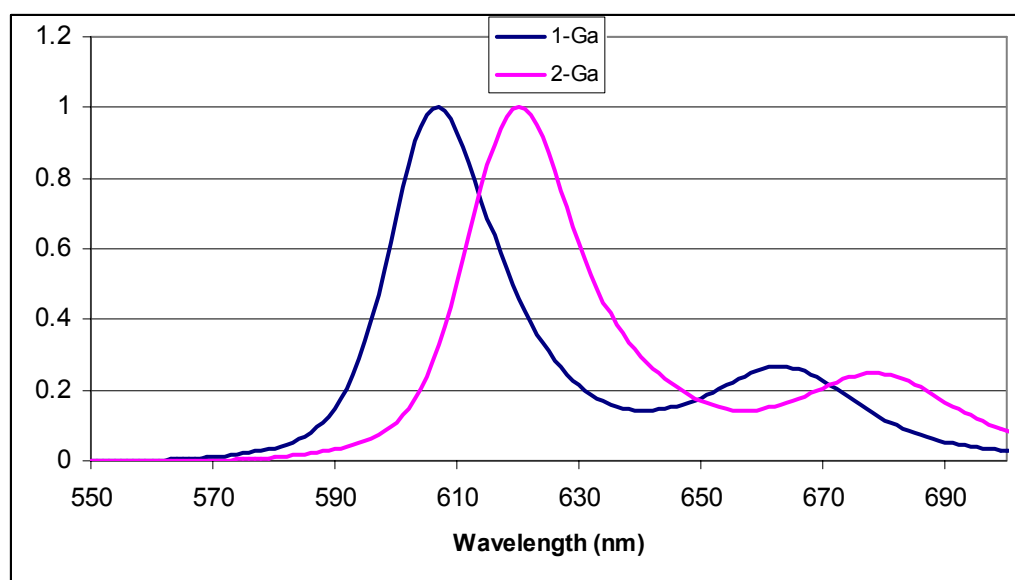


Figure 4.1. Singlet emission spectra for **1-Ga** (blue, in toluene) and **2-Ga** (pink, in pH 7.0 buffer). Peak intensity is normalized to 1 (arbitrary units).

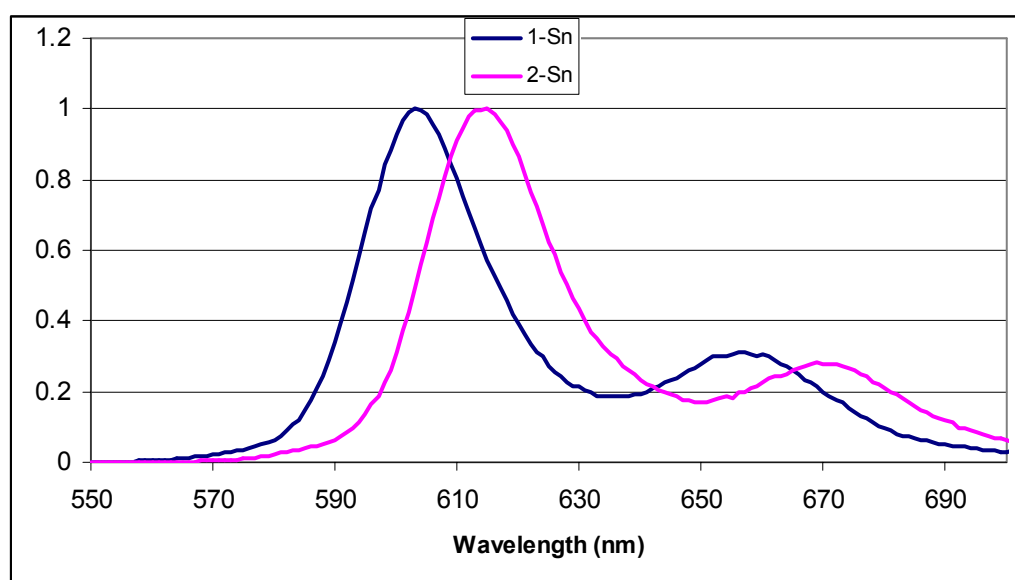


Figure 4.2. Singlet emission spectra for **1-Sn** (blue, in toluene) and **2-Sn** (pink, in pH 7.0 buffer). Peak intensity is normalized to 1 (arbitrary units).

On first glance, it would appear that the situation is very different for the two metal-free corroles (see figure 4.3). In this pair, it is the emission of the nonsulfonated corrole that is significantly red-shifted in comparison to the sulfonated. While this could appear to be a demonstration of the unpredictable effects of β substitution, closer inspection reveals the difference lies in the nature of the emitting species. While all the other corroles studied here show a 10-20 nm difference between the emission peak and the lowest energy Q-band peak, the difference in **1** is 46 nm. This difference can be explained by the protonation state of the molecule. The spectrum of **2** was measured in pH 7.0 buffer. However, as seen in chapter 2, at this pH one of the core protons of **2** has been lost, reducing the steric strain on the molecule, and this spectrum is really the singlet emission of $\mathbf{2}^-$. Note that the spectrum of **1** was measured in toluene, which would not give it the same opportunity for deprotonation as **2**. Thus, to gauge the effect of the sulfonate groups for these molecules, a comparison must be made between **1** and **2** at an intermediate pH where **2** will be core neutral, such as pH 3.8 (see figure 4.4). From these spectra, it can be easily seen that the effect of the sulfonate groups does indeed hold for the free-base corroles, and a red-shift is observed between like species. It is also expected that if **1** were to be deprotonated to $\mathbf{1}^-$, the fluorescence spectrum would blue-shift 25-35 nm.

An interesting effect is seen upon further protonation of **2**, as seen in figure 4.5. The emission spectrum for $\mathbf{2}^+$ shows a peak slightly blue-shifted compared to the peak of $\mathbf{2}^-$. If steric distortion is responsible for the large red-shift observed in going from $\mathbf{2}^-$ to **2**, these data would suggest that the distortion is counterbalanced when a fourth proton is added to the corrole macrocycle. This can be explained by the fourth proton adding to the opposite

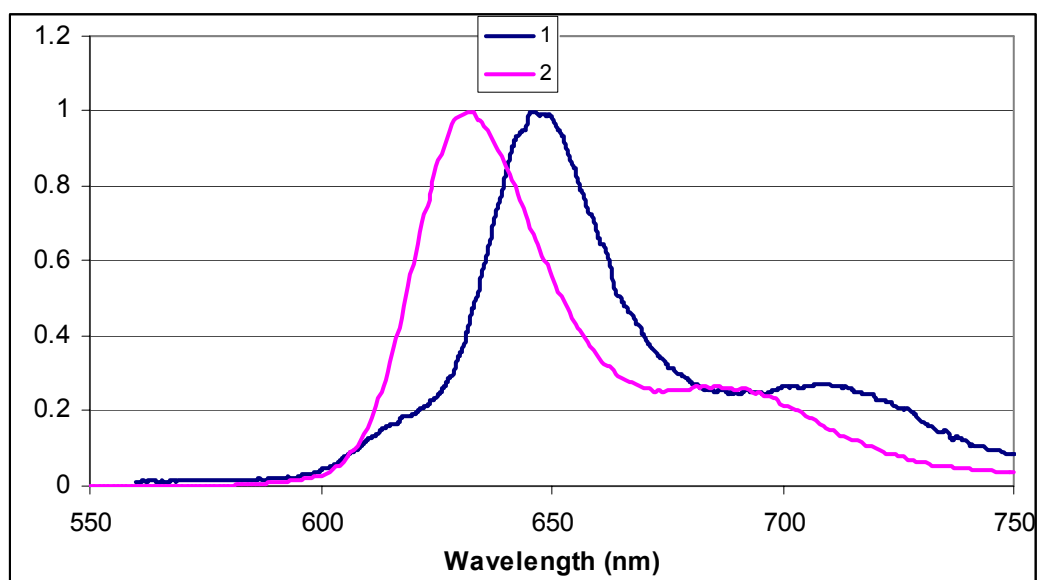


Figure 4.3. Singlet emission spectra for **1** (blue, in toluene) and **2** (pink, in pH 7.0 buffer). Peak intensity is normalized to 1 (arbitrary units).

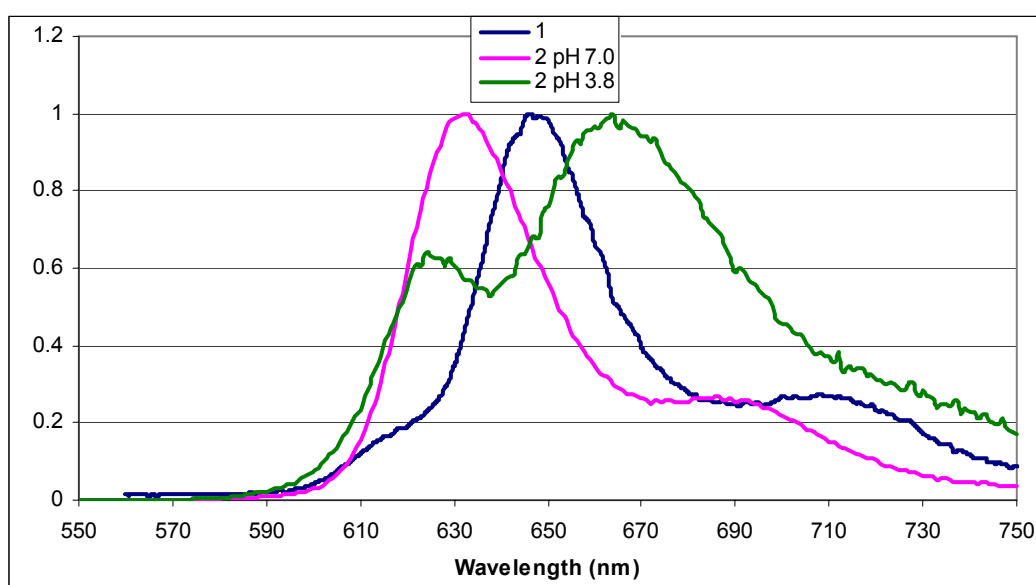


Figure 4.4. Singlet emission spectra of **1** (blue, in toluene), **2⁻** (pink, in pH 7.0 buffer), and **2** (green, in pH 3.8 buffer). Peak intensities have been normalized to 1 (arbitrary units).

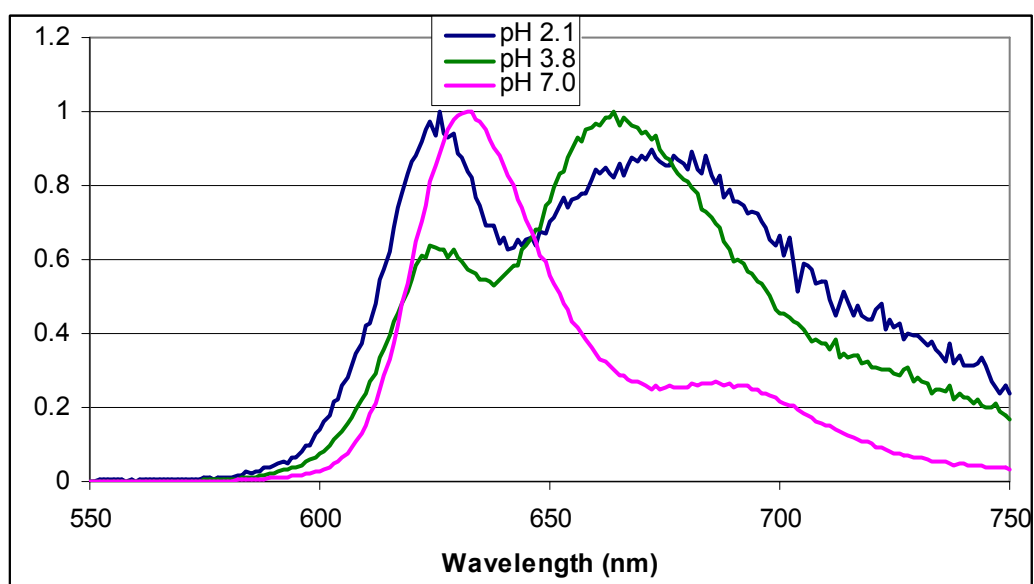


Figure 4.5. Emission spectra of 2^- (pink, in pH 7.0 buffer), 2 (green, in pH 3.8 buffer), and 2^+ (blue, in pH 2.1 buffer). Peak intensities have been normalized to 1 (arbitrary units). Note there is some contamination of 2^+ in the spectrum of 2 and vice versa.

side of the corrole than the previous proton, forcing the macrocycle to distort back toward planarity. An idealized case is shown in figure 4.6. It is important to note that while the pyrrole rings in the figure are all shown as being perfectly planar, this is not likely to be the case. However, the rings are likely closer to being in the mean plane of the four nitrogens of **2**⁺ than in the case of **2**.

Singlet Lifetimes

This part of the project also investigated lifetimes of corrole singlet excited states by monitoring emission with a picosecond laser and streak camera set up. The data for **1** are shown in figure 4.7, along with the lifetime fit. As seen in the figure, the lifetime of **1** can be calculated to be 5 nanoseconds. The figure also illustrates a problem encountered in the measurement of these lifetimes, namely multiple decay times. The data for **1** show ~25% decaying with a lifetime of 1 nanosecond. It is thought that this is due to oxygen quenching. While care was taken to degas the solution (three freeze-pump-thaw cycles), the lifetimes (and as will be seen shortly, the quantum yields) show great sensitivity to the presence of any oxygen. While this makes absolute determination of the lifetimes difficult, they can still be estimated, albeit with proportionally large error bars. All six of the fluorescent corroles tested herein were found to have singlet lifetimes of 5 ± 3 ns.

Singlet Quantum Yields

The final characterization of the singlet excited state was measurement of the quantum yields. Much like the lifetimes, the quantum yield measurements suffered from

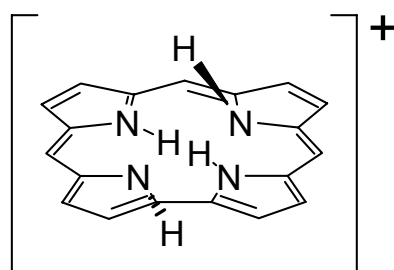


Figure 4.6. An idealized planar structure of 2^+ . Note that while the pyrrole rings are shown as being in the mean plane of the four nitrogens, this is not likely to be the actual case. See text for further discussion.

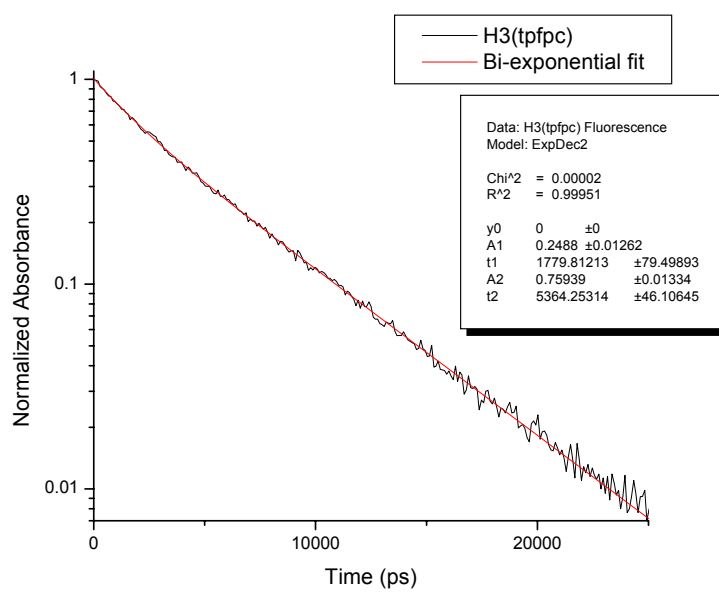


Figure 4.7. Fluorescence emission decay (black) and fit (red) for **1**.

reproducibility problems. Through variations in the concentration of the solutions used, the standard used, and the methods used to prepare the solutions, yields varying by a full order of magnitude were obtained. Reported here are best values based on a number of experiments on degassed solutions in which care was taken to avoid aggregation effects, and with a standard that has been very well studied in the group, ruthenium trisbipyridine.

The general set-up used for measuring quantum yields involved the preparation of solutions of the compounds at low concentrations. For the particular fluorimeter used for these experiments, overall absorbance at the excitation wavelength needed to be below 0.1 absorbance units to ensure linearity of response. In general, the solutions used herein were kept at absorbances below 0.05 units. A solution containing ruthenium trisbipyridine was also made to the same specifications. All solutions were made to have approximately the same absorbance at the excitation wavelength for a given set of experiments. The solutions were degassed by three freeze-pump-thaw cycles in atmosphere controlled cuvettes, and the emission spectra were measured. The quantum yields were then calculated from the following equations^[22]:

$$\Phi_f = \Phi_{ref} \left(\frac{n^2}{n_{ref}^2} \right) \left(\frac{\int F(\nu) d\nu}{A} \right) \left(\frac{A_{ref}}{\int F_{ref}(\nu) d\nu} \right) \quad (\text{eq. 4.1})$$

$$F(\nu) = F(\lambda)\lambda^2 \quad (\text{eq. 4.2})$$

In eq. 4.1, Φ is the quantum yield (0.042 for Ru(bpy)₃), n is the refractive index of the solvent, $\int F(\nu)d\nu$ is the area under the curve of fluorescence intensity vs. wavenumber, and

A is the absorbance at the excitation wavelength (430 nm for these experiments). Unsubscripted quantities are those of the sample; quantities subscripted “ref” are for the reference solution. Since the fluorescence spectra were measured versus wavelength, equation 4.2 was used to convert the intensities to a function of wavenumber. Due to the various solubilities of the corroles, no one solvent could be used for all six, so several solvents were used. Table 4.2 presents the average results from these experiments. Given the spread of values obtained, the errors in these numbers are estimated to be $\pm 15\%$.

As can be seen in the table, the free-base and gallium corroles all possess quantum yields of 10% or higher, while the tin complexes are roughly an order of magnitude lower, as expected, given that the heavy atom effect should come into play for the tin corroles, promoting intersystem crossing to the triplet state.

Triplet States

An attempt was also made to detect the presence of this triplet state for four metallocorroles through the use of transient absorbance, thereby giving lifetime information as well. The triplet lifetime of **1** had previously been measured at 870 μs ^[8]. The metallocorrole solutions were observed at 850 nm, beyond the presence of any intensity from fluorescence. In all four cases, a long-lived excited state was observed, and like the singlet observations, the decay was biexponential, with $\sim 80\%$ of the sample decaying with the shorter lifetime. These lifetimes are given in table 4.3. The biexponential nature of the decays again gives evidence of the sensitivity of these compounds to oxygen and concentration effects. While the solutions were made in as low a concentration as feasible

Compound	Φ_f
1	0.10
2 (pH 7.0)	0.18
2 (pH 2.1)	0.03
1-Ga	0.16
2-Ga	0.15
1-Sn	0.01
2-Sn	0.03

Table 4.2. Quantum yields for fluorescence of corroles in this study. **1**, **1-Ga**, **1-Sn** were measured in toluene, **2** in buffer at given pHs, **2-Ga** in methanol, and **2-Sn** in isopropanol. Error is estimated at 15%.

	τ_1 (μs)	τ_2 (ms)
1-Ga	110	0.45
2-Ga	730	2.0
1-Sn	100	1.0
2-Sn	120	1.2

Table 4.3. Excited triplet lifetimes for four metallocorroles.

to still obtain a measurable transient absorbance signal, it is possible that even at this concentration there was some corrole aggregation. No aggregation effects were seen in this concentration range by absorbance, however. Given the previously measured lifetime of **1**, it seems reasonable that the triplet state could decay with the shorter lifetimes measured, as the heavy atom effect would be expected to shorten this value compared to the free-base.

Conclusions

The relative positions of the singlet emission bands of the corroles provide further support for the four-orbital model discussed in chapter 3. As well, it has been seen that the position of the singlet emission bands for the free-bases can be used to determine the protonation state of the molecule, or at the least, give an estimate of the planarity.

While the excited states of these compounds show great sensitivity toward concentration and oxygen, their quantum yields and lifetimes can be estimated. Interestingly, the quantum yields measured for the free-bases and gallium complexes (10 and 18% for the free-bases, 15 and 16% for the gallium corroles) are much higher than their porphyrin counterparts. Tetrakis(pentafluorophenyl)porphyrin has a measured quantum yield of 3.2%^[23], and the zinc complex has a measured quantum yield of 7%^[24]. It is believed that the greater quantum yields for the corroles are properties related to the direct pyrrole-pyrrole linkage, as this structural element makes the macrocycle more rigid, thereby disfavoring relaxation to the ground state through ring bending and stretching. This effect is also manifested in the lifetimes of porphyrins, as evidenced by the much shorter singlet lifetime (<1.0 ns) of zinc tetrakis(pentafluorophenyl)porphyrin^[24].

INTERACTIONS WITH HSA

The data in this chapter concerning **2**, **2-Ga**, and **2-Mn** have been reproduced in part with permission from “Amphiphilic Corroles Bind Tightly to Human Serum Albumin,” Mahammed, A.; Gray, H. B.; Weaver, J. J.; Sorasaene, K.; Gross, Z., *Bioconj. Chem.* **2004**, *15*, 738. Copyright 2004 American Chemical Society. Interactions between HSA and **2-Sn** will be considered after this section.

Introduction

The bioinorganic chemistry of porphyrins is a broad field, ranging from natural to completely synthetic systems. The field also includes work on a large variety of porphyrin-like molecules (porphyrinoids), such as the chlorophyll-related chlorins and bacteriochlorins as well as completely synthetic phthalocyanines and expanded porphyrins^[25, 26]. A great deal of research has been devoted to the interactions of porphyrinoids with biomolecules, owing to their tendency to accumulate in cancer cells and to intercalate DNA^[27, 28]. Surprisingly, although corroles have been known for almost four decades^[29, 30], there has been very little work on their interactions with biological molecules. This situation does not reflect a lack of interest in these tetrapyrrolic macrocycles (they are related to the cobalt-chelating corrin in vitamin B₁₂ by virtue of an identical carbon skeleton and to porphyrins by being fully conjugated), but only because

their syntheses heretofore have been long and tedious. This situation has recently changed in dramatic fashion: facile synthetic methodologies have been introduced during the last 5 years, allowing for the preparation of more than 100 new corroles^[11, 14, 31-39]; transition metal complexes (Cr, Mn, Fe, Rh) of the most extensively investigated derivative (tris(pentafluorophenyl)corrole, **1**) function as versatile catalysts for a variety of organic reactions^[16, 40-43]; and the Ga(III) and Al(III) complexes of corrole **1** are highly fluorescent, with quantum yields (0.37 up to 0.76) that exceed those of all other porphyrinoids^[8, 44]. In addition, it has been discovered recently that electrophilic substitution of **1** offers a facile and highly selective synthetic method for the preparation of corroles with polar head groups located in only one half of the macrocycle (amphiphilic corroles)^[15, 45]. This finding is key for the utilization of corroles in biological systems, since amphiphilic porphyrinoids have been shown to be the molecules of choice for many applications^[46-48].

As the most abundant protein in blood plasma, human serum albumin (HSA) plays a role in many biological processes^[49-51]. Available are high resolution X-ray structures of HSA as well as information about its binding affinities to many natural and synthetic molecules^[52]. However, with the exception of one preliminary report, there are no X-ray structures of HSA conjugates with any porphyrinoid or related macrocyclic molecule^[53]. Accordingly, information about noncovalent binding of porphyrinoids to HSA comes from data acquired by spectroscopic methods^[54]. Selected results from such investigations are set out in table 5.1^[55-64].

No.	Ligand ^a	Binding sites	Association constant, K (M ⁻¹)	Method	Ref.
1	uroporphyrin I	N=1	$(8.8 \pm 0.51) \cdot 10^4$	b	[55]
2	uroporphyrin I	N=1	$2.0 \cdot 10^4$	c	[56]
3	heptacarboxylporphyrin	N=1	$(2.39 \pm 0.16) \cdot 10^5$	b	[55]
4	coproporphyrin I	N=1 another weak site	$(1.61 \pm 0.11) \cdot 10^6$ $(3.1 \pm 0.3) \cdot 10^5$	b b	[55]
5	coproporphyrin I	N=1	$(1.3 \pm 0.11) \cdot 10^5$	d	[56]
6	protoporphyrin IX	N=1	$(9.34 \pm 0.3) \cdot 10^6$	b	[55]
7	protoporphyrin IX	N=1	$0.5 \cdot 10^6$	c	[57]
8	protoporphyrin IX	N=1	$1.3 \cdot 10^6$	c	[56]
9	protoporphyrin IX	N=1	$2.8 \cdot 10^8$	e	[58]
10	hemin	N _{strong} = 1 N _{weak} ≥ 4	$5 \cdot 10^7$ ----	f & c	[59]
11	mesoporphyrin IX		$(2.5 \pm 0.7) \cdot 10^7$	e	[60]
12	Mg-mesoporphyrin IX		$(1.7 \pm 0.5) \cdot 10^7$	e	[59]
13	Al (PcS1)	N _{strong} = 1 N _{weak} = 8	$(4.2 \pm 0.8) \cdot 10^7$ $(3.8 \pm 0.9) \cdot 10^4$	f	[61]
14	Al (PcS2) (opp)	N _{strong} = 1 N _{weak} = 8	$(2.8 \pm 1.1) \cdot 10^7$ $(4.0 \pm 0.7) \cdot 10^4$	f	[61]
15	Al (PcS2) (adj)	N _{strong cooperative site} = 1 N _{weak} = 8	$(5.8 \pm 0.6) \cdot 10^6$ $(2.7 \pm 0.8) \cdot 10^4$	f	[61]
16	Al (PcS3)	N _{strong cooperative site} = 1 N _{weak} = 8	$(2.5 \pm 1.2) \cdot 10^6$ $(2.5 \pm 0.7) \cdot 10^4$	f	[61]
17	Al(PcS4)	nonsaturable	----	f	[61]
18	Al(PcS2)		10^4	f	[62]
19	tpss		$(5.0 \pm 2) \cdot 10^6$ $(0.2 \pm 0.1) \cdot 10^6$	f c	[63]
20	Zn(2,6-Cl, 3SO ₃ H)tp	N= 7	----	f	[64]

a) Abbreviations: PcS1, PcS2, PcS3, PcS4: phthalocyanine with 1, 2, 3, and 4 sulfonato groups, respectively, where opp and adj stand for the relative positions of the sulfonato groups in PcS2 on opposite and adjacent benzopyrrole rings, respectively; tpss: 5,10,15,20-tetrakis(p-sulfonatophenyl)porphyrin; (2,6-

Cl, 3-SO₃H)tp: 5,10,15,20-tetrakis(2,6-dichloro-3-sulfonatophenyl)porphyrin. b) Affinity capillary electrophoresis. c) Fluorescence quenching of HSA by the porphyrinoid. d) Equilibrium dialysis. e) HSA-initiated changes in the fluorescence of the porphyrinoid. f) HSA-initiated changes in the absorbance of the porphyrinoid.

Table 5.1. Association constants of HSA:porphyrinoid conjugates.

In many cases, the conclusions about the number of binding sites and the association constants are based on a limited number of spectroscopic measurements, a likely reason for the significant scattering in published results that is evident from inspection of rows 6-9. Nevertheless, it is clear that only negatively charged porphyrinoids associate with HSA; and, in most cases, the protein has one well-defined high-affinity site and several other lower-affinity sites^[61]. Another important finding is the inverse relationship between the association constants and the number of charged groups. The strongest association to HSA occurs with porphyrinoids that contain only two carboxylato or sulfonato groups located on the pyrrole, benzopyrrole, or phenyl rings. Intriguingly, these dipolar and amphiphilic molecules are also the most active derivatives in photodynamic therapy. A major drawback, however, is that porphyrins or phthalocyanines with a limited (<4) number of polar head groups are not readily accessible, as illustrated by the bis-sulfonated phthalocyanines that are obtained and used as a mixture of at least eight nonseparable isomers, even after separation of derivatives with a different degree of sulfonation^[65].

In sharp contrast to all other synthetic porphyrinoids, the amphiphilic 2,17-bis(sulfonato)-5,10,15(trispentafluorophenyl)corrole (**2**) with its two precisely located sulfonate groups can be obtained in very simple synthetic steps from readily available starting materials^[15, 45]. Accordingly, investigations of the association of **2** and its gallium(III) and manganese(III) complexes (**2-Ga**, and **2-Mn**, respectively) to HSA were performed as a first step toward utilization of corroles in bioinorganic applications. Employing several complementary physical methods, it was found that all three corroles form noncovalent conjugates with HSA. The binding affinities of these conjugates decrease according to $\mathbf{2} \geq$

2-Ga > **2-Mn**. It is apparent that corrole **2** and its metal complexes will be fully bound to HSA under physiological conditions; accordingly, any biological activity observed for these molecules likely will be attributable to their protein conjugates.

Experimental Procedures

Chemicals. Preparations of corrole **2** and its metal complexes are described in chapter 2, and in previous publications^[15, 45]. HSA was purchased from Sigma (essentially fatty acid free, catalogue no. A 1887) and used as received. Throughout these studies, 0.1 M phosphate buffer solutions of pH 7.0 were used. The extinction coefficients of the corroles under these conditions are: **2**: ϵ (414 nm) = 71000 M⁻¹cm⁻¹; **2-Ga**: ϵ (424 nm) = 75000 M⁻¹cm⁻¹; **2-Mn**: ϵ (422) = 21000 M⁻¹cm⁻¹; and for HSA, ϵ (280 nm) = 37400 M⁻¹cm⁻¹. Importantly, perfectly linear plots of O.D. vs. corrole concentration were obtained in the range of 10⁻⁶-10⁻⁴ M, ruling out self-aggregation phenomena at the concentrations that were used in these studies. Further support for this conclusion comes from the practically identical extinction coefficients measured in aqueous and polar organic solvents (CH₃CN, MeOH).

Electronic Spectroscopy. UV-vis absorption measurements were performed on a HP8452A diode array spectrophotometer, using 3 mL of corrole solutions at 2-10 × 10⁻⁵ M and adding either μ L portions of HSA solution or mg amounts of solid HSA.

Emission Spectroscopy. The fluorescence of HSA or the corroles was measured on an AB2 Luminescence Spectrometer. For titration of HSA's fluorescence, μ L portions of

concentrated corrole solutions were added to 3 mL solutions of HSA wherein the absorbance at the excitation wavelength of 280 nm was less than 0.15. For titration of **2** or **2-Ga**, either μL portions of a concentrated HSA solution or mg amounts of solid HSA were added to 3 mL solutions of the corroles until no further changes in the emission intensity occurred.

Circular Dichroism Spectroscopy. CD spectra were recorded in the visible range on an Aviv model 62A DS Circular Dichroism Spectrometer using 3 mL of corrole solutions at 2×10^{-5} M and adding either μL portions of concentrated HSA solution or mg amounts of solid HSA. UV-CD spectra were recorded using an HSA concentration of 1.8×10^{-6} M (in a 4-mm cuvette) and 3.7×10^{-6} M (in a 10-mm cuvette) with varying ratios of **2-Ga**.

Results and Discussion

Binding of Corroles to HSA. Electronic spectra of corroles when treated with increasing amounts of HSA are shown in figure 5.1. For **2** and **2-Ga**, respective shifts of the Soret bands from 416 to 424 nm and from 424 to 430 nm are observed. For metal-free **2**, this effect could indicate changes in the protonation state of the inner N_4 core from triply- to doubly-protonated. The pK_a for this process has been determined to be 5.2 in water^[66], and it might be quite different in a more hydrophobic environment. However, this explanation is not believed to be correct: the changes in the Q-bands upon titration with HSA are very different from those observed upon NH-deprotonation of **2** in aqueous solutions^[66], so the results are likely attributable to a "solvent effect" that would manifest itself in the interior of the protein. The same interpretation also accounts for the Soret shift of **2-Ga**. Spectral

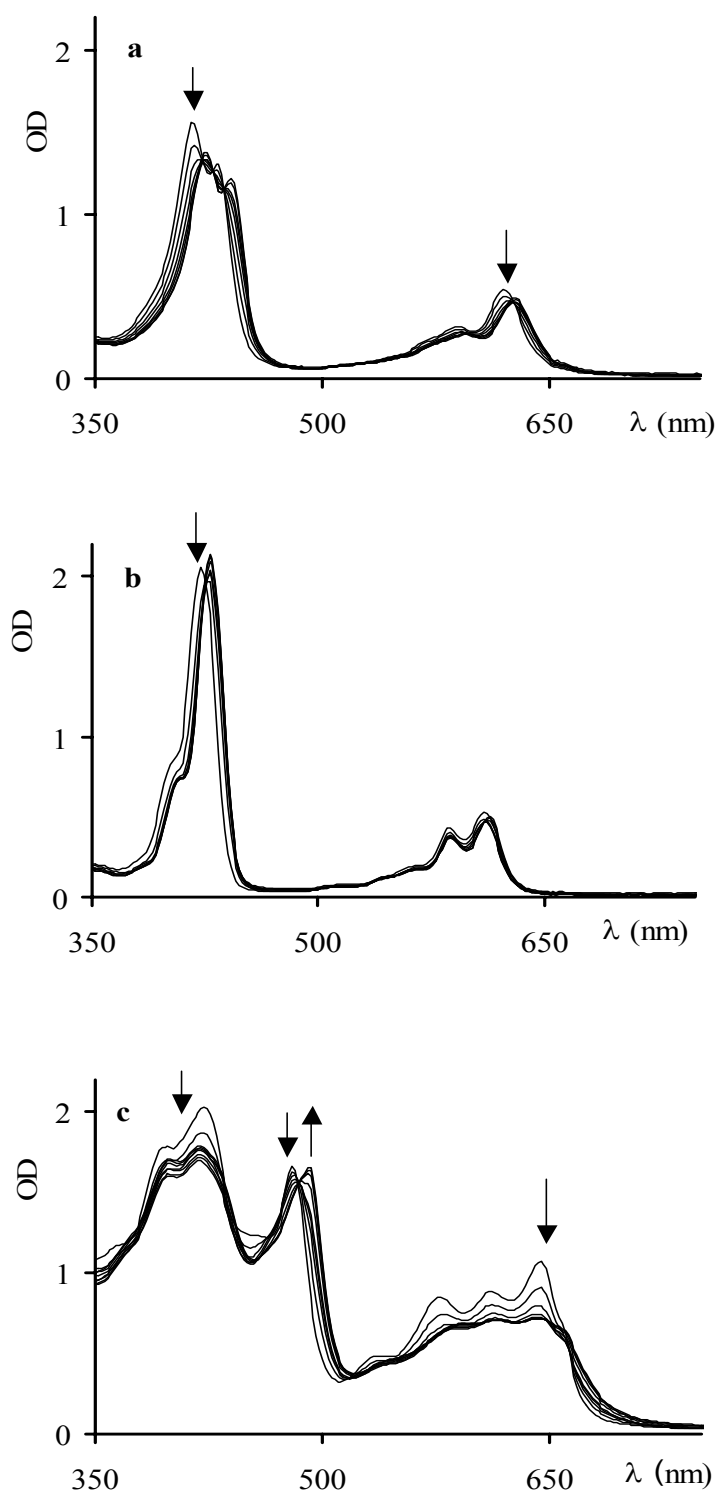


Figure 5.1. Changes in the UV-vis spectra of (a) corrole **2** and its metal complexes (b) **2-Ga**, and (c) **2-Mn**, upon titration with increasing amounts of HSA. $[2] = 2.2 \times 10^{-5}$ M, $[2\text{-Ga}] = 2.7 \times 10^{-5}$ M, $[2\text{-Mn}] = 10^{-4}$ M; $[\text{HSA}] = 0\text{-}10^{-4}$ M.

changes for **2-Mn** were most pronounced: most bands just decreased in intensity, but the 480 nm band was clearly replaced by a 492 nm band. It is known that this particular band (No. V in manganese(III) porphyrins) is very sensitive to axial ligation. Adding imidazole to an aqueous solution of **2-Mn** gave almost the same spectrum as addition of HSA, suggesting the participation of histidine residues in the binding of this metal complex.

In all three cases, there were no more spectral changes after the addition of about 1 equivalent of HSA, suggesting very strong association. More detailed information was obtained by following the intensity changes at selected wavelengths (figure 5.2). The majority of the intensity increase at 438 and 428 nm for **2** and **2-Ga**, respectively, is complete much before a 1:1 ratio is achieved, suggesting that there are multiple HSA binding sites for these corroles. This phenomenon is even more pronounced for **2-Mn**: the intensity at 422 nm decreases sharply up to a [HSA]:[**2-Mn**] ratio of 0.04 and increases slightly when a 1:1 ratio is approached. Taken together, the results clearly indicate that several corrole molecules associate with one protein and that redistribution takes place at higher [HSA]:[corrole] ratios in favor of the 1:1 conjugate. As the number of binding sites in protein-chromophore conjugates and the corresponding binding constants are frequently determined from Scatchard plots^[67], this was also attempted with this system. However, this method and the underlying equations require the presence of unbound chromophore, while later indications show that there is no free corrole at the lowest concentrations that can be measured by UV-vis (10^{-6} M). Accordingly, none of the binding constants can be determined by UV-vis titrations.

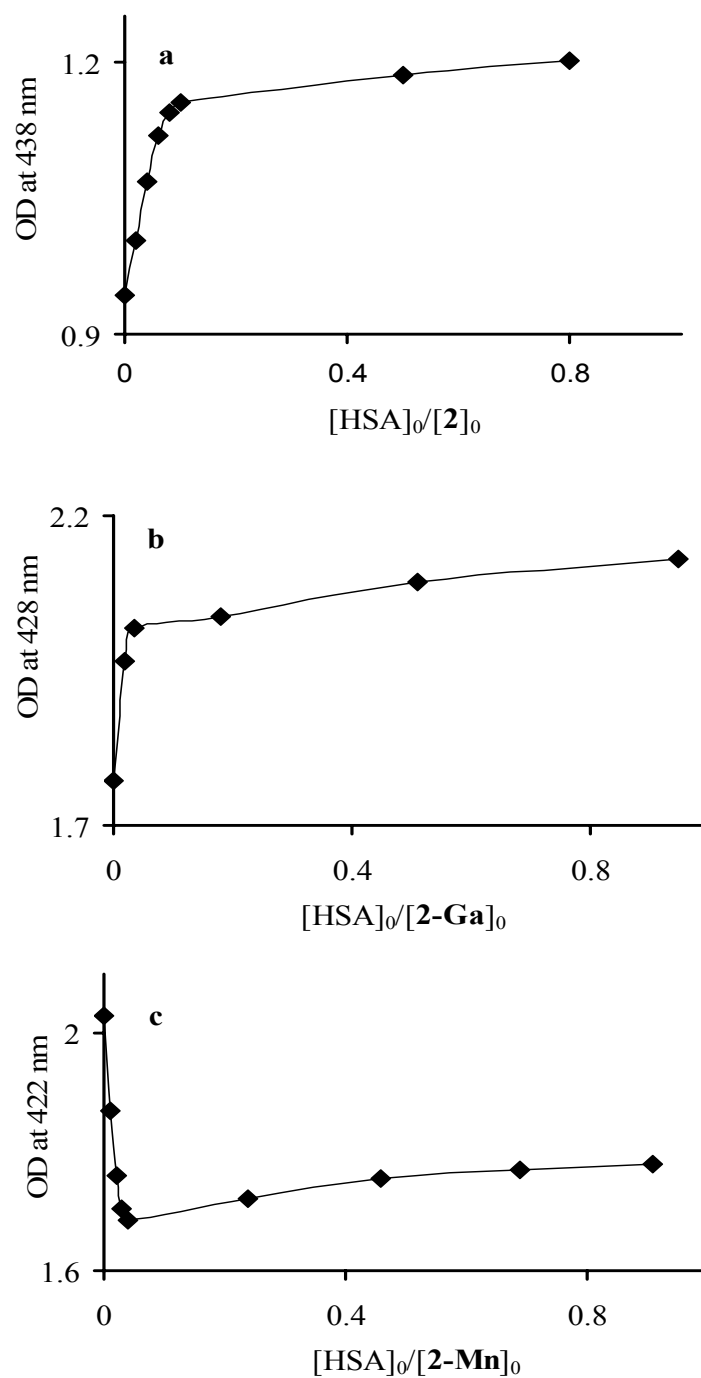


Figure 5.2. UV-vis spectral changes at selected wavelengths as a function of the $[HSA]:[corrole]$ ratio for (a) **2**, (b) **2-Ga**, and (c) **2-Mn**.

Effect of HSA on Corrole Fluorescence. Binding of corroles to HSA can be quantified by monitoring the highly intense fluorescence of **2** and **2-Ga**, allowing experiments to be performed at significantly lower corrole concentrations. Another major advantage of fluorescence monitoring is that free and bound corroles might have different emission maxima and/or intensities. The differences in emission wavelengths of both **2** and **2-Ga** in the presence and absence of HSA are only a few nanometers, but the fluorescence intensities are very sensitive to the [HSA]:[corrole] ratio (figure 5.3). These effects are further demonstrated for selected wavelengths in figure 5.4: the initial fluorescence of **2** is reduced to less than 40 percent at a [HSA]:[**2**] ratio of 0.1:1, and it is 60 percent of the initial intensity at a 1:1 ratio. The results for **2-Ga** were even more pronounced: about 40 percent reduction at a [HSA]:[**2-Ga**] ratio of 0.1:1 and 130 percent of the initial intensity at a 1.1:1 ratio. The latter phenomenon suggests that the extent of non-radiative decay of the excited state is lowered upon binding of the fluorophore to the protein (less degrees of freedom), reflected in increased fluorescence. Nevertheless, the intensity becomes lower when many corrole molecules are bound to the same protein because of self-quenching.

For quantitative elucidation of the dissociation constants (K_d) assigned to the high-affinity binding sites, the fluorescence intensities of equimolar conjugates were measured as a function of concentration, with the expectation of a nonlinear correlation if there is significant dissociation. However, a linear correlation was obtained in the range [**2-Ga**] = [HSA] = 2×10^{-6} - 4×10^{-8} M, thereby confirming that no significant dissociation takes place, even at very low (40 nM) conjugate concentrations.

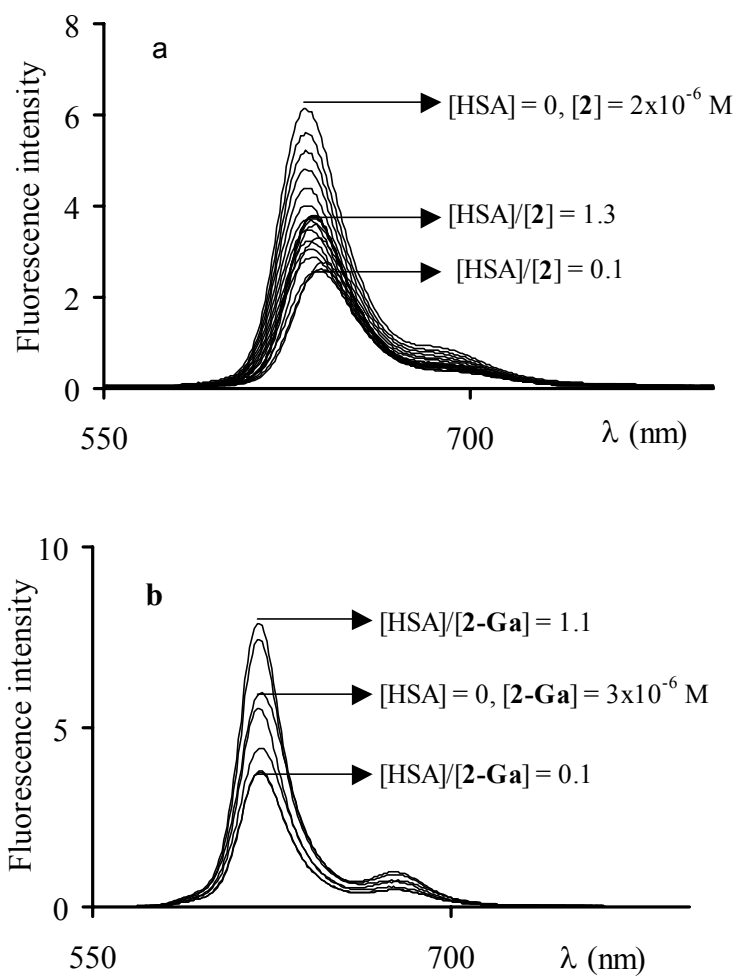


Figure 5.3. Emission spectra of corrole **2** (a, $\lambda_{exc.} = 436$ nm) and **2-Ga** (b, $\lambda_{exc.} = 426$ nm) as a function of added HSA.

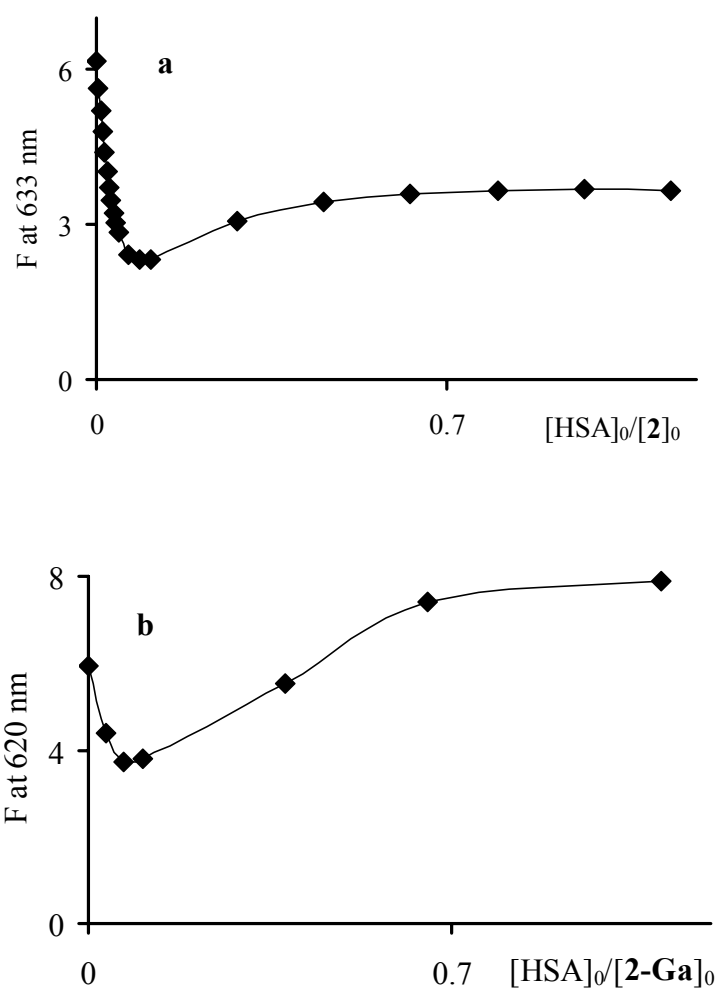


Figure 5.4. Fluorescence intensity at selected wavelengths of a) **2** and b) **2-Ga** as a function of the HSA:corrole ratio.

Circular Dichroism (CD). CD spectra of corrole solutions as a function of HSA concentration are shown in figure 5.5. Since HSA does not absorb visible light, the CD spectrum at long wavelengths ($\lambda > 360$ nm) can only be attributed to corrole interactions with the chiral environment of the folded protein. Intriguingly, the **2-Mn** CD signal (figure 5.5c) is centered at around 490 nm, which is the region of the spectrum that is most sensitive to axial ligands. Moreover, the response to HSA addition is irregular, as can be seen from the shifts of λ_{\max} and the inversion from negative to positive ellipticity at 482 nm. This phenomenon is amplified at 440 and 425 nm, respectively, in the spectra of **2** and **2-Ga** (figure 5.5a-b). These data accord with the earlier conclusions about weak and strong binding sites, which in the present case is observed by redistribution of weakly bound corroles (under the conditions of $[\text{corrole}] \gg [\text{HSA}]$) as the $[\text{corrole}]:[\text{HSA}]$ ratio approaches 1:1. The results show that there are multiple chiral binding sites, albeit with significant differences in wavelengths and ellipticities.

CD spectra of HSA in the region 200-250 nm as a function of added **2-Ga** were also obtained to monitor possible changes of protein secondary structure in response to corrole binding^[68]. As can be seen in figure 5.6, HSA gives rise to a strong CD signal at 222 nm, attributable to α -helical structures. The intensity of the signal drops as a function of the $[\text{2-Ga}]:[\text{HSA}]$ ratio (0.4%, 1.1%, , 1.5%, 2% at 1:1, 2:1, 3:1, and 4:1, respectively); and, at a ratio of 10:1, roughly 8 percent of helical structure is lost. Although there is some degree of conformational change, these corrole-induced perturbations of protein secondary structure are smaller than those observed for BSA-porphyrin conjugates^[67].

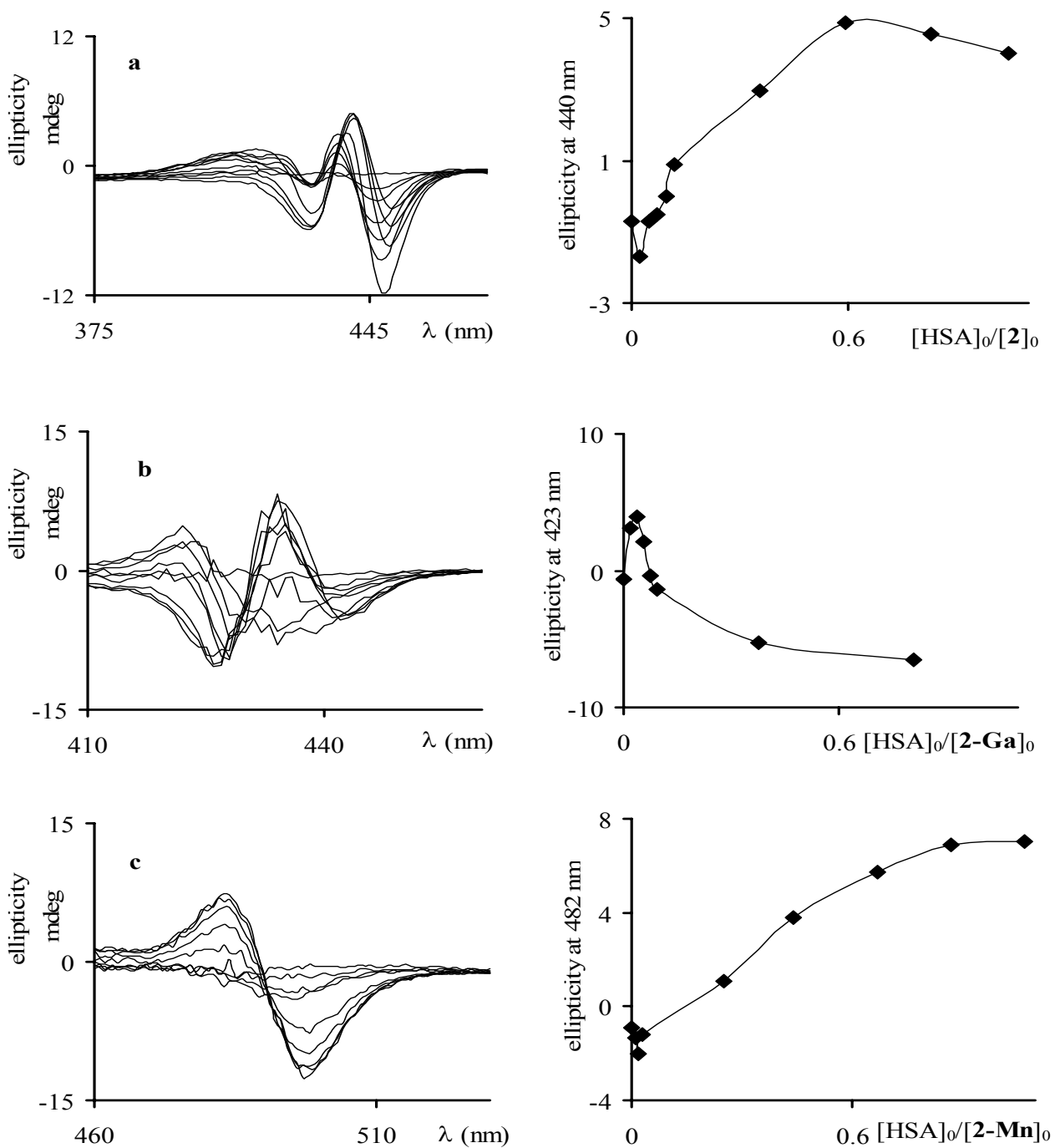


Figure 5.5. HSA titrations of (a) **2**, (b) **2-Ga**, and (c) **2-Mn**, followed by CD spectroscopy. $[2] = 2.11 \times 10^{-5}$ M, $[2-Ga] = 2.7 \times 10^{-5}$ M, $[2-Mn] = 10^{-4}$ M; $[HSA] = 0-10^{-4}$ M.

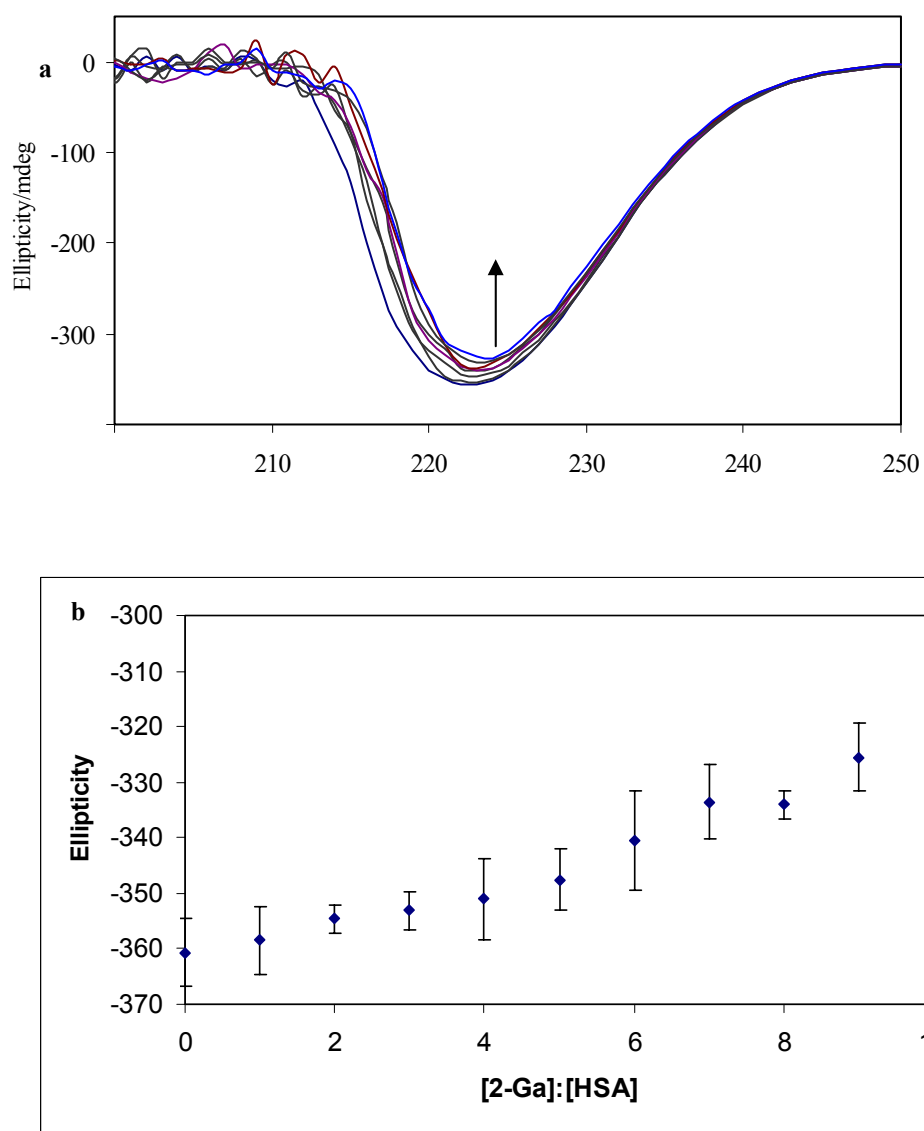


Figure 5.6. a) CD spectra of HSA as a function of [2-Ga]:[HSA] (0,1,2...10) at constant [HSA] (3.7×10^{-6} M). b) Ellipticity at 222 nm as a function of [2-Ga]:[HSA].

Quenching of Trp²¹⁴ Emission. One of the earliest and simplest methods that was used for investigating heme binding is fluorescence quenching of the single tryptophan residue (Trp²¹⁴) in HSA^[59]. The advantage of this approach is that it reports selectively on binding sites that are not too distant from the fluorophore. Results obtained by exciting HSA's Trp²¹⁴ at 280 nm and recording its emission ($\lambda_{\text{max}} = 340$ nm) as a function of the concentration of **2-Ga** are shown in figure 5.7a. Notably, full and selective quenching was achieved, as can be seen from the residual emission ($\lambda_{\text{max}} = 310$ nm) due to the many tyrosine residues that are present in HSA. More quantitative information was obtained from plots of fluorescence intensity as a function of the [HSA]:[corrole] ratio (figure 5.7b). The responses (slopes) of **2** and **2-Ga** are practically identical, and that of **2-Mn** somewhat smaller. The up to 50% quenching at equimolar concentrations of HSA and corrole obtained in the first two cases implies that **2** and **2-Ga** occupy close to Trp²¹⁴ binding sites with very high-affinity. If **2-Mn** also associates to similar binding sites, figure 5.7b may be analyzed as reflecting an opposite relationship between the steepness of the slopes and the K_d of the HSA:corrole conjugates. This would lead to relative K_d from high-affinity sites in the order of **2** ~ **2-Ga** < **2-Mn**.

The roughly 50% quenching at a 1:1 ratio between HSA and **2** or **2-Ga** may be interpreted either one of two limiting ways: 100% quenching efficiency by sites that are only 50% occupied (= large K_d) or 50% quenching efficiency by sites that are 100% occupied (= small K_d). Two sets of experiments were performed to distinguish between these possibilities. The first consisted of dilution experiments on 1:1 mixtures of HSA and the corroles. For all three corroles (data for **2-Ga** is shown in the inset of figure 5.8) there was

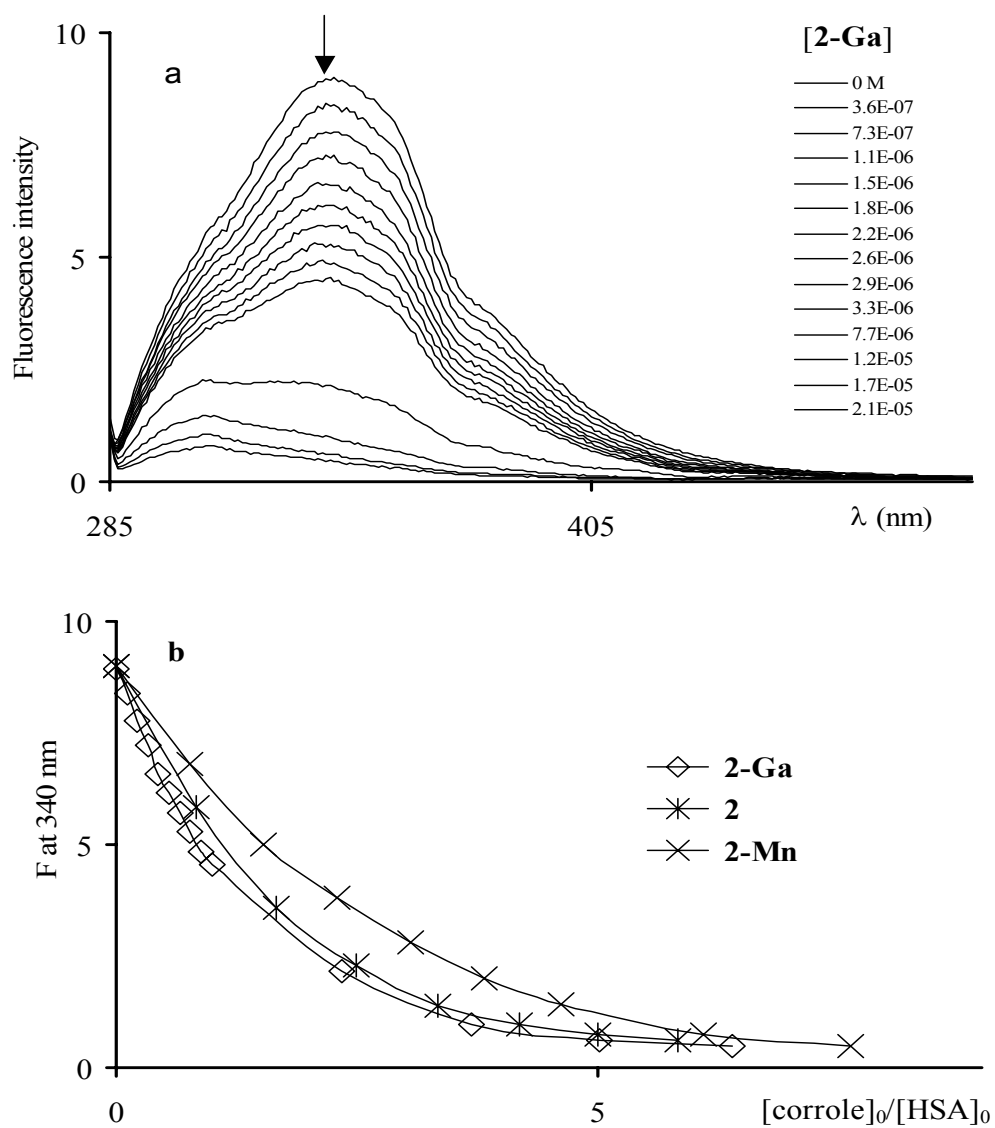


Figure 5.7. Quenching of the emission of HSA by (a) increasing amounts of **2-Ga** and (b) the dependence of the emission on the $[\text{corrole}]/[\text{HSA}]$ ratio.

$\lambda_{\text{exc.}} = 280 \text{ nm}$, $[\text{HSA}] = 3.3 \times 10^{-6} \text{ M}$.

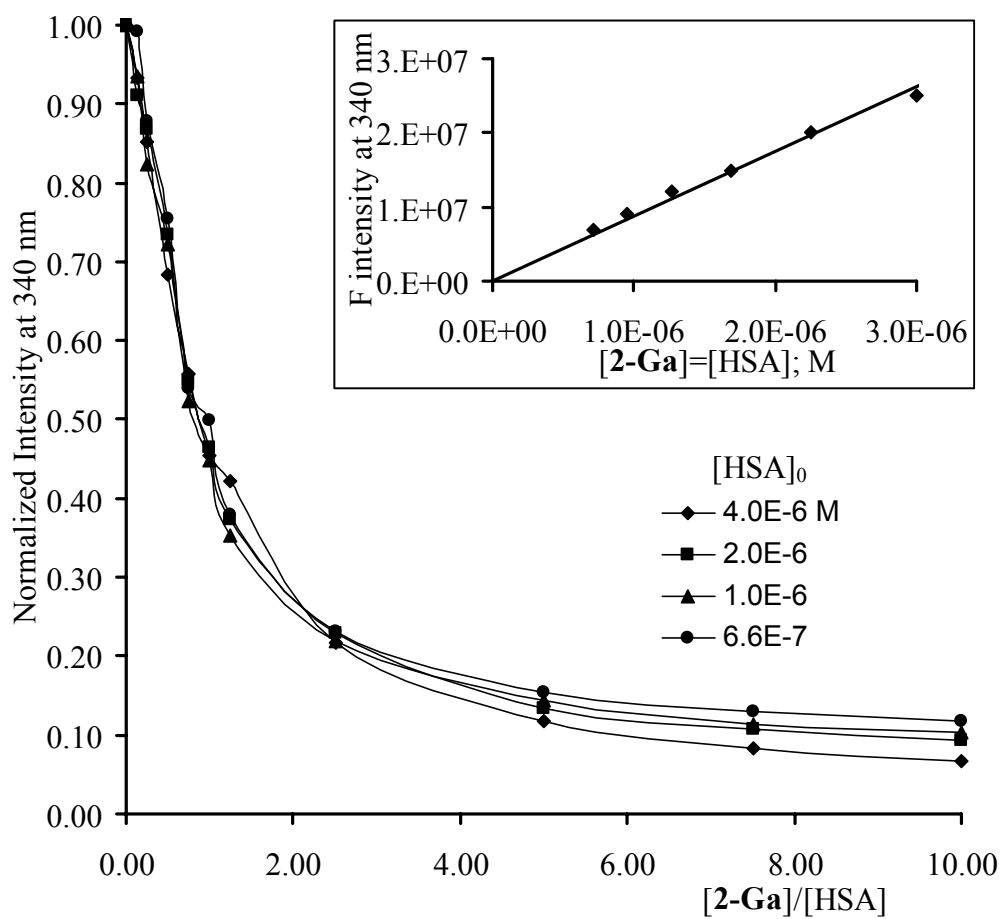


Figure 5.8. Normalized fluorescence intensity of HSA as a function of the $[2\text{-Ga}]:[\text{HSA}]$ ratio at different initial concentrations of HSA. Inset: Fluorescence intensity at 340 nm of equimolar concentrations of **2-Ga** and HSA at different absolute concentrations.

no deviation from linearity in the concentration versus fluorescence-intensity plots in the range 4×10^{-6} to 7×10^{-7} M ($K_d < 10^{-8}$ M for the conjugates). Figure 5.8 shows the other set of experiments: measuring fluorescence intensity of HSA as a function of the relative amount of **2-Ga**, at four different absolute concentrations. The normalized plots are identical as long as the corrole is not in excess of HSA, clearly confirming the absence of any dissociation. The plots become different only after the $[\mathbf{2-Ga}]:[\text{HSA}]$ is above 1, indicating the presence of slightly weaker secondary binding sites. Importantly, although a reliable measurement of K_d is problematic because of the large number of corrole molecules that can be accommodated by HSA, the trends of figure 5.8 show that dissociation from weaker binding sites is very small as well. Therefore, the approximately 50% quenching seen at a 1:1 ratio between HSA and corrole is consistent with incomplete quenching of Trp²¹⁴ fluorescence by corroles that occupy high affinity sites.

Binding Sites for 2-Ga. Since the three-dimensional structure of HSA is known, an attempt was made to estimate the distance between Trp²¹⁴ and a corrole binding site *via* standard Förster energy transfer equations, using the roughly 50% fluorescence quenching by **2-Ga**.

$$R_0^6 = 8.8 \times 10^{-5} (\kappa^2 n^{-4} \phi_{\sigma} J) \quad (1)$$

$$J = \frac{\int_0^{\infty} F_o(\lambda) E_A(\lambda) \lambda^4 d\lambda}{\int_0^{\infty} F_o(\lambda) d\lambda} \quad (2)$$

Equations 1-2 were used for evaluation of the Förster distance^[69, 70], where J is the overlap between the luminescence spectrum of the donor and the absorption spectrum of the

acceptor (weighted by λ^4), ϕ_0 is the luminescence quantum yield in the absence of energy transfer, n is the refractive index, and κ is an orientation factor dependent on the alignment of the donor and acceptor dipoles ($\kappa^2 = 2/3$ for random alignment). According to the above expressions, the experimental data yielded a value for the overlap integral J between the fluorescence spectrum of the protein HSA and the absorption spectrum of the quencher **2-Ga** of 6.26×10^{14} . Based on the J value and Equation 1, the Förster distance (R_0) between **2-Ga** and Trp²¹⁴ (HSA) was calculated to be 30 Å. Moreover, models of the **2-Ga**-HSA conjugate based on crystallographic data for [Ga(tpfc)(py)] (tpfc = 5,10,15-tris(pentafluorophenyl)corrolate; py = pyridine) and HSA were constructed (Structural models were built using the Accelrys DS ViewerPro 5.0 software package. The structure of **2-Ga** was obtained by addition of two sulfonate groups and removal of the axial pyridine from the published crystal structure^[8]: **2-Ga** was then inserted into putative HSA binding sites (crystal structure from reference 53)). In the HSA crystal structure, a heme (Fe^{III}-protoporphyrin IX) is located in a hydrophobic pocket in sub-domain IB; and there are additional interactions involving Tyr¹⁶¹, Ile¹⁴², Tyr¹³⁸, His¹⁴⁶, and Lys¹⁹⁰ with the heme. In one of the proposed structures, where noncovalent interactions are dominant (figure 5.9a), **2-Ga** replaces the heme in the hydrophobic cavity; at this site, the distances between **2-Ga** and Trp²¹⁴ are 20-24 Å (from the edge of the corrole-from the metal), in fair agreement with the estimated distance based on fluorescence quenching. Figures 5.9b and 5.9c show two **2-Ga**-HSA interactions that involve metal-coordination to His. As examples, it was proposed that **2-Ga** could bind to surface-exposed His³ and His¹⁰⁵ with distances between His-bound **2-Ga** and Trp²¹⁴ of 24-30 and 30-34 Å, respectively. It is also noted that

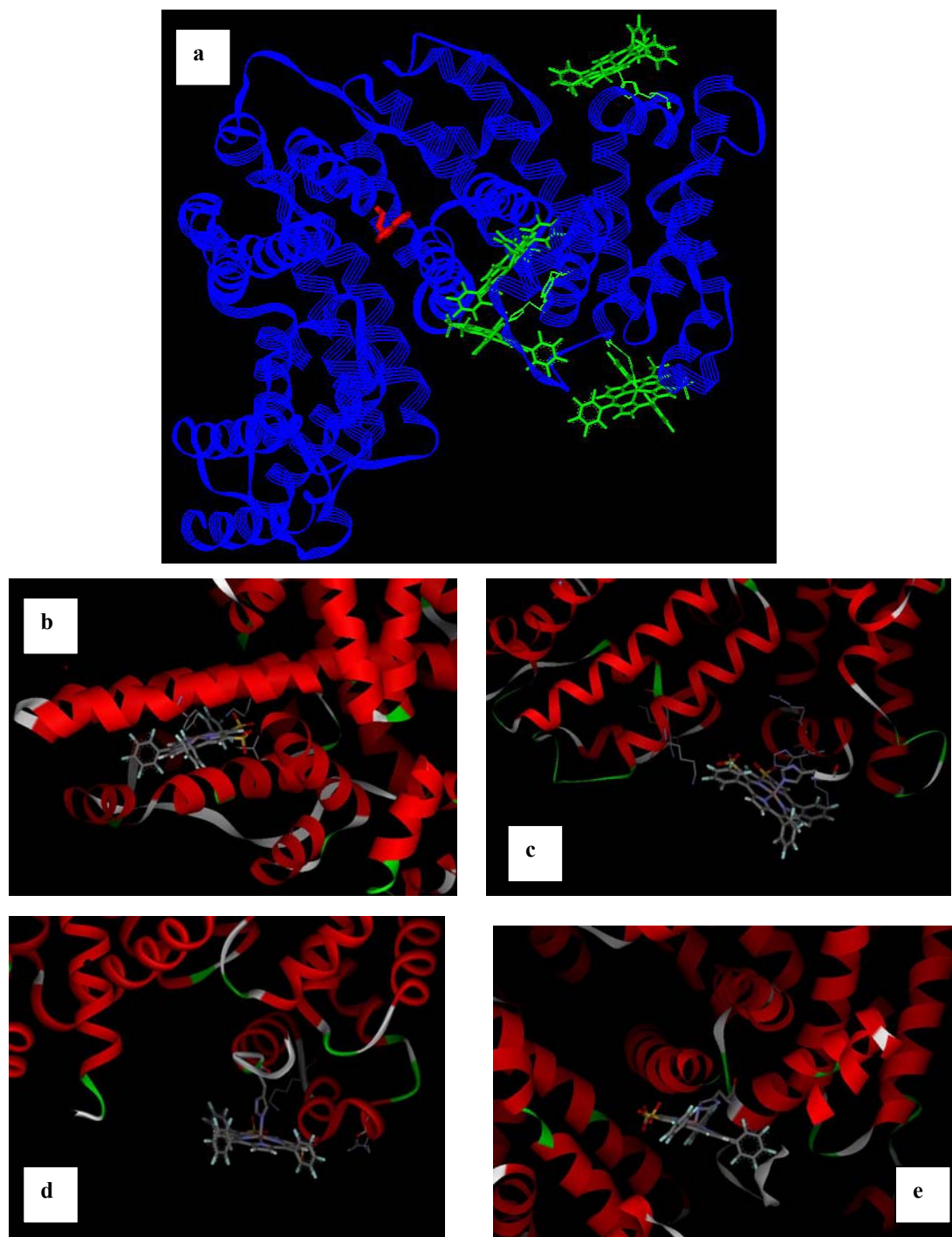


Figure 5.9. Structural models depicting four potential binding sites for **2-Ga** to HSA. (a) HSA with corroles (green) in all four potential binding sites. Trp²¹⁴ is shown in red. (b) **2-Ga** in place of the heme of methemalbumin. (c) **2-Ga** coordinated to His³. (d) **2-Ga** coordinated to His¹⁰⁵. (e) **2-Ga** coordinated to His¹⁴⁶. The proposed locations were chosen as follows: one is the heme binding site; others are histidine binding sites whose positions are consistent with the Trp²¹⁴ quenching experiments, except for d.

coordination of **2-Ga** to His¹⁴⁶ located in the heme binding pocket (figure 5.9d) is unlikely due to a considerable difference between the Förster distances measured in the model and that estimated from quenching experiments (16-19 Å vs. 30 Å).

Concluding Remarks

Reported here are results from an investigation of interactions between corroles and biomolecules. Corrole **2** is especially promising for biomedical research because of its structural similarity to the most active porphyrin-based drugs and because amphiphilicity is easily achieved. Our work has focused on interactions with HSA because any medical application must take into account associations with the most abundant protein in serum. Two metal complexes of **2** were investigated, with the goal of elucidating any effects due to ligation to relevant residues of the protein.

The changes in the electronic absorption spectra of **2**, **2-Ga**, and **2-Mn** as well as in the emission spectra of **2** and **2-Ga** as a function of increasing amounts of HSA revealed many protein binding sites. With corrole in excess, both absorption and emission intensities decreased, which is behavior that is frequently encountered when porphyrins form aggregates, usually because of limited solubility in water. However, the corroles of the current investigation do not aggregate in aqueous solutions and, accordingly, it is proposed that the above phenomena are due to self quenching of many corrole molecules that are aggregated/associated in binding pockets within the protein. Examination of published crystal structures of HSA reveals the presence of a large calixarene-like amphiphilic pocket that seems appropriate for accommodation of the corroles. When the [corrole]:[HSA] ratio

approaches 1:1, the absorption and emission intensities increase, thereby indicating redistribution of corroles from the weaker binding pocket to high-affinity sites. Many different methods were used to investigate the interactions of corroles with HSA. The results clearly show that all derivatives form tightly bound conjugates with the protein, with dissociation constants in the nM range in the order $2 \leq 2\text{-Ga} < 2\text{-Mn}$. Under biologically relevant conditions (HSA concentrations 2 to 3 orders of magnitude larger than those examined here) all the derivatives will be fully bound to proteins. This information is of prime importance for any potential utilization of the corroles in bioinorganic systems such as for therapeutic applications and biomimetic catalysis, approaches that are currently under investigation in the Gray and Gross laboratories.

2-Sn/HSA Interactions

2-Sn behaves much like the other sulfonated corroles when exposed to HSA. As can be seen in figure 5.10, a ~5 nm red shift is seen in the Soret bands of the corrole absorption spectrum upon HSA binding and, as with **2-Ga**, there is a slight increase in peak absorption. Note that, as with the previous corroles, the shift of the Soret band is complete before a 1:1 ratio is reached. A strong CD signal induced upon binding is also seen in figure 5.10, indicating a preferred orientation for the corrole in its binding pocket.

The fluorescence data for HSA and **2-Sn** are much like those seen with the other corroles as well. As seen in figure 5.11, the fluorescence of **2-Sn** is quenched upon binding to HSA, and the quenching levels off at $[\text{HSA}]/[\text{2-Sn}] = 1$, at approximately 20% of its initial value. Interestingly, no recovery of intensity, as in the cases of **2** and **2-Ga**, is observed.

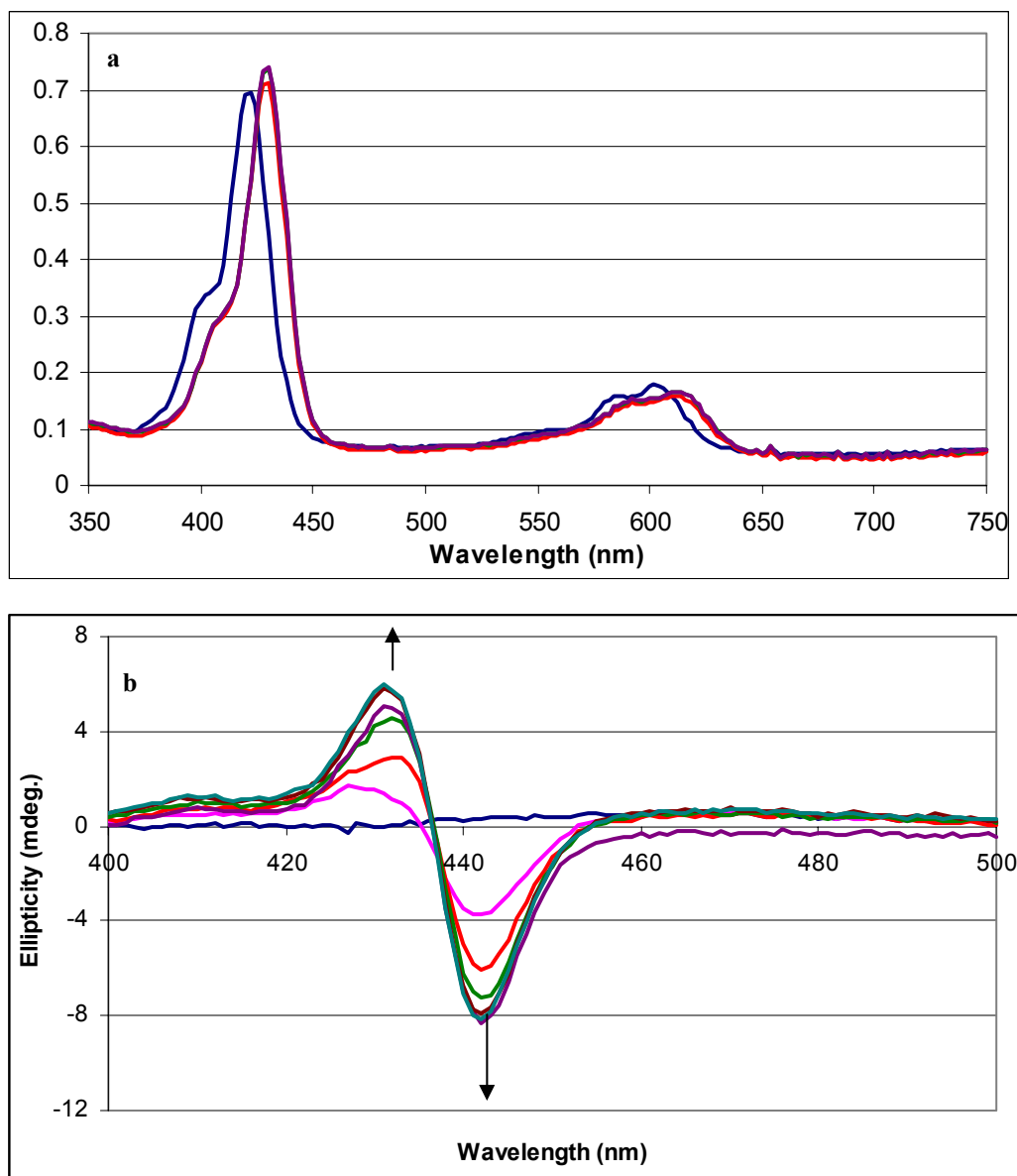


Figure 5.10. a) UV-vis spectra of HSA titrated into **2-Sn** at pH 7. $[\text{HSA}]/[\text{2-Sn}] = 0$ (blue), 0.75 (red), 1.1 (green), 1.5 (purple). b) CD spectrum of HSA titrated into **2-Sn** at pH 7. $[\text{HSA}]/[\text{2-Sn}] = 0$ (blue), 0.37 (pink), 0.75 (red), 1.1 (green), 1.5 (purple), 1.9 (brown), 2.3 (teal).

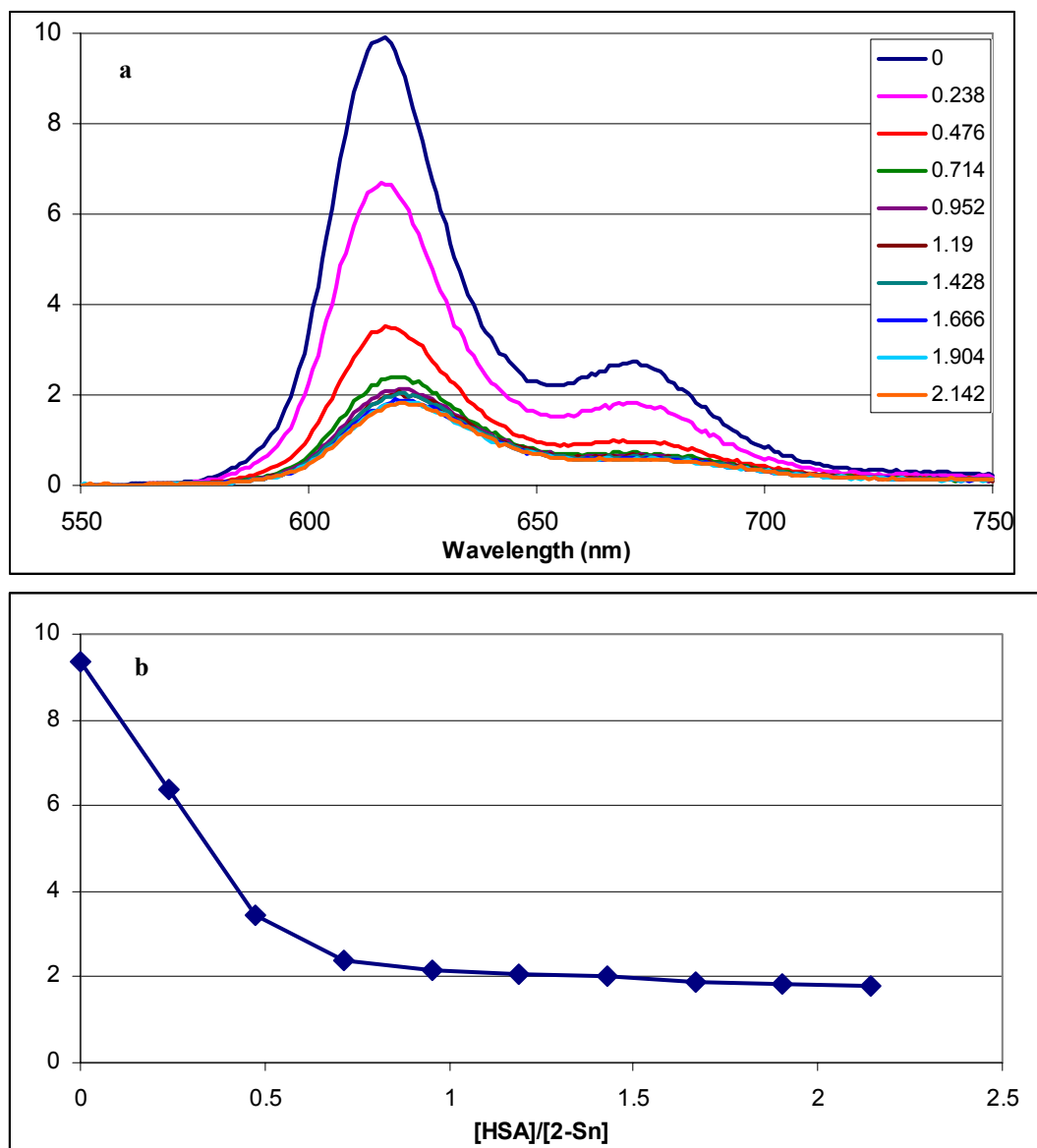


Figure 5.11. Fluorescence of 2-Sn at varying ratios of HSA. a) Emission spectra. Ratios are given in legend. b) Peak emission versus ratio.

Studies of the tryptophan fluorescence in HSA further the similarities between **2-Sn** and the other corroles. As seen in figure 5.12, addition of **2-Sn** quenches the fluorescence of this residue, reaching ~50% quenching at a 1:1 ratio, with the amount of quenching not leveling off until $[\mathbf{2-Sn}]/[\text{HSA}] > 2$.

2-Sn/HSA Conclusions

Studies of **2-Sn**/HSA aggregates indicate that they behave in the same manner as the other corroles studied. Thus, it seems safe to assume that the tin corrole is binding in the same manner, and likely in the same sites, as other corroles. Furthermore, the linearity of fluorescence emission for a 1:1 conjugate of **2-Sn**:HSA upon dilution indicates that the corrole binds to HSA with a similar dissociation constant, and, as with the other corroles, dissociation is undetectable by the methods used herein.

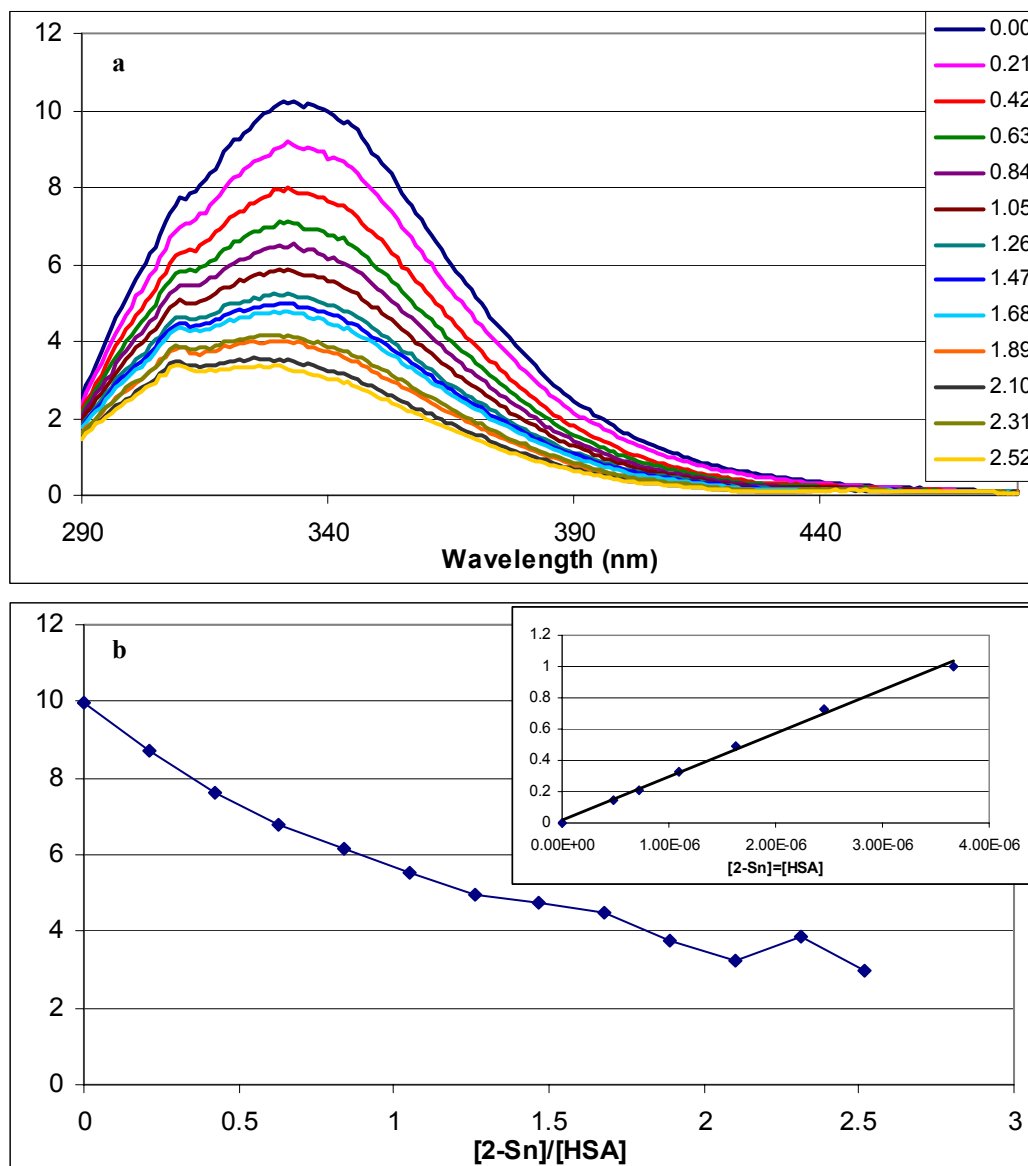


Figure 5.12. HSA tryptophan fluorescence at varying ratios of **2-Sn**. a) Emission spectra. Ratios are given in legend. b) Peak emission versus ratio. Inset shows dilution of a 1:1 mixture of HSA and **2-Sn**; concentration is given as molarity.

SOLAR CELLS**Introduction**

In our fast-growing world, alternative energy sources are quickly becoming a concern. It was shown in the early 1990s that dye-sensitized solar cells (DSSCs) are a very promising technology toward alternative energy conversion^[71]. These cells involve coating nanocrystalline TiO₂ with a dye capable of absorbing sunlight and sensitizing the semiconductor. The dye absorbs photons of visible light, promoting electrons into the excited state. The electrons are injected into the conduction band of TiO₂, leaving an oxidized dye and reduced semiconductor. The injected electron is then free to pass to the back electrode and go around a circuit to do work. The oxidized dye is reduced by an ion pair in solution, which in turn is reduced to its original state at the counter electrode, completing the circuit^[71].

One of the best dyes currently known for these solar cell applications is Ru(4,4'-dicarboxylic acid-2,2'-bipyridine)₂(NCS)₂, more popularly known as the N3 dye. While it is not entirely known why this compound performs so much better than others, it has shown that in developing dyes for DSSCs, two important factors must be considered. The potential dye must have strong absorption bands in the visible spectrum, and the dye must be able to bind to the TiO₂ surface. Quick inspection of the absorption spectra of corroles

shows that they do indeed satisfy this first requirement. As well, the sulfonate groups of corroles derived from **2** can provide the binding ability called for in the second factor. Therefore, a portion of this work was spent looking at the ability of corroles to act as the dyes in DSSCs.

2-Ga versus Ruthenium Dyes

Initial work started on corrole-TiO₂ systems started with **2-Ga**, with some preliminary work having also been performed with **2** and **2-Sn** as well. The first experiments were to qualitatively determine if the corroles could in fact bind to the TiO₂ surface.

Slides prepared in lab were soaked in an ethanol solution containing **2-Ga** for approximately 24 hours to ensure maximum adsorption onto the TiO₂ surface. After the 24 hour soaking period the dyes are ready for use in a working solar cell with a 0.5M LiI, 0.05M I₂, 20mM pyridine, 20mM pyridinium triflate, and acetonitrile electrolyte. It can also be seen after this soaking period that the dye has indeed bound to the surface, as the slide takes on the green color of the dye (see figure 6.1). By running current-voltage curves on the coated slides, the efficiency can be determined with equation 6.1:

$$E = (J_{sc} \times V_{oc} \times ff) / I_s \quad (\text{eq. 6.1})$$

In this equation E is the efficiency of the cell, J_{sc} is the short circuit current (the amount of current at zero applied voltage), V_{oc} is the open circuit potential (the potential at zero current), ff is the fill factor (a measure of the shape of the curve, see figure 6.2), and I_s is the power of the sun (100 mW/cm²). Comparison of the curve obtained for **2-Ga** to those

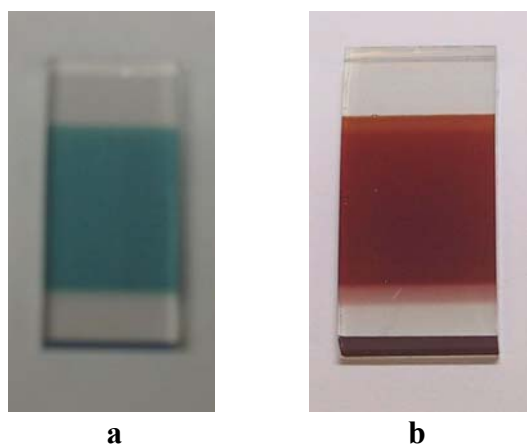


Figure 6.1. TiO_2 slides coated with a) **2-Ga** and b) **N3**. In both cases the colored area is 1 x 1.5 cm.

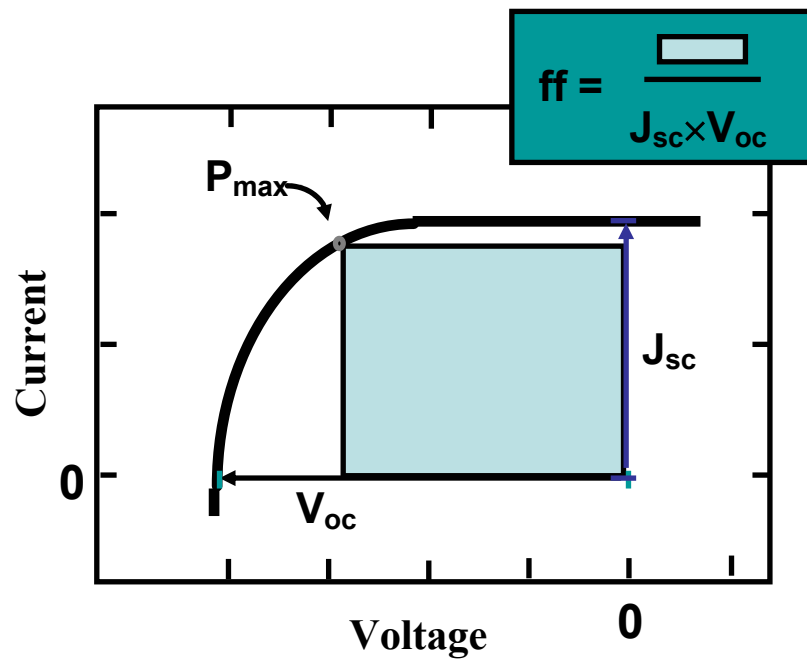


Figure 6.2. Model diagram of current-voltage curve showing important parameters for calculating efficiency. P_{max} is the maximum power from the cell. The remaining terms are defined in the text.

obtained from various ruthenium-diimine dyes (figure 6.3) shows that the corrole based slide has similar parameters to various ruthenium dyes studied, falling in between the best dye, N3, and the worst dye studied, a ruthenium tris(bipyridine) based dye. The overall efficiency of the corrole slide was 1.56%, about half of that found for N3 (3.14%), but more than twice that of the poorest dye (0.69%) (see table 6.1).

2, 2-Ga, and 2-Sn Dyes versus N3

Work was then done to introduce other corrole compounds into the solar cells as well, namely **2** and **2-Sn**. Interestingly, it was found that the free-base performed slightly worse than **2-Ga**, at 0.82% efficiency; however, both were significantly better than **2-Sn** at 0.12% efficiency (see figure 6.4, table 6.2). The reasons behind these differences are still under investigation.

One important factor to consider in the adsorption of these dyes to the TiO₂ cells is whether or not the dye is being changed upon adsorption. However, as seen in figure 6.5, the overall absorption spectrum of the dyes when bound to the surface shows the same typical shape of a corrole spectrum, and the shift in band position seen is similar to that seen with ruthenium-based dyes.

Another experiment performed in characterization of these dyes was incident photon-to-current conversion efficiency (IPCE) measurements. As seen in figure 6.6, the conversion efficiencies of **2-Ga** and **2** rival that of the N3 dye in their Soret and Q-band regions, while

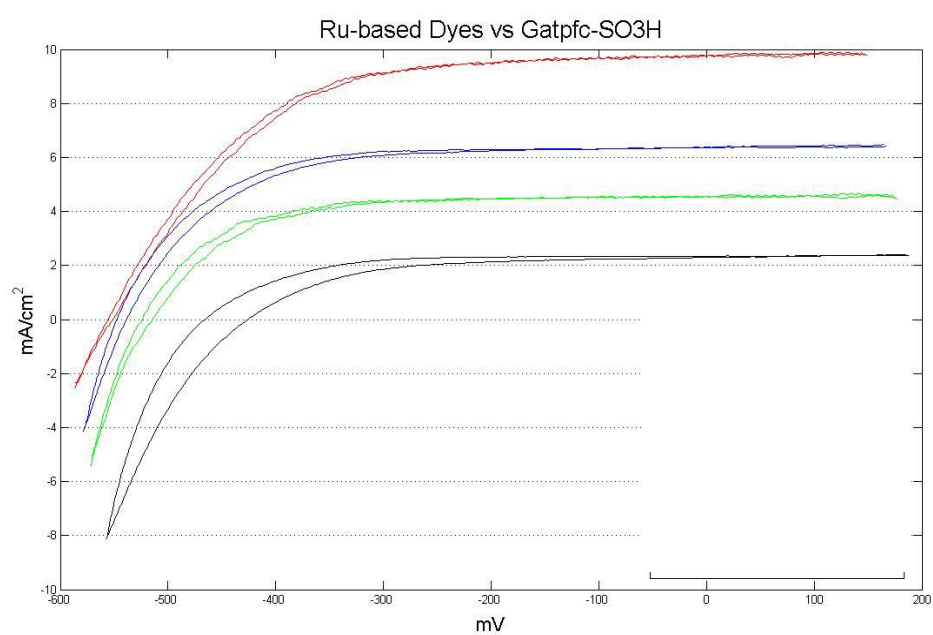


Figure 6.3. Current-voltage curves for N3 dye (red), a ruthenium-diimine dye (blue), **2-Ga** (green), and the poorest ruthenium-diimine dye used in this study (black).

	N3	$[\text{Ru}(\text{H}_2\text{L}')_2(\text{CN})_2]^{2+}$	$[\text{Ru}(\text{H}_2\text{L}')\text{L}_2]^{2+}$	2-Ga
V_{oc} (mV)	556	548	466	524
J_{sc} (mA)	9.76	6.36	2.34	4.55
Fill Factor	0.58	0.64	0.63	0.66
Efficiency	3.14	2.13	0.69	1.56

Table 6.1. Efficiency parameters for **2-Ga** slides vs. Ru-diimine dyes.

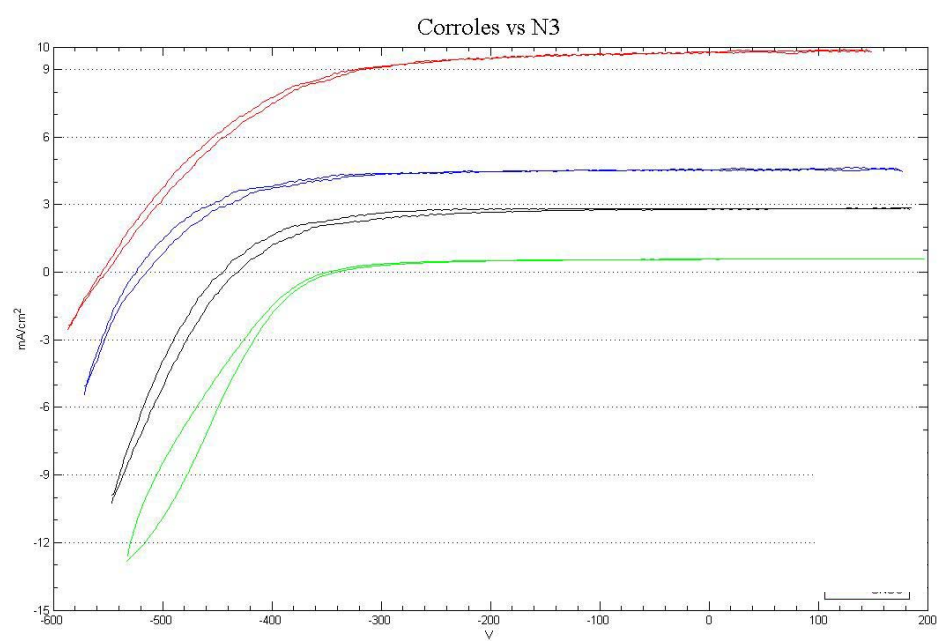


Figure 6.4. Current-voltage curves of N3 (red), **2-Ga** (blue), **2** (black), and **2-Sn** (green).

	N3	2-Ga	2-Sn	2
V _{oc} (mV)	556	524	348	444
J _{sc} (mA)	9.76	4.55	0.58	2.83
Fill Factor	0.58	0.66	0.60	0.65
Efficiency	3.14	1.56	0.12	0.82

Table 6.2. Efficiency parameters for corrole dyes vs. N3.

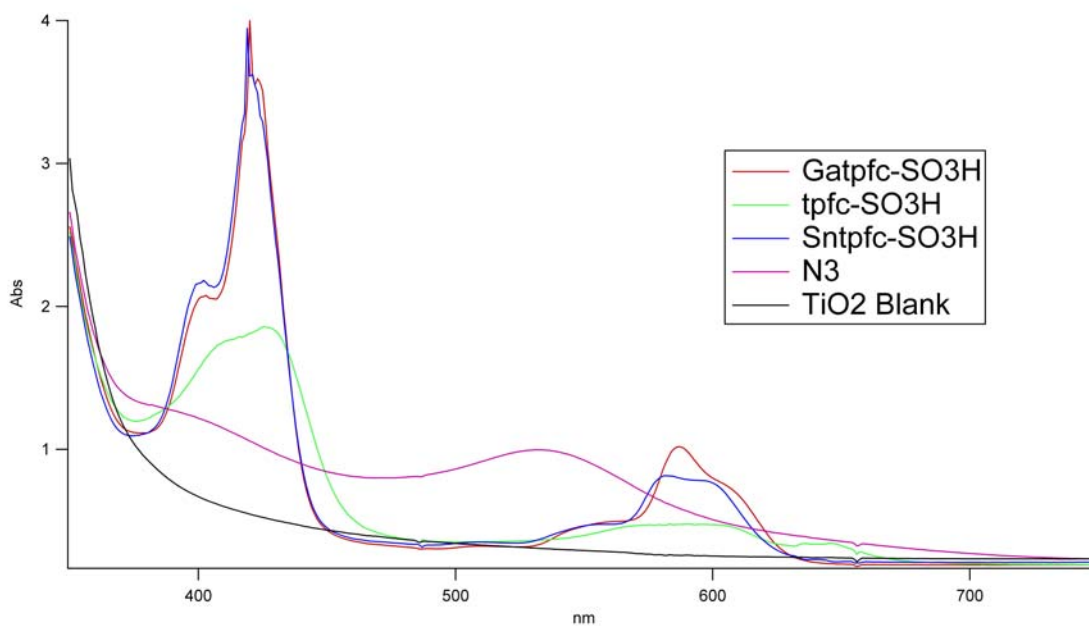


Figure 6.5. Absorption spectra of N3 (purple), **2-Ga** (red), **2** (green), **2-Sn** (blue), and TiO₂ blank (black). Corroles show slight blue shifting of Q-bands. Soret of **2-Ga** shows ~9 nm blue shift; Soret of **2** and **2-Sn** show 2-3 nm red shifts. These shifts are similar to those seen for ruthenium-diimine dyes.

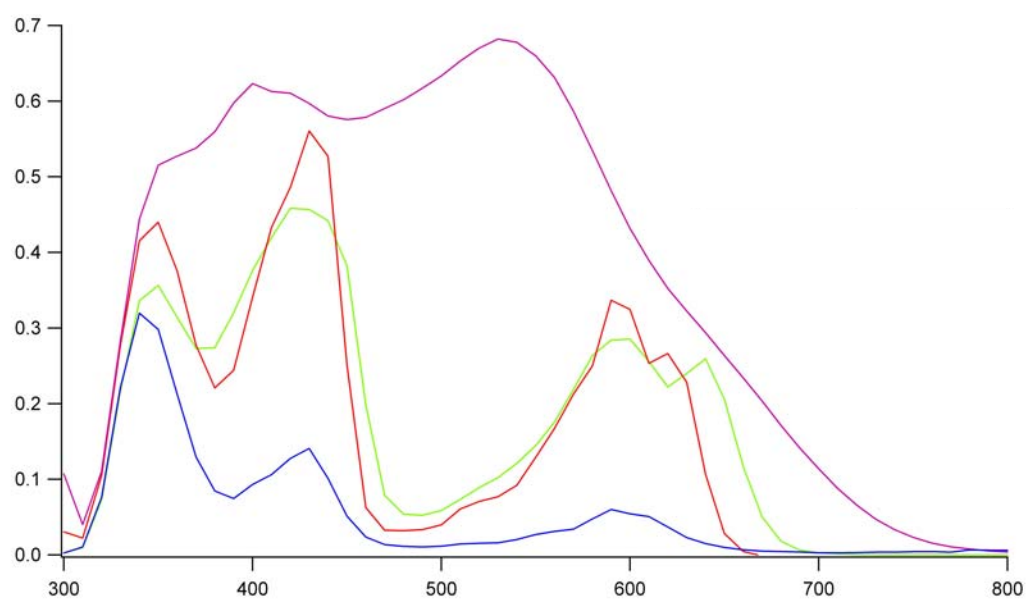


Figure 6.6. IPCE curves of N3 (purple), **2-Ga** (red), **2** (green), and **2-Sn** (blue).

2-Sn shows relatively poor conversion efficiency across the board in comparison with the other dyes.

Conclusions

The corrole based dyes used in this work show great promise for making efficient solar cells and have demonstrated good binding to the TiO₂ surface. However, the kinetics of the cell processes with corroles dyes is not fully understood, and future work will be devoted to elucidating these events. As well, it has been seen qualitatively that the corrole dyes do fall off the surface of the solar cells, and over time the cell loses its color. Research is also being planned toward developing new types of corroles with different binding groups, such as carboxylic acids or phosphonate groups, with the goal of providing stronger overall binding to the surface and making a more robust cell.

Appendix A

ANTI-CANCER DRUGS

Work on this project involved collaboration with Dr. Lali Medina-Kauwe, now at Cedars-Sinai Medical Center, on the development of corroles as anti-cancer drugs. Given the high fluorescence of corroles, and their known toxicity to cancerous cells^[6], the water-soluble corroles seemed an ideal place to start on a search for drugs. While Dr. Medina-Kauwe worked on developing a protein to specifically enter cancer cells, we provided compounds for testing in cellular systems with model proteins, in particular with HSA. It was hoped that the fluorescent corroles could be used as a diagnostic tool for early cancer detection. If the corrole is bound to a transport protein specific for cancer cells, unknown cells could be exposed to the mixture and tested for the fluorescent markers. It was then hoped to develop a phosphorescent corrole that could be delivered to the cells and used to activate triplet oxygen in the cell to singlet oxygen, inducing cell death in a photodynamic therapy manner. If the absorbance of the corroles could not be shifted into tissue penetrating wavelengths, we planned to put more effort into developing a corrole that could activate a catalytic oxygen cycle, based on the findings that the chromium complex of **1** catalyzes the aerobic oxidation of phosphines^[72].

While **2**, **2-Ga**, **2-Mn**, and **2-Sn** were all used to varying extents in the project, it was **2-Ga** that served as the best model compound. It was found that a transport protein could indeed deliver this corrole compound into cells (see figure A.1). Even more remarkable was the

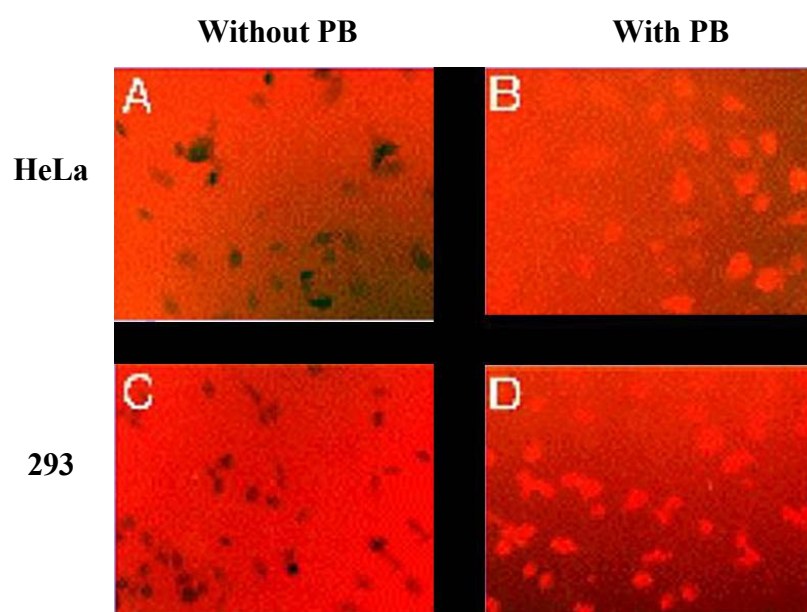


Figure A.1. Corrole delivery to cells. PB: a proven gene delivery protein. HeLa: human cervical carcinoma cells. 293: monkey kidney cells. Micrographs (courtesy of Dr. Medina-Kauwe) were taken under UV light at 10x magnification.

increased toxicity the corrole seemed to show toward cancer cells versus non-cancerous cells. The mechanism of this specific toxicity is still under investigation. This toxicity was seen with **2** and **2-Mn** as well. Work with **2-Sn** is underway.

Appendix B

WORK WITH MAYRA SHEIKH

While working on this project, I had the opportunity to work with Mayra Sheikh, an undergraduate student at Caltech, both as a SURF co-mentor and as a graduate supervisor for her Chem 10 work. During this time, three different projects were attempted. The first, measuring quantum yields of many of the corroles discussed herein, has been presented in Chapter 4. Results from the other two projects will be summarized here.

The first of these remaining projects had the eventual goal of producing a water-soluble chromium corrole complex. Previous work in the group by Dr. Alexandre Meier had shown the chromium corrole capable of acting as an oxidation catalyst for some compounds^[72]. While this was limited to phosphines in the initial work, it was hoped that moving to an aqueous system would allow a greater range of substrates. Initial work in this area, performed by Meier and repeated by Sheikh in the beginning stages of her project, had attempted to metallate **2** by the same method used to metallate **1**, refluxing with $\text{Cr}(\text{CO})_6$ or CrCl_2 ^[73]. This method did not yield the desired results, however, as it appeared to cause the dissociation of at least one sulfonate group from **2** and resulted in a compound that was not water soluble.

The second method attempted in this project was to prepare the chromium version of **1** as detailed in the literature^[73] and to use that compound as the starting point for the corrole

sulfonation reaction in place of **1**. While the reaction did produce green products characteristic of sulfonated corroles, mass spectrometry and EPR spectrometry did not confirm the presence of the desired compound.

While it was not determined why these reactions would not produce the desired bis-sulfonated chromium corrole, it was decided to attempt a different method for a water-soluble chromium corrole. It had been seen earlier that the para-fluorines of **1** could be substituted with pyridine, which was then methylated to form a water-soluble corrole, 5,10,15-tris(4-(2-(1-methylpyridyl))tetrafluorophenyl)corrole (**4**, see figure B.1)^[11]. While the synthesis of this free-base was attempted, it proved to be extremely sensitive to any change in reaction conditions, and the compound was not made. However, other projects in the group had made use of an imidazole substitution reaction in the para position of decafluorobiphenyl^[74]. It was therefore decided to attempt a combination of these two reactions to produce an imidazole substituted corrole.

1 was dissolved in THF under argon, followed by addition of 7 equivalents of imidazole and 14 equivalents of K₂CO₃, and stirred for 6 hours. A mass spectrum of the mixture revealed the main component of the solution to be unreacted free-base. However, peaks were observed for addition of one, two, and three imidazole groups to the corrole (at 42%, 13%, and 1% peak intensity relative to the unreacted starting material, respectively. See figure B.2a). Column separation of this solution (with 4:1 hexanes:dichloromethane as eluent) provided the unreacted free-base and a mixture of the various substituted imidazole

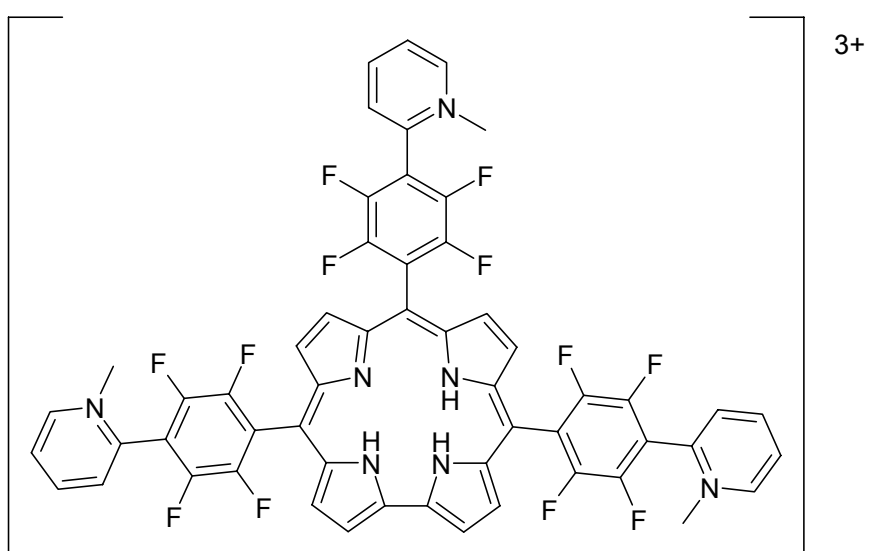


Figure B.1. Previously reported 5,10,15-tris(4-(2-(1-methylpyridyl))tetrafluorophenyl)corrole, **4**.

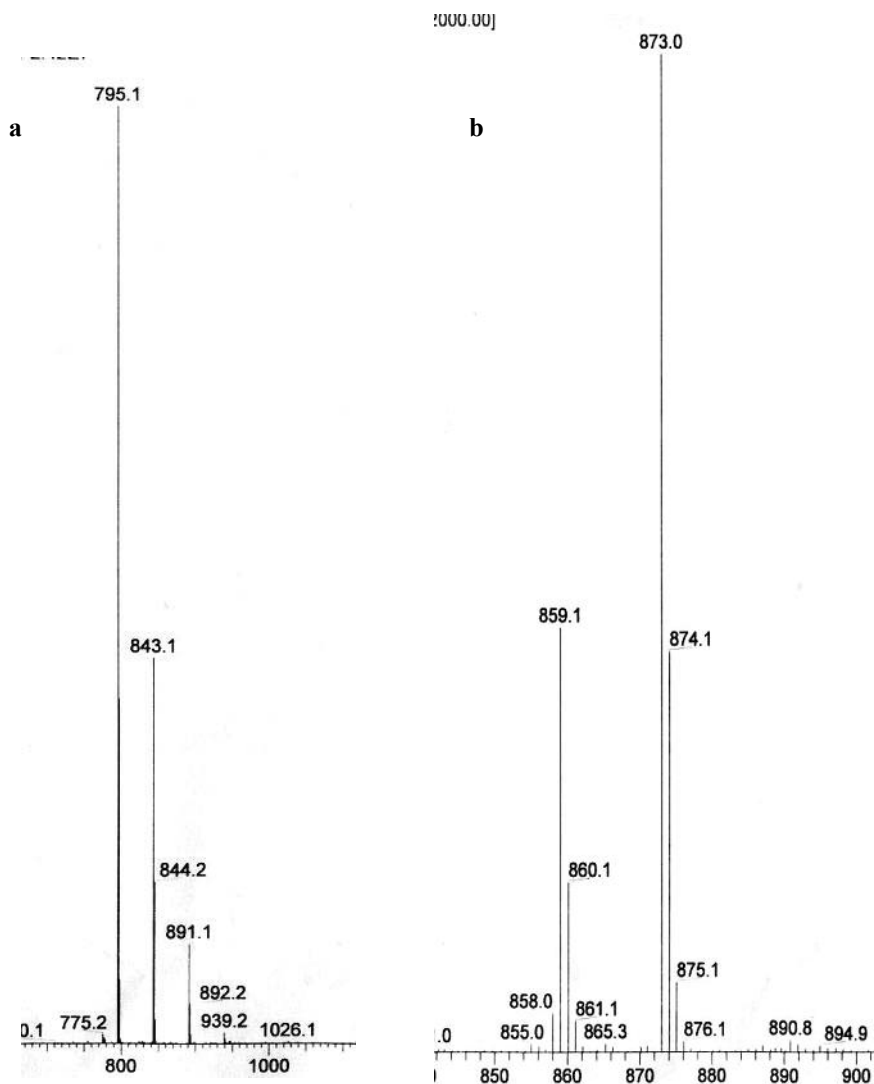


Figure B.2. a) Mass spectrum of reaction mixture from imidazole substitution reaction, negative ions. Unreacted free-base is seen at 795 m/z. Substitution of a fluorine atom by an imidazole molecule adds 48 mass units. Mono, bis, and tris substituted peaks can be observed. B) Mass spectrum of methylation reaction, positive ions. Main peak at 873 corresponds to a dimethyl-monoimidazole corrole, with a peak at 859 corresponding to a monomethyl-monoimidazole corrole.

corroles. Optimization of this reaction to provide a greater portion of triply substituted corrole, as well as separation conditions to resolve the isomers, is ongoing.

While the previous reaction was being optimized, the isomer mixture was used as a starting point for the methylation reaction to ionize the corrole. The isomer mixture was dissolved in distilled DMF and placed under argon. An excess of iodomethane was added, and the solution stirred for three hours at 70 °C. A mass spectrum of the reaction mixture (see figure B.2b) showed primarily a bismethylated-monoimidazole corrole, with a monomethylated corrole at approximately 45% relative to the bismethylated. Two possible structures for the bismethylated molecule are shown in figure B.3. When the DMF from the reaction solution was evaporated, the solid remaining proved to be water soluble, indicating the creation of a new water-soluble corrole. As with the imidazole substitution reaction, optimization of this reaction is ongoing, but again the crude reaction mixture was used as a starting point for the next step, metallation with a chromium salt to provide a water-soluble chromium corrole.

This reaction was performed in the same manner as metallation of **1** with chromium hexacarbonyl. The ionized free-base corrole was refluxed in THF, and 5-10 mg aliquots of Cr(CO)₆ were added every 15 minutes. The reaction was monitored by UV-vis and appeared to be complete after 3 hours. While a separation method for the solution is still being determined, the main peak in the mass spec of the crude reaction mixture shows a surprising result (see figure B.4). The peak at 971 m/z corresponds to a chromium(III)

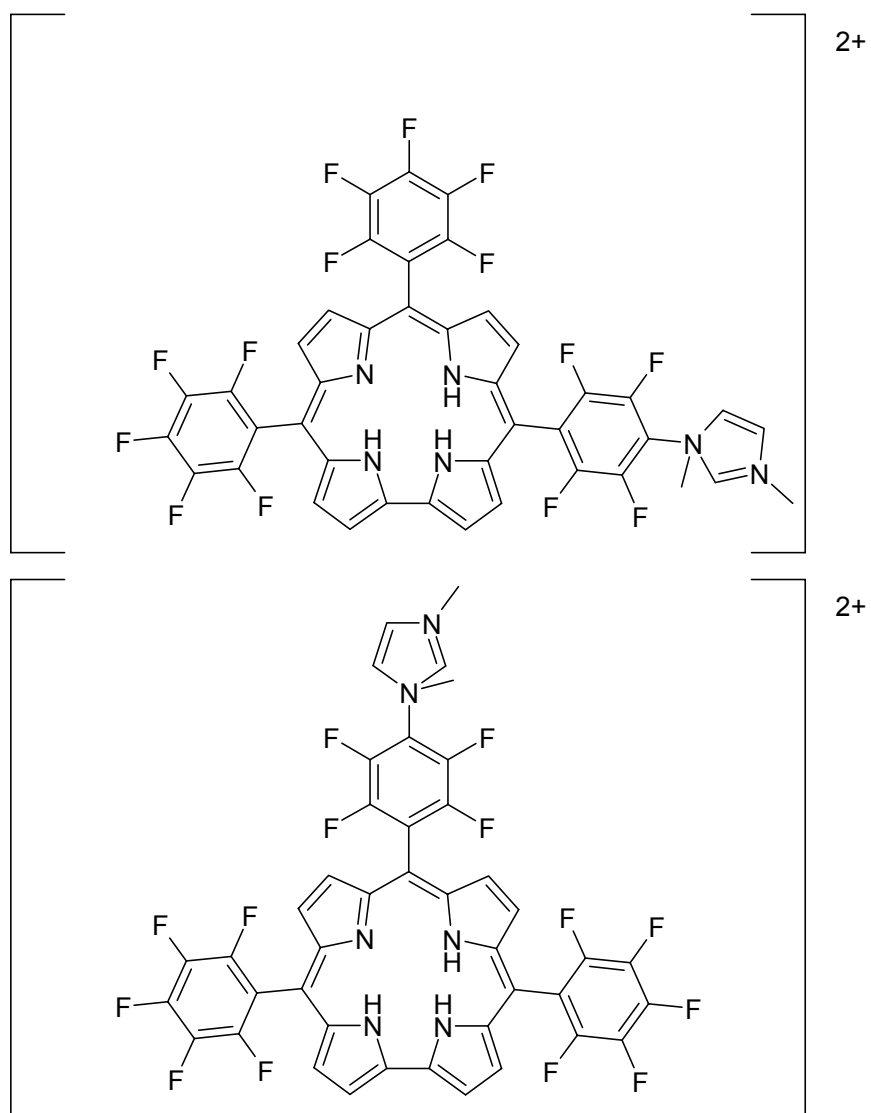


Figure B.3. Two possible structures for the observed bismethylated-monoimidazole corrole.

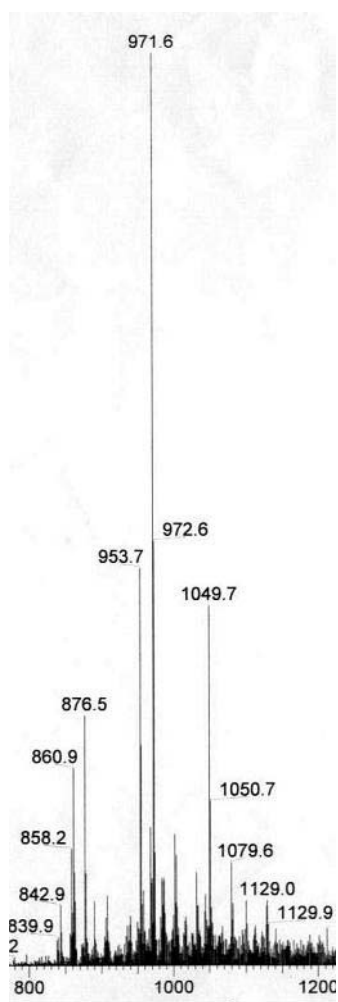


Figure B.4. Mass spectrum of crude reaction mixture from chromium insertion reaction.

corrole with two imidazole groups and two methyl groups. Analysis and full characterization of the products from this reaction are pending.

The final project with Sheikh was the synthesis of a water-soluble manganese nitrido corrole. Work by other groups had shown it was possible to synthesize a nitridomanganese(V) version of **1**^[75], so we attempted to use those methods to obtain a nitrido derivative of **2-Mn**.

In the procedure, **2-Mn** is stirred with sodium azide in acetonitrile while being irradiated with an arc lamp. Mass and UV-vis spectra provided evidence that a Mn(V) nitrido complex was formed; it remains to optimize the reaction conditions to obtain pure product.

BIBLIOGRAPHY

- [1] Johnson, A. W., Kay, I. T., *J. Chem. Soc.* **1965**, 1620.
- [2] Gryko, D. T., *Eur. J. Org. Chem.* **2002**, 1735.
- [3] Van Caemelbecke, E., Will, S., Autret, M., Adamian, V. A., Lex, J., Gisselbrecht, J. P., Gross, M., Vogel, E., Kadish, K. M., *Inorg. Chem.* **1996**, *35*, 184.
- [4] Will, S., Lex, J., Vogel, E., Adamian, V. A., Van Caemelbecke, E., Kadish, K. M., *Inorg. Chem.* **1996**, *35*, 5577.
- [5] Meier-Callahan, A. E., Di Bilio, A. J., Simkhovich, L., Mahammed, A., Goldberg, I., Gray, H. B., Gross, Z., *Inorg. Chem.* **2001**, *40*, 6788.
- [6] Aviezer, D., Cotton, S., David, M., Segev, A., Khaselev, N., Galili, N., Gross, Z., Yayon, A., *Cancer Research* **2000**, *60*, 2973.
- [7] Mahammed, A., Gray, H. B., Weaver, J. J., Sorasaene, K., Gross, Z., *Bioconj. Chem.* **2004**, *15*, 738.
- [8] Bendix, J., Dmochowski, I. J., Gray, H. B., Mahammed, A., Simkhovich, L., Gross, Z., *Angew. Chem. Int. Ed.* **2000**, *39*, 4048.
- [9] Weaver, J. J., Sorasaene, K., Sheikh, M., Goldschmidt, R., Tkachenko, E., Gross, Z., Gray, H. B., *J. Porphyrins Phthalocyanines* **2004**, *8*, 76.
- [10] Paolesse, R., Licoccia, S., Boschi, T., *Inorganica Chimica Acta* **1990**, *178*, 9.
- [11] Gross, Z., Galili, N., Saltsman, I., *Angew. Chem. Int. Ed.* **1999**, *38*, 1427.
- [12] Jimenez, H. R., Julve, M., Faus, J., *J. Chem. Soc., Dalton Trans.* **1991**, 1945.
- [13] Huang, C. Z., Li, Y. F., Li, N., Li, K. A., Tong, S. Y., *Bull. Chem. Soc. Jpn.* **1998**, *71*, 1791.
- [14] Gross, Z., Galili, N., Simkhovich, L., Saltsman, I., Botoshansky, M., Bläser, D., Boese, R., Goldberg, I., *Org. Lett.* **1999**, *1*, 599.
- [15] Saltsman, I., Mahammed, A., Goldberg, I., Tkachenko, E., Botoshansky, M., Gross, Z., *J. Am. Chem. Soc.* **2002**, *124*, 7411.
- [16] Simkhovich, L., Mahammed, A., Goldberg, I., Gross, Z., *Chem. Eur. J.* **2001**, *7*, 1041.

- [17] Gouterman, M., *J. Mol. Spec.* **1961**, *6*, 138.
- [18] Gouterman, M., Wagnière, G. H., Snyder, L. C., *J. Mol. Spec.* **1963**, *11*, 108.
- [19] Hush, N. S., Dyke, J. M., Williams, M. L., Woolsey, I. S., *J. Chem. Soc. Dalton Trans.* **1974**, 395.
- [20] Ghosh, A., Wondimagegn, T., Parusel, A. B. J., *J. Am. Chem. Soc.* **2000**, *122*, 5100.
- [21] Lide, D. R., editor, *CRC Handbook of Chemistry and Physics*, 76th ed., CRC Press, **1995**.
- [22] Kilså, K., *Energy and Electron Transfer in Porphyrin-based Donor-bridge-acceptor Systems*, Ph.D. thesis, Chalmers University of Technology (Göteborg), **2000**.
- [23] Grancho, J. C. P., Pereira, M. M., Miguel, M. d. G., Rocha Gonsalves, A. M., Burrows, H. D., *Photochem. Photobiol.* **2002**, *75*, 249.
- [24] Khalil, G., Gouterman, M., Ching, S., Costin, C., Coyle, L., Goulin, S., Green, E., Sadilek, M., Wan, R., Yearyeen, J., Zelelow, B., *J. Porphyrins Phthalocyanines* **2002**, *6*, 135.
- [25] Sessler, J. L., Tvermoes, N. A., Davis, J., Anzenbacher, P., Jursikova, K., Sato, W., Seidel, D., Lynch, V., Black, C. B., Try, A., Andrioletti, B., Hemmi, G., Mody, T. D., Magda, D. J., Kral, V., *Pure Appl. Chem.* **1999**, *71*, 2009.
- [26] MacDonald, I. J., Dougherty, T. J., *J. Porphyrins Phthalocyanines* **2001**, *5*, 105.
- [27] Via, L. D., Magno, S. M., *Curr. Med. Chem.* **2001**, *8*, 1405.
- [28] Dougherty, T. J., Gomer, C. J., Henderson, B. W., Jori, G., Kessel, D., Korbelik, M., Moan, J., Peng, Q., *J. Natl. Cancer. Inst.* **1998**, *90*, 889.
- [29] Sessler, J. L., Weghorn, S. J., *Expanded, Contracted, & Isomeric Porphyrins*, Pergamon, Oxford, **1997**.
- [30] Paolesse, R., *The Porphyrin Handbook, Vol. II*, Academic Press, New York, **2000**.
- [31] Paolesse, R., Jaquinod, L., Nurco, D. J., Mini, S., Sagone, F., Boschi, T., Smith, K. M., *Chem. Commun.* **1999**, 1307.
- [32] Simkhovich, L., Goldberg, I., Gross, Z., *J. Inorg. Biochem.* **2000**, *80*, 235.
- [33] Cho, W.-S., Lee, C.-H., *Tetrahedron Lett.* **2000**, *41*, 697.
- [34] Gryko, D. T., *Chem. Commun.* **2000**, 2243.

- [35] Briñas, R. P., Brückner, C., *Synlett.* **2001**, 442.
- [36] Gryko, D. T., Jadach, K., *J. Org. Chem.* **2001**, 66, 4267.
- [37] Ka, J.-W., Cho, W.-S., Lee, C.-H., *Tetrahedron Lett.* **2000**, 41, 8121.
- [38] Paolesse, R., Nardis, S., Sagone, F., Khoury, R. G., *J. Org. Chem.* **2001**, 66, 550.
- [39] Asokan, C. V., Smeets, S., Dehaen, W., *Tetrahedron Lett.* **2001**, 42, 4483.
- [40] Gross, Z., Simkhovich, L., Galili, N., *J. Chem. Soc., Chem. Commun.* **1999**, 599.
- [41] Gross, Z., Golubkov, G., Simkhovich, L., *Angew. Chem. Int. Ed.* **2000**, 39, 4045.
- [42] Golubkov, G., Bendix, J., Gray, H. B., Mahammed, A., Goldberg, I., Di Bilio, A. J., Gross, Z., *Angew. Chem. Int. Ed.* **2001**, 40, 2132.
- [43] Simkhovich, L., Gross, Z., *Tetrahedron Lett.* **2001**, 42, 8089.
- [44] Mahammed, A., Gross, Z., *J. Inorg. Biochem.* **2002**, 88, 305.
- [45] Mahammed, A., Goldberg, I., Gross, Z., *Org. Lett.* **2001**, 3, 3443.
- [46] Allen, C. M., Langlois, R., Sharman, W. M., La Madeleine, C., Van Lier, J. E., *Photochem. Photobiol.* **2002**, 76, 208.
- [47] Boyle, R. W., Dolphin, D., *Photochem. Photobiol.* **1996**, 64, 469.
- [48] Bonnett, R., *Rev. Contemp. Pharmacother.* **1999**, 10, 1.
- [49] Chuang, V. T. G., Kragh-Hansen, U., Otagiri, M., *Pharm. Res.* **2002**, 19, 569.
- [50] Kragh-Hansen, U., Chuang, V. T. G., Otagiri, M., *Biol. Pharm. Bull.* **2002**, 25, 695.
- [51] Peters, T., *All About Albumin: Biochemistry, Genetics, and Medical Applications*, Academic Press, San Diego, **1996**.
- [52] Sugio, S., Kashima, A., Mochizuki, S., Noda, M., Kobayashi, K., *Protein Eng.* **1999**, 12, 439.
- [53] Wardell, M., Wang, Z., Ho, J. X., Robert, J., Ruker, F., Ruble, J., Carter, D. C., *Biochem. Biophys. Res. Commun.* **2002**, 291, 813.
- [54] Bertucci, C., Domenici, E., *Curr. Med. Chem.* **2002**, 9, 1463.
- [55] Ding, Y. S., Lin, B. C., Huie, C. W., *Electrophoresis* **2001**, 22, 2210.

- [56] Morgan, W. T., Smith, A., Koskelo, P., *Biochim. Biophys. Acta* **1980**, 624, 271.
- [57] Datta-Gupta, N., Malakar, D., Dozier, J., *Res. Commun. Chem. Pathol. Pharmacol.* **1989**, 63, 289.
- [58] Rotenberg, M., Cohen, S., Margalit, R., *Photochem. Photobiol.* **1987**, 46, 689.
- [59] Beaven, G. H., Chen, S. H., Dalbis, A., Garatzer, B. W., *Eur. J. Biochem.* **1974**, 41, 539.
- [60] Bardos-Nagy, I., Galantai, R., Kaposi, A. D., Fidy, J., *Int. J. Pharm.* **1998**, 175, 255.
- [61] Gantchev, T. G., Ouellet, R., van Lier, J. E., *Arch. Biochem. Biophys.* **1999**, 366, 21.
- [62] Ambroz, M., MacRobert, A. J., Morgan, J., Rumbles, G., Foley, M. S. C., Phillips, D., *J. Photochem. Photobiol., B* **1994**, 22, 105.
- [63] Andrade, S. M., Costa, S. M. B., *Biophys. J.* **2002**, 82, 1607.
- [64] Davila, J., Harriman, A., *J. Am. Chem. Soc.* **1990**, 112, 2680.
- [65] Bishop, S. M., Khoo, B. J., MacRobert, A. J., Simpson, M. S. C., Phillips, D., *J. Chromatogr.* **1993**, 646, 345.
- [66] Mahammed, A., Gray, H. B., Weaver, J. J., Gross, Z., *Tetrahedron Lett.* **2003**, 44, 2077.
- [67] Chatterjee, S., Srivastava, T. S., *J. Porphyrins Phthalocyanines* **2000**, 4, 147.
- [68] Cai, X., Dass, C., *Curr. Org. Chem.* **2003**, 7, 1841.
- [69] Dunn, A. R., Dmochowski, I. J., Winkler, J. R., Gray, H. B., *J. Am. Chem. Soc.* **2003**, 125, 12450.
- [70] Turro, N. J., *Modern Molecular Photochemistry*, Benjamin/Cummings Inc., Menlo Park, **1978**.
- [71] Kilså, K., Mayo, E. I., Brunshwig, B. S., Gray, H. B., Lewis, N. S., Winkler, J. R., *J. Chem. Phys.* **2004**, 40, 15640.
- [72] Mahammed, A., Gray, H. B., Meier-Callahan, A. E., Gross, Z., *J. Am. Chem. Soc.* **2003**, 125, 1162.
- [73] Meier, A. E., *Gallium and Chromium Corroles*, Ph.D. thesis, California Institute of Technology (Pasadena), **2003**.

- [74] Dunn, A. R., *Sensitizer-linked substrates as probes of heme enzyme structure and catalysis*, Ph.D. thesis, California Institute of Technology (Pasadena), **2003**.
- [75] Eikey, R. A., Khan, S. I., Abu-Omar, M. M., *Angew. Chem. Int. Ed.* **2002**, *41*, 3591.